

EIHE 2023



7 – 11 February, 2023

DAE Convention Centre,
Anushaktinagar, Mumbai



Souvenir Cum bulletin of Indian Society for ElectroAnalytical Chemistry



Souvenir Cum Bulletin of
Indian Society for ElectroAnalytical Chemistry
Being released during
2nd International Conference On
Electrochemistry in Industry, Health & Environment

EIHE 2023

February 7-11, 2023

DAE Convention Centre, Anushaktinagar,
BARC, Mumbai

Editors

Sudipa Manna

A. K. Satpati

Organized by



Indian Society for ElectroAnalytical Chemistry
Mumbai, India
www.iseac.org.in

EIHE 2023

Indian Society for Electro Analytical Chemistry (ISEAC)

Welcomes you to the

International Conference

on

Electrochemistry in Industry, Health & Environment – 2023

ISBN No. 978-81-961201-1-5

February, 2023

Printed by

Shradha Xerox Centre

Shop No 4, Arjun Centre, Govandi Station Rd,

Deonar, Govandi East, Mumbai,

Maharashtra 400088

डॉ. अजित कुमार मोहान्ती
Dr. Ajit Kumar Mohanty



निदेशक, भाभा परमाणु अनुसंधान केंद्र
Director, Bhabha Atomic Research Centre
सदस्य, परमाणु ऊर्जा आयोग
Member, Atomic Energy Commission



MESSAGE

Electrochemistry is one of the frontier areas of research in chemistry, which has provided microscopic understanding of the mechanism and strategies in solving several recent societal challenges, especially in relation with the energy, environment and health care. Over the years, these subject areas are gradually becoming interdisciplinary in nature with applications in many industrial challenges like, Li-ion battery, redox flow battery, supercapacitors, solar energy harvesting devices, biomedical sensors, electrochemical synthesis, electrochemical deposition of materials and fabrication of devices. Electrochemical techniques have also been utilized in the preparation and characterization of some of the advanced radiopharmaceuticals. I am glad that our Research Centre has the finest state-of-the-art facilities for this kind of frontline research and are actively pursuing this discipline, covering almost all of its dimensions, from laboratory scale studies to the industrial scale applications.

I am delighted to know that the 2nd DAE-BRNS international conference on, "Electrochemistry in Industry, Health and environment (EIHE 2023)" is jointly organized by Analytical Chemistry Division, Chemistry Group, Bhabha Atomic Research Centre, with the Indian Society for Electroanalytical Chemistry (ISEAC) during February 7 to 11, 2023 at DAE Convention Centre, Anushaktinagar, Mumbai. This conference has attracted participation of scientists from all over the world whose interaction with young researchers will pave the way into cutting-edge research in the coming days.

I am sure that the deliberations of the conference will be very exciting and will offer a common platform for the intense scientific discussions and exchange of ideas amongst the budding researchers in this field. It will bring out new ideas and understandings to carry forward quest for collaborative and interdisciplinary research.

I wish EIHE-2023 a grand success.

Date : 02.02.2023

Ajit Kumar Mohanty
(Dr Ajit Kumar Mohanty)



भाभा परमाणु अनुसंधान केंद्र, ट्रॉम्बे, मुंबई- 400 085, भारत • Bhabha Atomic Research Centre, Trombay, Mumbai 400 085, India
दूरभाष/Phone: +(91) (22) 2550 5300, 2551 1910 • फैक्स/Fax: +(91) (22) 2559 2107, 2550 5151
ई-मेल/E-mail: director@barc.gov.in





भारत परमाणु अनुसंधान केंद्र
BHABHA ATOMIC RESEARCH CENTRE

2-206-S, Modular Labs.,
Trombay, Mumbai-400 085, INDIA

Phone : +91-22-2559 5330
 +91-22-2559 3670

Email : aktyagi@barc.gov.in



सत्यमेव जयते

Government of India
Bhabha Atomic Research Centre
Chemistry Group

Dr. A.K. Tyagi

FNASc, FASc, FNAE
Distinguished Scientist, DAE &
Director, Chemistry Group, BARC




Message

The International conference under the thematic title of **"Electrochemistry in Industry, Health and Environment, EIHE-2023"** is being organised by **Analytical Chemistry Division, Chemistry Group, Bhabha Atomic Research Centre** along with Indian Society for Electroanalytical Chemistry (ISEAC) at DAE Convention Centre, Anushaktinagar, Mumbai 400094 during February 7-11, 2023. Under the scope of this conference the expediency of electrochemistry will be discussed in the context of important scientific and technological issues related to the recent societal problems. The topics of the conference includes; Catalytic electrochemistry, Photoelectrochemical water splitting for hydrogen generation using solar energy, Electrochemical instrumentations and devices, Energy storage systems like, Battery and Supercapacitor, Electrochemistry at nanoscale, Electrochemistry in Nuclear Energy/molten salt processes, Electrochemical Sensors and Biosensors for Health, Medical and Environmental Sciences.

I welcome all the invited speakers from India and overseas for accepting our invitation, I am sure that your presence in the conference will encourage the young researchers and students to take up challenging activity in this exciting field. I request all the students to remain attentive during the scientific deliberation and interact with the experts to enhance your scientific horizon in electrochemistry.

As chairman organising committee of **EIHE 2023**, I express my heartiest welcome to all the delegates of **EIHE 2023** once again and my best wishes to all of you in your future endeavours.


(A.K. Tyagi)

Dated : 02.02.2023



Prof. P. D. Naik
Vice Chancellor (Officiating)
& Dean

होमी भाभा राष्ट्रीय संस्थान

प्रशिक्षण विद्यालय परिसर, अणुशक्तिनगर, मुंबई-400 094, भारत

Homi Bhabha National Institute

Training School Complex, Anushaktinagar, Mumbai – 400 094, India

Tel. No. 91-22-25595398 • Mob. : 9221798549

Email : deanhbni@hbni.ac.in • pdnaik@barc.gov.in



Message from President, Indian Society for Electroanalytical Chemistry (ISEAC)

Wish you a very happy and productive new year 2023. As the President, Indian Society for Electroanalytical Chemistry (ISEAC), I welcome you to this International Conference "Conference on Electrochemistry in Industry, Health and Environment (EIHE 2023)".

Electrochemistry and its applications aspects are immensely useful in solving various societal problems. ISEAC has broadened the scope of the Society to include activities from all branches of Electrochemical Sciences and Technologies. The main aim of ISEAC is to promote electrochemistry in India, to disseminate scientific and technological knowledge within the country and to strengthen national and international cooperation in the area of Electrochemistry. ISEAC with support from DAE units organises one discussion meeting and one international conference every alternate year to provide a platform for discussion on the recent development in electrochemistry and allied fields.

ISEAC appeal to all electrochemist and allied field researchers to be a part of the ISEAC family. To encourage the researchers to join ISEAC as a member, we have kept a life membership fee nominal, Rs. 4000/- and the student membership fee is Rs. 1000/- (for 5-year validity).

It is encouraging to see a large number of participants registered for this international event, EIHE 2023, which indicates the popularity of the symposium among researchers and the importance and interest in the field. I take this opportunity to thank the authorities of Bhabha Atomic Research Centre for the kind support rendered in the organisation of this event at the beautiful campus of Anushaktinagar and BRNS for sponsoring the conference.

As president of ISEAC, I welcome you all to this international event and wish you all a fruitful interaction and the best for your future research endeavours.


(P. D. Naik)



Indian Society for ElectroAnalytical Chemistry
(Reg. No. MAH/MUM/1173/2006 GBBSD)
Bhabha Atomic Research Centre, Mumbai - 400085



Dr. Ashis Kumar Satpati
Secretary, ISEAC and Convener, EIHE-2023
Head, Electrochemical Methods Section,
Analytical Chemistry Division
Bhabha Atomic Research Centre, Trombay,
Mumbai 400085, Phone: 022-25590744 (O)
Email: aksatpati@gmail.com

Dear Delegates

Greetings from ISEAC

On behalf of ISEAC and the organising team EIHE 2023, I welcome you all in this international event "Electrochemistry in Industry, Health and Environment, EIHE-2023" at Anushaktinagar, Mumbai. I thank all of you for coming here to attend this conference.

We have tried our best to organise this international event, and thank you for your cooperation and enthusiasm. Since its inception, scope of the society has been broadened to cover the entire spectrum of the scientific activities in the field, this has resulted the increased number of life members from the scientific fraternity across various institutes. I take this forum to request all of you to enhance the activities of the society and promote your colleagues and students to become the life member of this organisation.


In addition to the abstract booklet we are coming out with a Souvenir cum Bulletin of ISEAC during this conference containing articles on different aspects of electrochemical science and technology are being published in this volume, I thank all the authors for their contribution in the bulletin. I encourage all of you to participate in writing short articles for this series of Bulletin.

Being stationed at Bhabha Atomic Research Centre, we enjoy the fame of this institute and excellent logistics support, we thank our authorities for the same. I thank Heavy Water Board (HWB), Atomic Energy Regulatory Board (AERB), Nuclear Power Corporation of India Limited (NPCIL), American Chemical Society (ACS), Royal Chemical Society (RSC), Elsevier, for supporting this event. I sincerely thank all the industrial partners for their support.

From this very conference let us collectively make an effort to take the activities of the society forward and a make our presence at higher level. I wish all of you for excellent outcome from your research, ISEAC will provide all possible platform to promote your research activities. Let us join together and bring the fascinating science in the field of *ELECTROCHEMISTRY* to its fullest potential for the benefit of the society.

On behalf of the team of organising committee EIHE 2023 and the Secretary, ISEAC, I express my sincere appreciations once again to DAE-BRNS, the ISEAC life members, all sponsors and the delegates of EIHE 2023 to make this event possible.

February 02, 2023


02-02-2023
(A K Satpati)

Address of Correspondence: Analytical Chemistry Division, 3rd Floor, Modular Labs,
Bhabha Atomic Research Centre, Mumbai – 400085, India
Email: electrochembarc@gmail.com, **Web:** www.iseac.org.in
Contact: (+91)22-25590744/0326



Indian Society for ElectroAnalytical Chemistry

Reg. No. MAH/MUM/1173/2006 GBBS

(Website: www.iseac.org.in; Email: electrochembarc@gmail.com)

Since foundation, the Society has evolved magnificently to represent a truly National Organization and at present, it comprises more than 325 life-members from different parts of India and Overseas. The Executive committee of ISEAC, which manages the activities of ISEAC, is being elected triennially by all the members of ISEAC.

International Events organized by ISEAC:

ISEAC organizes International Conferences, Discussion Meets and Workshop cum Symposium on Electrochemistry and allied topics in association with the Departments of Government of India, International Society of Electrochemistry and other Scientific Organizations and Industries. ISEAC has organized thirteen International Events in India. This is 16th event organized by the society; however, it has been planned to continue the EIHE series from the year 2020 onwards, therefore this conference is 2nd conference in the series.

1. International Conference on Electrochemistry in Industry Health and Environments (EIHE 2020) at DEA Convention Centre, Anushaktinagar, Mumbai during January 21-25, 2020.
2. Discussion meeting on Spectro electrochemistry (DM-ISEAC-2022) at Multipurpose hall, Training School Hostel, Anushaktinagar, Mumbai 400094 on 16-07-2022
3. International Conference on Electrochemistry in Advanced Materials, Corrosion and Radiopharmaceuticals (CEAMCR-2018) at DEA Convention Centre, Anushaktinagar, Mumbai during February 15-17, 2018.
4. Twelfth ISEAC Discussion Meet in Electrochemistry (12th ISEAC-DM-2016) held at The Acres Club, Chembur, Mumbai during December 7-8, 2016.
5. Eleventh ISEAC International Discussion Meet on Electrochemistry and its Applications (ISEAC-DM-2014) held at Hotel Radisson Blu, Amritsar during February 20-25, 2014.
6. Fifth ISEAC Triennial International Conference on Advances and Recent Trends in Electrochemistry (ELAC-2013) held at Sitara Hotel, Ramoji Film City, Hyderabad during January 16-20, 2013.
7. ISEAC International Symposium cum Workshop on Electrochemistry (ISEAC-WS-2011) at Cidade de Goa, Dona Paula, Goa during December 7-10, 2011.
8. Fourth ISEAC International Discussion Meet on Electrochemistry and its Applications (DM-ISEAC-2011) at Mascot Hotel, Thiruvananthapuram, Kerala during February 7-10, 2011.

9. *Fourth International Conference on ElectroAnalytical Chemistry and Allied Topics (ELAC-2013) at Toshali Sands, Puri, Orissa during March 16-18, 2010.*
10. *Discussion Meet on ElectroAnalytical Techniques and Their Applications (DM-ELANTE-2008) held at Tea County, Munnar, Kerala during February 25-28, 2008.*
11. *Third International Conference on ElectroAnalytical Chemistry and Allied Topics (ELAC-2007) at Toshali Royal View Resort, Shilon Bagh, Shimla during March 10-15, 2007.*
12. *Discussion Meet on Role of Electrochemistry in Biosensors, Nanomaterials, Fuel Cells and Ionic Liquids (DM-BNFL-2006) held at Bhabha Atomic Research Centre, Mumbai during September 24-25, 2006.*
13. *Discussion Meet on Coulometry (DM-COUL-2005) at Bhabha Atomic Research Centre, Mumbai on May 5, 2005.*
14. *Second International Conference on ElectroAnalytical Chemistry and Allied Topics (ELAC-2004) held at The International Centre, Dona Paula, Goa during January 18-23, 2004.*
15. *Workshop cum Seminar on ElectroAnalytical Chemistry and Allied Topics (ELAC-2000) held at Bhabha Atomic Research Centre, Mumbai during November 27 – December 1, 2000.*

Objectives of ISEAC:

- *Promote the growth of Electrochemistry in India.*
- *Provide a common world-wide platform to the experts, scientists and scholars working in the area of Electrochemistry and its Allied Sciences.*
- *Disseminate scientific and technological knowledge in the area of Electrochemistry to advance both national and international collaborations.*
- *Share the information on Electrochemistry with other International Societies viz. European Society for Electroanalytical Chemistry (ESEAC), Society for Electroanalytical Chemistry (SEAC) and International Society of Electrochemistry (ISE), Bioelectrochemical Society (BES).*
- *Work in harmony with other Indian Electrochemical Societies viz. Society for the Advancement of Electrochemical Science and Technology (SAEST) based at CECRI, Karaikudi and Electrochemical Society of India (ECSI) based at Indian Institute of Science, Bengaluru.*
- *Provide incentive by way of awards to researchers for the best thesis, the best paper published in the journal and the best paper presented in National and International Conferences/Symposia.*

- *Encourage young as well as experienced Indian researchers for participation in International Electrochemistry Conferences by providing partial funds, if possible.*

Procedure to join ISEAC:

ISEAC has the provision for individual to join as Life-members and for company to join as Corporate Member. The Life-membership fee w.e.f. April 1, 2011 is Rs. 4000/- (Rs. Four thousands only) for Indians and € 300/- (Euro three hundred only) for others. The Fee has to be transferred electronically (NEFT or wire transfer) to ISEAC Bank Account and then you have to sign-up through “Join ISEAC as Life-Member” icon available on www.iseac.org.in with the fund transfer details.

Name of Bank: State Bank of India, BARC Branch, Mumbai-400 085, India

Branch code: 1268

Beneficiary name: Indian Society for ElectroAnalytical Chemistry (ISEAC)

Account number: 34209997299

BIC (Swift Code): SBININBB508

IFSC code (for within India): SBIN0001268

Please contact us for any further information:

The Secretary,

Indian Society for ElectroAnalytical Chemistry (ISEAC)

Analytical Chemistry Division,

Bhabha Atomic Research Centre, Trombay,

Mumbai – 400 085, India

Email: electrochembarc@gmail.com;

web.: www.iseac.org.in

Phone: +91-22-2559 0744 (office hours only); 8369268926 (after office hours)

You are Welcome to Join

ISEAC

EIHE-2023

Conference on Electrochemistry in Industry, Health and Environment

February 7-11, 2023

**DAE Convention Centre, Anushaktinagar, Mumbai – 400094,
India**

Organised by



In association with



Academic partners

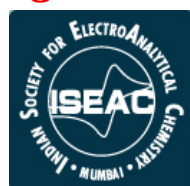


DAE-BRNS
2nd International Conference on
EIHE-2023

Electrochemistry for Industry, Health and Environment
February 7-11, 2023

At DAE Convention Centre, Anushaktinagar, Mumbai – 400094, India

Organised by



Programme Schedule

February 07, 2023; Tuesday

- 9:30- 13:00 hrs : Registration at *DAE Convention Centre*
- 13:00 – 14:00 hrs : Lunch at dining hall, DAE Convention Centre
- 14:30 – 16:00 hrs : **Inauguration of the Conference (Auditorium A)**
- 16:00 – 16:30 hrs : High Tea at Lobby & Group photograph
- 16:30- 18:45 hrs : **Session 1 (Auditorium A)**

Chairperson: Prof. J. P. Mittal, UM-DAE-CEBS

Plenary Lecture (40+5 minutes)

- 16:30- 17:15 hrs : **IT-01; Prof Christopher M.A. Brett, Department of Chemistry, CEMMPRE, Faculty of Sciences and Technology, University of Coimbra, Portugal**

Modified electrodes with electroactive redox polymers and nanomaterials for sensor and biosensor platforms

Invited Lecture (25+5 minutes)

IT-11; Prof. Amreesh Chandra; Indian Institute of Technology Kharagpur

Pseudo-2D Nanostructure based High Performance Hybrid Supercapacitors: Correlating Theoretical and Experimental Studies

IT-49; Prof. Sangaraju Shanmugam, *Department of Energy Science & Engineering, Daegu Gyeongbuk Institute of Science and Technology (DGIST) Daegu, 42988, South Korea*

Electrochemical Synthesis of Sustainable Carbon-Free Fuels

IT-14; Prof. Kinshuk Dasgupta, *Materials Group, Bhabha Atomic Research Centre, Mumbai*

Tuneable synthesis of graphene oxide by electrochemical exfoliation of graphite

- 19:00 – 20:30hrs : **Cultural programme (Auditorium A)**
- 20:30-21:30 hrs : **Dinner at dining hall, DAE Convention Centre**

February 08, 2023; Wednesday

- 09:30 – 11:15hrs : **Session 2 (Auditorium A)**

Chairperson: Prof. S. Mukhopadhyay, E& IG, BARC

Plenary Lecture (40+5 minutes)

- 9:30-10:15 hrs : **IT-08; Prof. P. Vadgama**, *Queen Mary University of London, United Kingdom*

Sensors for in vivo biochemical monitoring: A Membranes and materials adaptation

Invited Lecture (25+5 minutes)

- 10:15-10:45 hrs : **IT-07; Prof. Muhammed Musthafa O T**, *Indian Institute of Science Education and Research, Pune*

Electrochemical Neutralization: Concepts to Devices

- 10:45-11:15 hrs : **IT-38, Prof. Rama Kant**, *Department of Chemistry, University of Delhi*

Electron Transfer in Nano-Structured and Atomically Stepped Electrodes: Theoretical Aspects

- 11:15-11:30 hrs : **Tea at Lobby**

- 11:30–13:00 hrs : **Session 3 (Auditorium A)**

Chairperson: Prof. Archana Sharma, BTDG, BARC

Invited Lecture (25+5 minutes)

- 11:30-12:00 hrs : **IT-17; Prof. Amartya Mukhopadhyay**, *Indian Institute of Technology Bombay*

		Layered' transition metal oxides as cathode materials for Na-ion batteries
12:00-12:30 hrs	:	<i>IT-05 Prof. Annamalai Senthil Kumar, Vellore Institute of Technology, Vellore</i>
		In-Situ Activation of Pencil Graphite Electrode Surface and Its Active Site Mapping Using Scanning Electrochemical Microscopy and Electrocatalysis
12:30-13:00 hrs	:	<i>IT-21 Prof. M R Pai, Chemistry Division, Bhabha Atomic Research Centre, Mumbai</i>
		Solar Water Splitting Using Earth Abundant Conjugated Photocatalysts
13:00-14:00 hrs		Lunch at dining hall, DAE Convention Centre
14:00-16:00 hrs		Session 4 Chairpersons: Dr. Sangita D Kumar, ACD, BARC Dr. Sanjukta A. Kumar, ACD, BARC
		Poster Presentations: P-1 to P-82 at Poster Hall (Except CPs selected for oral presentation)
15:30-16:00 hrs		Tea during poster session
16:00-18:30 hrs		Session 5 (Auditorium A & Auditorium B)

Invited Lecture (20+2 minutes)

Auditorium A

Chairperson:

Prof. H. Pal, HBNI

Prof. Sunil K Ghosh, HBNI

IT-22: Prof. Chinmoy Bhattacharya, Dept. of Chemistry, Indian Institute of Engineering Science & Technology, (IEST), Shibpur

BiVO₄ - a futuristic Semiconductor for Photoelectrochemical Applications

IT-46; Prof. Bhaskar R. Sathe, Department of Chemistry, Dr. Babasaheb Ambedkar Marathwada University Aurangabad

New Modifications of Graphene for Water Splitting and Fuel Cell Reactions

IT-23; Prof. Nagraj Shetty, School of Advanced Sciences, KLE Technological University, Hubballi, Karnataka

Electrochemical sensors for the detection and degradation of toxic molecules

IT-09: Rituraj Mishra, Bharat Petroleum Corporation LTD

Investigative Research on the Critical Electrochemical Corrosion Driven by Combined Cathodic and Anodic Interference on a Pipeline

Auditorium B

Chairperson:

Prof. A.C. Bhasikuttam, RPCD, BARC

Prof. P.A. Hassan, ChD, BARC

IT-28; Prof. Subramanyam Sarma, Department of Chemistry, YOG VEMANA UNIVERSITY

Electrocatalysis of reduced graphene oxide-supported nanocomposites for fuel cell reactions

IT-10: Prof. Sanghamitra Chatterjee, Department of Chemistry, Institute of Chemical Technology, Mumbai

Theranostic Applications of Carbon Nanomaterial Modified Sensors: A Promising Future

IT-41; Dr. D. K Sahoo, Material Processing & Corrosion Engineering Divisison, Bhabha Atomic Research Centre

Electrowinning of light rare earth metals and alloys using molten salt electrolysis route

IT-52; Dr. V. S. Tripathi, Radiation & Photochemistry Division, BARC, Mumbai

IT-51 ; Dr. Ruma Gupta, Fuel Chemistry Division, Bhabha Atomic research Centre

Electrochemical fate of Actinides: Aqueous and Non aqueous routes

IT-35; Dr. Bholanath Mahanty, Radiochemistry Division, Bhabha Atomic Research Centre

Membrane based potentiometric sensors for lanthanides and actinides

Electrodeposition of Rhodium and Platinum-Rhodium alloy on stainless steel substrate: a durable catalyst surface

IT-45; Prof. D. Banerjee, Nuclear Recycle Group, Bhabha Atomic Research Centre, Mumbai

Electrodeposition of Radioruthenium: Process Development and its Applications for the Treatment of Eye Cancer

IT-58: Ms. Sutanwi Lahiri, Laser & Plasma Technology Division, Bhabha Atomic Research Centre, Mumbai

Application of cavitation in graphite decontamination

18:45 hrs : Tea at *Lobby*

20:00-21:00 hrs : Dinner at dining hall Training School Hostel, Anushaktinagar

February 09, 2023; Thursday

09:30–11:00 hrs : **Session 6 (online) (Auditorium A)**

Chairperson: Prof. T.K. Ghanty, BSG, BARC

Plenary Lecture (40+5 minutes)

09:30–10:15 hrs : *IT-16; Prof. Shalini Prasad, Department of Bioengineering and Biomedical Engineering, The University of Texas at Dallas*

Electrochemically mediated multi-modal detection strategy-driven sensor platform to detect and quantify pesticides

10:15-11:00 hrs : *IT-55; Prof. Ritu Goswami Katak, Department of Chemistry, Durham University, Durham, United Kingdom*

Electrochemical Interactions at 'soft' liquid-liquid interfaces

11:00–11:15 hrs : Tea at *Lobby*

11:15–13:00 hrs : **Session 7 (online & offline); (Auditorium A)**

Chairperson: Prof. Swapan K Ghosh, UM-DAE-EBES

Plenary Lecture (40+5 minutes)

11:15-12:00 hrs : *IT-29; Prof. Ignacy Cukrowski, Department of Chemistry, Faculty of Natural and Agricultural Sciences, University of Pretoria, South Africa*

Metal-Ligand Equilibria: A Unified Theory and Protocol for Voltammetry and Potentiometry

Invited Lecture (25+5 minutes)

- 12:00 – 12:30 hrs : *IT-02; Prof. Ramanathan S, Dept. of Chemical Engineering, IIT Madras, Chennai*
Electrochemical reaction mechanism identification from potentiodynamic polarization data
- 12:30– 13:00 hrs : *IT-03; Prof. Sayan Bhattacharyya, IISER Kolkata*
Solid State Chemistry Approach Towards Green Hydrogen
- 13:00 – 14:00 hrs : **Lunch at dining hall, DAE Convention Centre**
- 14:00 – 16:00 hrs : **Session 8**
Chairperson:
Prof. N. Choudhury, ChD, BARC
Prof. S. Nath, RPCD, BARC
Poster Presentations: CP-82 to CP-152 at Poster Hall (Except CPs selected for oral presentation)
Tea during 15:30-16:00
- 16:00 – 17:30 hrs : **Session 9; Invited Lecture (20+2 minutes)**

Auditorium A

Chairperson:

Dr. S. Adhikari, SIRD, BARC

Shri M.K. Saxena, RACD, BARC

IT-24; Mr. Rooshin Vadgama, UCL Cancer Institute, University College London

The Effect of Low Dose Radiation on Neurotransmission

IT-57; Prof. Drishty Satpati, Radiopharmaceuticals Division, Bhabha Atomic Research Centre, Mumbai, India

Applications of Electrochemistry In Development of Radiopharmaceuticals

IT-13; Prof. P.C. Mondal , Department of Chemistry, Indian Institute of Technology Kanpur

Molecular thin films for electrochemical supercapacitors: Are we heading toward the molecular power banks?

IT-53; Prof. Ruma Ghosh, Department of Electrical Engineering, Indian Institute of Technology Dharwad

Nanomaterials based Sensors for Healthcare Applications

Auditorium B

Chairperson:

Dr. A. K. Tripathi, ChD, BARC

Dr. G. Sugilal, FRD, BARC

IT-36; Prof. Rosy, Department of Chemistry, IIT(BHU) Varanasi

Hexagonal Boron Nitride for Na- Ion/Metal Batteries

IT-47; Dr. Thandavarayan Maiyalagan, Department of Chemistry, SRM Institute of Science and Technology, Kattankulathur

Non-Precious Electrocatalysts for Electrochemical Water Splitting; Current status and future prospects

IT-44; Dr. Pramod Bhatt, Solid State Physics Division, Bhabha Atomic Research Centre, Mumbai

Multifunctional Prussian Blue Analogues Molecular Magnets for Energy Storage Applications

IT-04; Dr. Shailendra K. Jha, CSIR -National Metallurgical Laboratory, Jamshedpur

Electrochemically Shape-controlled and Confined Micro and Nanostructured Materials for Methanol Electrooxidation

17:30-18:50 hrs

Session 10: Oral Presentations (5+2minutes)

Chairperson:

Dr. Amrit Prakash, RMD, BARC

Dr. D. Mandal, AMMD, BARC

Auditorium A

Oral presentations

CP 3,5,6,8,14,16,17,19,20,23 & 24

Chairperson:

Dr. Sulekha Mukhopadhyaya, ChED, BARC

Shri Kalyan Bhanja, HWD, BARC

Auditorium B

Oral Presentations

CP 29,31,34,43,46,48,51,57,60,64,67

18:50 hrs

:

Tea at *Lobby*

20:00 21:00 hrs

:

Dinner at Anushaktinagar

February 10, 2023; Friday

09:30 – 11:15 hrs

:

Session 11; (Auditorium A)

Chairperson: Prof. J. Chattopadhyay, RSD, BARC

09:30 – 10:15 hrs

:

IT-26; Prof. Stijn F. L. Mertens, Department of Chemistry, Lancaster University, United Kingdom

Electrochemistry beyond Redox Processes: from Collective to Single Molecule Switching

Invited Lecture (25+5 minutes)

10:15-10:45 hrs

IT-62; Prof. Suddhasatwa Basu, IIT Delhi

Electro and photo-electro conversion of Furfural to Various Platform Chemicals

10:45–11:15 hrs

:

*IT-40; Prof. S. K. Ghosh, Materials Processing & Corrosion Engineering Division
Bhabha Atomic Research Centre, Trombay, Mumbai*

Electrochemical Investigation of Uranyl Species in Ethaline-DES and Possibility of UO₂ Deposition

11:15 – 11:30 hrs

:

Tea at *Lobby*

11:30 – 13:00 hrs

:

Session 12: (Auditorium A)

Chairperson: Prof. S. Kannan, RC&IG, BARC

Invited Lecture (20+2 minutes)

IT-18; Prof. Bharatkumar Suthar, Indian Institute of Technology Bombay

Electrochemical impedance of porous electrodes for battery applications

IT-56; Prof. S. N. Sawant, Chemistry Division, Bhabha Atomic Research Centre, Trombay-Mumbai

Electrochemical Biosensors for Cancer Biomarker Detection

IT-50: Prof. Abhijit Chatterjee, Department of Chemical Engineering, Indian Institute of Technology Bombay, Mumbai

Tackling complexity in electrocatalysis: A modeling framework to capture structure and complexity at the solid-liquid interface

IT-20: Prof. Arnab Dutta, Chemistry Department, Indian Institute of Technology, Bombay

Designing artificial H₂ producing cobalt catalysts with neurotransmitter and vitamin

13:00 – 14:00 hrs : Lunch at dining hall, DAE Convention Centre

14:00 – 16:00 hrs : Session 13

Chairperson:

Dr. T. Das, RPhD, BARC

Dr. K. K. Swain, ACD, BARC

Poster Presentations: P-153 to P-215 at Poster Hall (Except CPs selected for oral presentation)

Tea during 15:30-16:00

16:00 – 17:10 hrs : Session 14; Invited Lecture (20+2 minutes)

Auditorium A

Chairperson: Prof. Awadhesh Kumar, RPCD, BARC

IT-30; Prof. S Pande, Department of Chemistry, Birla Institute of Technology and Science, Pilani, Rajasthan

Effect of Cation Doping on Ni-based System for Overall Water-Splitting Reaction

IT-32; Prof. Mrinmoyee Basu, Department of Chemistry, BITS Pilani, Pilani Campus, Rajasthan

Carbon-based Dots as Efficient Sensitizer in Photoelectrochemical Water Splitting Reactions

IT- 31 : Prof. Kathiresan M, Electro Organic and Materials Electrochemistry Division, CSIR-Central Electrochemical Research Institute

Porous Organic Polymer and its Composites for Electrocatalysis

Auditorium B

Chairperson: Prof. Ashok Arya, G&AMD, BRAC

IT-34; Prof. S. B. Arya, National Institute of Technology Karnataka Surathkal

A critical issue of piping failure: Flow accelerated corrosion and erosion corrosion

IT-27; Prof. S. Senthil Kumar, CSIR-Central Electrochemical Research Institute (CSIR-CECRI), Karaikudi

Electrochemiluminescence based imaging for visualizing sebaceous fingerprint

IT-06; Prof. Venkataraman Dharuman, Department of Bioelectronics and Biosensors, Science campus, Alagappa University

Nanoparticles functionalized theranostic liposome for antibiotic resistant bacteria and electrochemical sensing

17:10-18:50 hrs

Session15: Oral Presentations (5+2minutes)

Chairperson:

Prof. H.N. Ghosh, RPCD, BARC

Prof. T. Bandyopadhyay, ChD, BARC

Auditorium A

Oral presentations

CP 72,77,84,88,92,102,105,110,113,115,118,119, 126, IT-33

Chairperson:

Auditorium B

Prof. D. K. Maity, HBNI

Shri Ajoy Singh, UED, BARC

Oral Presentations

CP 121, 133,136,164,173,178,187,205,209

Presentation by sponsors

18:50- 19:00 hrs

:

Tea

Evening Lecture

Chairperson: Shri Vivek Bhasin, NFG & RDDG, BARC

19:00-19:45 hrs

:

Prof. A. K. Tyagi, Director, Chemistry Group, BARC

Four golden years in Science: Shaping the modern world

20:00 21:00 hrs

:

Dinner at Anushaktinagar

February 11, 2023; Saturday

09:00 - 11:15 hrs

:

Session 16 (Auditorium A)

Chairperson: Prof. P.K. Mohapatra, RCD, BARC

Plenary Lecture (40+5 minutes)

09:00 - 10:15 hrs

:

IT-12; Prof. Ana Maria Oliveira-Brett, Department of Chemistry, CEMMPRE, Faculty of Sciences and Technology, University of Coimbra, Portugal

Bioelectrochemical Sensing of Biomolecules Oxidative Damage

Invited Lecture (20+2) minutes)

IT-54; Prof. Rajesh Ganesan, Materials Chemistry Division

Materials Chemistry and Metal Fuel Cycle Group, IGCAR

Applications of Electrochemical Sensors for Sodium Systems

IT-15: Prof. A. K. Satpati, Analytical Chemistry Division, Bhabha Atomic Research Centre, Mumbai

Characterisation of Semiconductor Photoelectrode Interfaces using Electrochemical/Spectroelectrochemical Investigations

IT-19: Prof. Amit Sinha, Powder Metallurgy Division, Materials Group, Bhabha Atomic Research Centre

Development of composite electrolyte and electrode materials for IT-SOFC

11:20– 11:30 hrs : Tea at Lobby

11:30 – 12:45 hrs : Session 17 (Auditorium A)

Chairperson: Prof. R. Tewari, MG, BARC

Invited Lecture (20+2 minutes)

IT-60: Prof. Balaji P. Mondal, Chemistry Division, Bhabha Atomic Research Centre, Mumbai

Lithium and sodium storage capacity of Mo₂C based composite

IT-42: Dr. V Nafees Ahmed, Chemical Technology Division, Bhabha Atomic Research Centre, Mumbai

Technology demonstration for Hydrogen production by Iodine Sulfur thermochemical process

IT-39: Prof. Pranjal Chandra, School of Biochemical Engineering, Indian Institute of Technology (BHU), Varanasi

Nanoengineered Electrochemical Sensors for Tracking Biomarkers In Miniaturized Settings

IT-61: Dr. Jyoti Prakash, Glass and Advanced Materials Division, Materials Group, Bhabha Atomic Research Centre, Mumbai

CNT aerogel electrochemical bio-sensor: A new era in ultra sensitive biomedical technology

12:45– 13:45 hrs : Lunch at dining hall, DAE Convention Centre

14:00 – 15:50 hrs : Session 18 (Auditorium A)

Chairperson: Prof. Y. K. Bhardwaj, RTDD, BARC

Invited Lecture (20+2 minutes)

IT-43: Prof. Dimple Dutta, Chemistry Division, Bhabha Atomic Research Centre, Mumbai

Design of Electrode Materials for Advanced Sodium-Ion Batteries

IT-48: Prof. Sunita Kumbhat, NanoBiosensor Laboratory, Jai Narain Vyas University, Jodhpur

Real time monitoring system for aflatoxins in real samples

IT-59; Dr. S. P. Koiry, Technical Physics Division, Bhabha Atomic Research Centre, Trombay-Mumbai

Electrochemical methods: Indispensable for the fabrication and characterization of organic solar cells

IT-25: Prof. Gunda Mohanakrishna, School of Advanced Sciences, KLE Technological University, Hubballi

Bioelectrochemical systems (BES) as a sustainable approach for water and wastewater treatment along with renewable energy generation

15:50- 16:00 hrs : **Tea**

16:00 - 17:30 hrs : **Valedictory Function at Auditorium A**

20:00 hrs Onwards : **Dinner at TSH, Anushaktinagar (only on prior intimation)**

Content		
Serial No.	Title and Authors	Page
1	Fabrication of an Electrochemical Sensor Based on Reduced Graphene Oxide Modified Glassy Carbon Electrode for an Antidiabetic Drug Repaglinide and its Analytical Application <i>Suma K. Pawar and J. Seetharamappa*</i>	26-42
2	Theranostic Applications of Carbon Nanomaterial Modified Sensors: A Promising Future <i>Nikita Agrawal, Rutesh Savalia and Sanghamitra Chatterjee*</i>	43-69
3	Electrochemical sensor applications based on biomass-derived carbon nanomaterials <i>Shweta J. Malode, Mahesh M. Shanbhag, Nagaraj P. Shetti*</i>	70-93
4	Bioelectrochemical Systems: A Versatile Process for Value Addition and Environmental Abatement <i>Gunda Mohanakrishna</i>	94-103
5	Metal/Metal oxide based Hybrid Electrocatalytic Systems for Enhanced Hydrogenation of CO₂ to Formate <i>Balaji B. Mulik*, Ajay V. Munde, and Bhaskar R. Sathe*</i>	104-123
6	Designing of photoelectrochemical device towards practical solar water splitting : A review on recent progress of BiVO₄ photoanodes <i>Ms. Sangeeta Ghosh, Mr. Aditya Poddar, Mr. Himanshu Sekhar Sahoo, Mr. Swarnendu Baduri, Mr. Debasish Ray, and Dr. Chinmoy Bhattacharya*</i>	124-148

Fabrication of an Electrochemical Sensor Based on Reduced Graphene Oxide Modified Glassy Carbon Electrode for an Antidiabetic Drug Repaglinide and its Analytical Application

*Suma K. Pawar and J. Seetharamappa**

Department of Chemistry, Karnatak University, Dharwad-580 003

**Email: drjseetharamappa@kud.ac.in*

Abstract

Repaglinide (RPG) is widely used in the treatment of non-insulin-dependent diabetes mellitus. A sensitive and versatile electrochemical method was developed for the determination of RPG employing electrochemically reduced graphene oxide modified glassy carbon electrode (ErGO/GCE). Graphene oxide suspension was drop casted on a glassy carbon electrode (GCE) and subjected to an electrochemical reduction in the potential range of -0.6 - 1.7 V. Both GO and ErGO were characterized by SEM, AFM, XRD and electrochemical techniques. RPG exhibited two irreversible oxidation peaks at 1.01 and 1.21 V on ErGO/GCE and at 0.94 and 1.14 V on bare GCE. Significant enhancement in the electrochemical response of RPG (3-fold) was observed at ErGO/GCE due to the higher electron transfer ability of reduced GO network on modified GCE. Effects of various parameters such as pH of the supporting electrolyte (Britton-Robinson buffer), accumulation time and amount of suspension were investigated on the electrochemical behavior of RPG. Scan rate studies revealed the electrode process to be diffusion controlled. The fabricated sensor (ErGO/GCE) for RPG exhibited the linear relationship between the peak current and concentration in the range of 0.5 - 66.7 μM and 0.1 - 48.5 μM for differential pulse voltammetric and square wave voltammetric methods, respectively. The applicability of the proposed method was examined by analyzing the commercially available tablets. Higher recovery (99.86 %) and low RSD values (0.3 %) indicated the accuracy and reproducibility of the proposed method. Further, the fabricated sensor was used to investigate the mechanism of interaction between RPG and bovine serum albumin (BSA). The binding constant of RPG-BSA and the ratio between these two were found to be $(2.6 \pm 0.04) \times 10^4 \text{ M}^{-1}$ and 1:1, respectively.

1. Introduction

Electrochemical techniques are powerful and versatile analytical tools that have found vast applications in the field of medicine, biotechnology, material science, food safety, energy storage, etc [1,2]. The massive attention gained by electrochemical methods over other techniques is mainly due to their eco-friendly nature, excellent sensitivity with large linear dynamic range, rapid analysis times and simultaneous determination of several analytes [3]. Among the electroanalytical techniques, the voltammetric method is frequently used in determining an analyte. Voltammetry is an example of a controlled-potential method with a three-electrode system where the potential is applied to the electrode-solution interface and the current that results from the oxidation/ reduction/ redox process of an analyte at an electrode surface is measured [4]. The sensitivity and selectivity of the voltammetric technique can be enhanced by modifying the working electrode with a variety of materials by adsorption, covalent bonding, coating and attaching the specific molecules to the electrode surface.

Graphene is an ideal material for electrochemistry because of its unique physicochemical properties such as high surface area, excellent thermal conductivity, electric conductivity and strong mechanical strength [5]. Because of these properties, graphene is considered an attractive candidate for tremendous applications including electronic devices, energy conversion, storage devices, sensors and biosensors [6]. The structure of graphene is characterized as the array of two-dimensional sheets of carbon atoms bonded by sp^2 bonds in a hexagonal lattice. These bonds and electronic configuration account for the astonishing properties of graphene [7]. Various techniques have been developed for the synthesis of graphene. Among these, the electrochemical reduction of graphene oxide to graphene has received great attention due to its fast and green nature [8]. In view of this, we have adopted a green method for the reduction of graphene oxide and developed an electrochemical sensor for an anti-diabetic drug, repaglinide (RPG).

Repaglinide (RPG), chemically known as 2-Ethoxy-4-(2-((3-methyl-1-(2-(1-piperidinyl)phenyl)butyl)amino)-2-oxoethyl)benzoic acid is a new carboxy methyl benzoic acid derivative. It belongs to a class of meglitinides and is used to treat diabetes type 2 (non-insulin-dependent diabetes mellitus). Diabetes mellitus is a chronic metabolic disorder characterized by a high blood glucose concentration. Impaired insulin secretion, resistance to tissue actions of insulin, or a combination of both are considered to be the cause of hyperglycemia. RPG is the first of a new class of oral antidiabetic drugs designed to regulate

postprandial glucose excursions in type 2 diabetic patients. Although RPG shows some chemical resemblance to other antidiabetic agents, it differs in its mechanism of action and excretion mechanism [9]. RPG lowers blood glucose levels by blocking ATP-dependent potassium channels in pancreatic β cells, which in turn stimulates insulin secretion [10]. Since, the administered RPG gets excreted through biliary excretion, it is considered to be an advantage for type 2 diabetic patients with impaired kidney function [11].

Literature survey revealed that analytical methods including HPLC [12], RP-HPLC [13,14], HPTLC [15], RPTLC [16], LC-MS/MS [11], spectrophotometric [17] and spectrofluorimetric [18] have been developed for the determination of RPG in pharmaceutical formulations and biological samples. El-Ries MAN *et al.*, have reported the electrochemical behavior of RPG at carbon paste and GCE [19]. The reported conventional methods require a long time and are expensive while the reported voltammetric method suffers from a shorter linearity range. In view of the vast applications of graphene-modified electrodes as electrochemical sensors, we have fabricated an electrochemical sensor based on electro-reduced graphene oxide (ErGO) film on GCE for the determination of RPG in pharmaceutical formulations and biological samples in the present study.

2. Materials and methods

2.1 Materials

A pure sample of RPG was obtained as a gift sample from Dr. Reddy's lab. Pvt. Ltd., India. A stock solution of 1 mM RPG was prepared in Millipore water. Britton-Robinson buffer (B.R.) was used as a supporting electrolyte. Working solutions of RPG were prepared daily by diluting the stock solution as required with B.R. buffer.

2.2 Materials and instrumental methods

Electrochemical investigations were carried out on a CHI-1110a Electrochemical Analyzer (CH Instruments Ltd. Co., USA, version 12.23). The system was constructed with three electrodes *viz.*, a working electrode (ErGO/GCE), an auxiliary electrode (platinum wire) and a reference electrode (Ag/AgCl).

XRD patterns of pristine graphite, graphite oxide and reduced graphene oxide were studied on an X-ray diffraction spectrometer, Philips X'Pert (Cu $K\alpha$, 1.5406 Å). FTIR and Raman spectra were recorded on an NXR-FT-Raman spectrometer, Nicolet, USA and Nicolet 6700, Nicolet USA, respectively. By using Carl Zeiss, Ultra 55 field emission scanning electron microscope

(FESEM) SEM images of graphite, graphite oxide and reduced graphene oxide were obtained. Atomic force microscopy (AFM) images were recorded on a Flex AFM system, in Switzerland.

2.3 Synthesis of graphene oxide

GO was synthesized from graphite powder by modified Hummer's method [20]. The resulting dark-yellow solid was then dried in an oven at 120 °C. The GO suspension was prepared by dispersing 10 mg of GO in 10 mL of water using ultrasonic agitation (1 h). The yellowish-brown suspension obtained was centrifuged to remove the unexfoliated GO [21]. This stable suspension was used to modify the GCE (**Figure 1**).

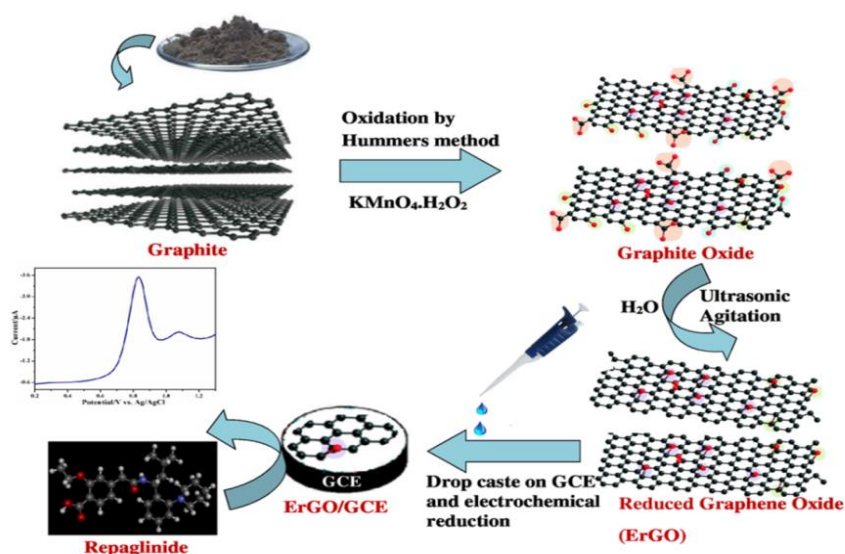


Figure 1. Schematic representation of fabrication of ErGO/GCE.

2.4 Fabrication of an electrochemical sensor GO/GCE and ErGO/GCE

Prior to modification, GCE was carefully polished with 0.5 μm alumina slurry on a wet polishing cloth and then rinsed thoroughly with Millipore water. 6 μL of yellowish-brown suspension of GO suspension was drop casted on the surface of GCE and dried under an IR lamp in order to obtain GO/GCE. Later, GO/GCE was subjected to an electrochemical reduction in phosphate buffer of pH 6 by employing the voltammetric sweep segments in the potential range of 0.6 to - 1.7 V which resulted in ErGO/GCE.

2.5 Analysis of Eureka tablets

Five Eurepa tablets containing RPG were crushed in a mortar. A portion of the powder equivalent to 1 mM RPG was diluted with methanol. For complete dissolution and homogenization, the stock solution was ultrasonicated for 15 min. Under optimized conditions, differential pulse voltammograms were recorded. The accuracy of the proposed method was examined by performing recovery studies. The content of RPG in the Eurepa tablet was determined from the regression equation obtained from the calibration graph.

2.6 Determination of RPG in spiked human urine samples

RPG fortified urine sample (1 mM) was prepared by treating 1 mL untreated urine of a healthy individual with 1 mL standard RPG solution (2 mM). A suitable aliquot of spiked urine sample was diluted with B.R. buffer without any pre-treatment. Under optimized conditions, differential pulse voltammograms were recorded and the amounts of RPG in spiked human urine samples were calculated using the calibration graph.

3. Results and discussion

3.1 Characterization of synthesized GO and ErGO

FTIR spectra

FTIR spectra of GO and ErGO are depicted in **Figure 2**. FTIR spectrum of GO exhibited characteristic bands at 3410 cm^{-1} (O-H stretching vibrations), 1589 cm^{-1} (C=C stretching) and 1098 cm^{-1} (C-O-C stretching). Upon electrochemical reduction of GO, the intensity of all the bands was found to be decreased.

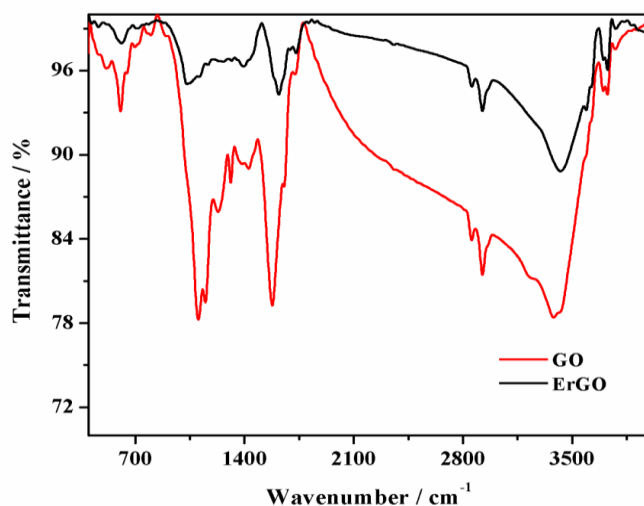


Figure 2. FTIR spectra of GO and ErGO.

Scanning electron microscopy (SEM)

The surface morphologies of graphene derivatives such as GO and ErGO films were characterized and the corresponding SEM images are shown in **Figure 3A** and **Figure 3B**, respectively. SEM micrographs demonstrated that the prepared GO material was composed of many cavities, stacked and crumpled flakes closely associated with each other. Upon electrochemical reduction of GO, the ErGO film showed a larger wrinkled and rougher surface. Such a rougher surface enhanced the incursion and diffusion of electrolyte ions. The electrochemical reduction of GO exposed more electrochemically active sites.

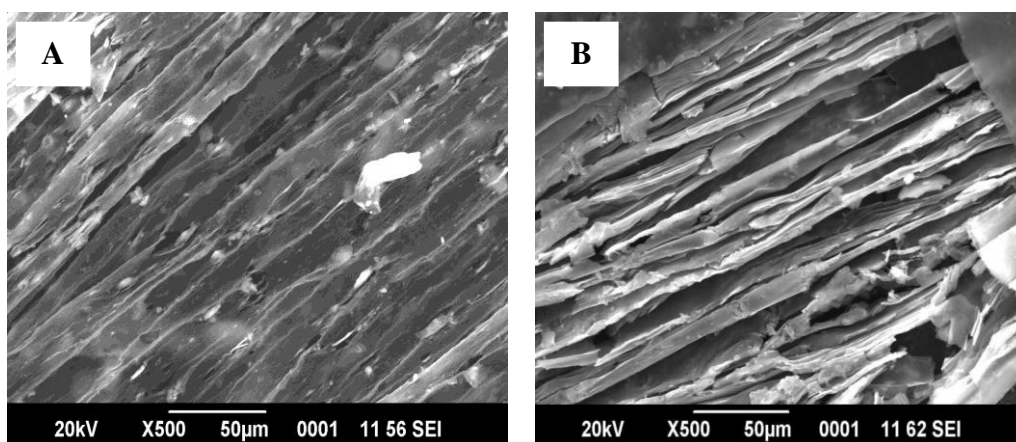


Figure 3.
FESEM

micrograph of exfoliated GO (A) and ErGO (B).

Atomic force microscopy (AFM)

In order to investigate the morphology, the thickness of the film and topography AFM studies were carried out. AFM images of GO and ErGO are displayed in **Figure 4A** and **Figure 4B**, respectively. It is evident from **Figure 4A** that GO is made up of many sheets-like structures closely associated with each other forming a disordered solid (thickness ~ 15.2 nm). Upon electrochemical reduction, the thickness was increased to ~ 28 nm indicating the formation of rough and edge planes on the surface of ErGO that are responsible for the higher surface area of the proposed electrode.

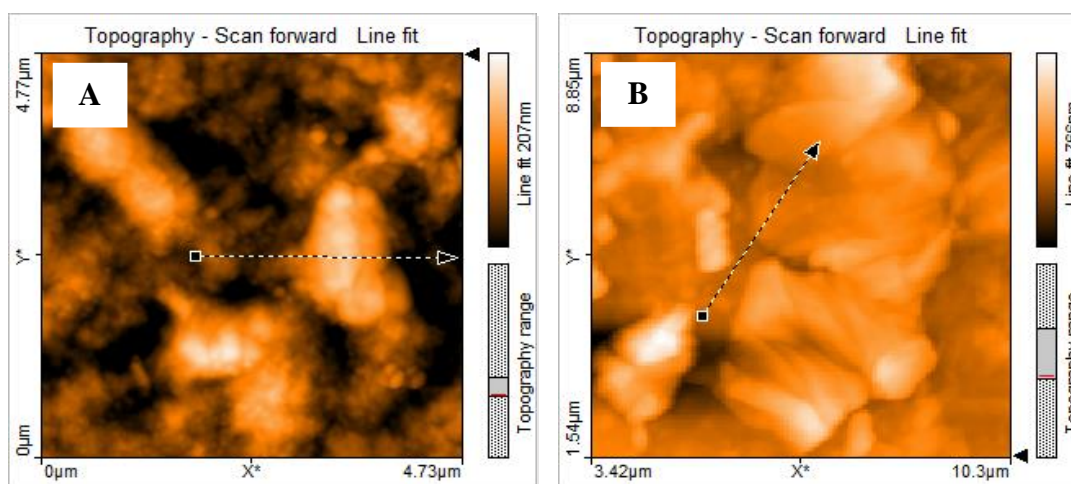


Figure 4. Atomic force micrograph of GO (A) and ErGO (B).

Powder X-ray diffraction measurements

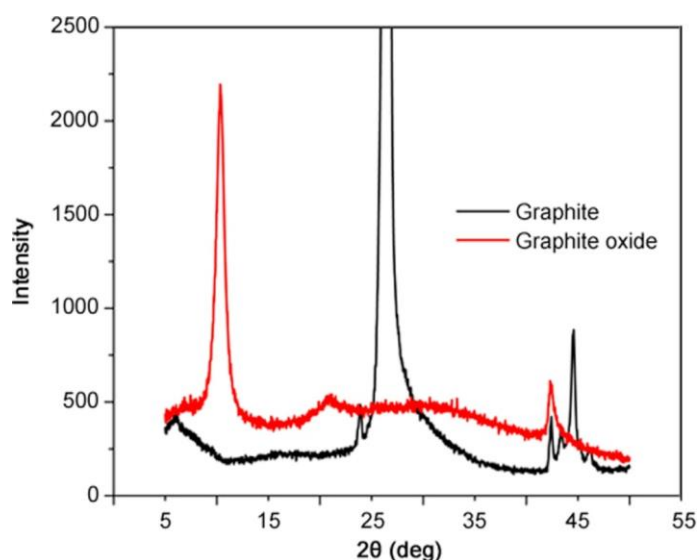


Figure 5. X-ray diffraction patterns of graphite oxide and pristine graphite.

XRD patterns of pristine graphite and GO are shown in **Figure 5**. For pristine graphite, an intense crystalline diffraction peak was observed at $\sim 26.48^\circ$. The successful oxidation of graphite to GO was evident by the disappearance of the peak at $\sim 26.48^\circ$ and the appearance of a new peak at 10.3° . During the oxidation of graphite to GO, oxygen-containing functional groups and water molecules were intercalated in between the graphene layers [22] and thus resulted in a subsequent increase in d -spacing from 3.36 to 8.55 Å.

3.2 Electrochemical characterization of ErGO/GCE

The fabricated electrode was electrochemically characterized by recording cyclic voltammograms using $K_3[Fe(CN)_6]$ as a redox probe. Cyclic voltammograms of 1 mM $K_3[Fe(CN)_6]$ at bare GCE and ErGO/GCE in 0.1 M KCl were recorded and the corresponding voltammograms are shown in **Figure 6**.

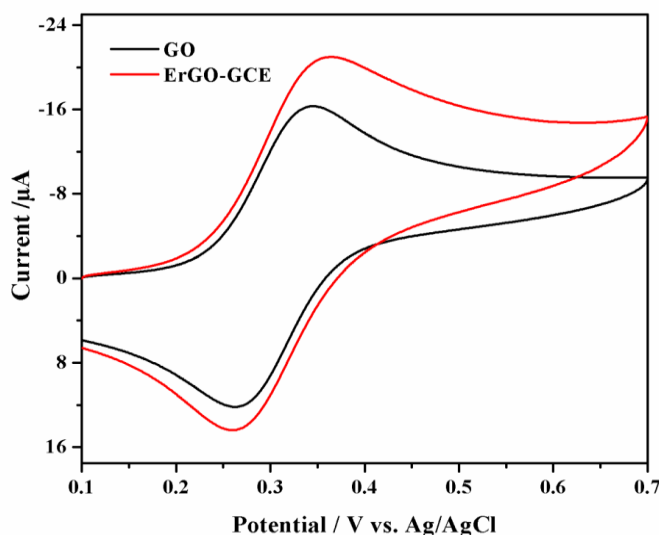


Figure 6. Cyclic voltammograms of 1mM potassium ferricyanide at bare GCE and ErGO/GCE.

A pair of well-defined redox peaks were observed that corresponds to the electron transfer of Fe^{II}/Fe^{III} couple at bare GCE. The highest redox peak current was observed at ErGO/GCE compared to that at bare GCE. The increased peak current at ErGO/GCE indicated that upon reduction the surface area and electronic conductivity of graphene increased and so accelerated the electron transfer kinetics of ferricyanide. The electroactive surface area of bare GCE and ErGO/GCE was calculated using the Randles-Sevcik equation shown below [23]:

$$I_p = 2.69 \times 10^5 n^3 / 2 A C_0 D_R^{1/2} v^{1/2} \dots\dots\dots (1)$$

where I_p denotes the peak current, n is the number of electrons transferred, A is the surface area of the electrode, D_R is the diffusion coefficient, C_0 is the concentration of $K_3[Fe(CN)_6]$ and v

is the scan rate. For 1 mM $K_3[Fe(CN)_6]$ in 0.1 M KCl electrolyte, $n = 1$ and $D_R = 7.6 \times 10^{-6} \text{ cm}^2 \text{ s}^{-1}$. From the slope of the plot of I_p versus $v^{1/2}$, the electrochemically active surface area of ErGO/GCE and bare GCE was calculated to be 0.61 and 0.05 cm^2 respectively. The larger surface area of ErGO/GCE facilitated the electron transfer rate.

3.3 Electrochemical behavior of RPG at ErGO/GCE

Cyclic voltammograms of 20 μM RPG at bare GCE and ErGO/GCE in B.R. buffer of pH 5 are shown in **Figure 7**. RPG exhibited an oxidation peak at 0.95 V on bare GCE in the forward scan and no peak was observed in the reverse scan, suggesting the irreversible nature of the electrode reaction. The peak current of this peak was enhanced significantly (3-fold) at ErGO/GCE compared to that at the bare electrode, signifying that the ErGO enhanced the electro-oxidation of RPG due to increased electroactive surface area.

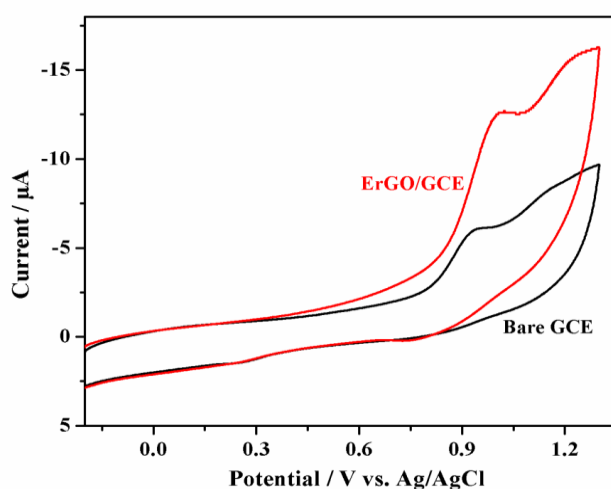


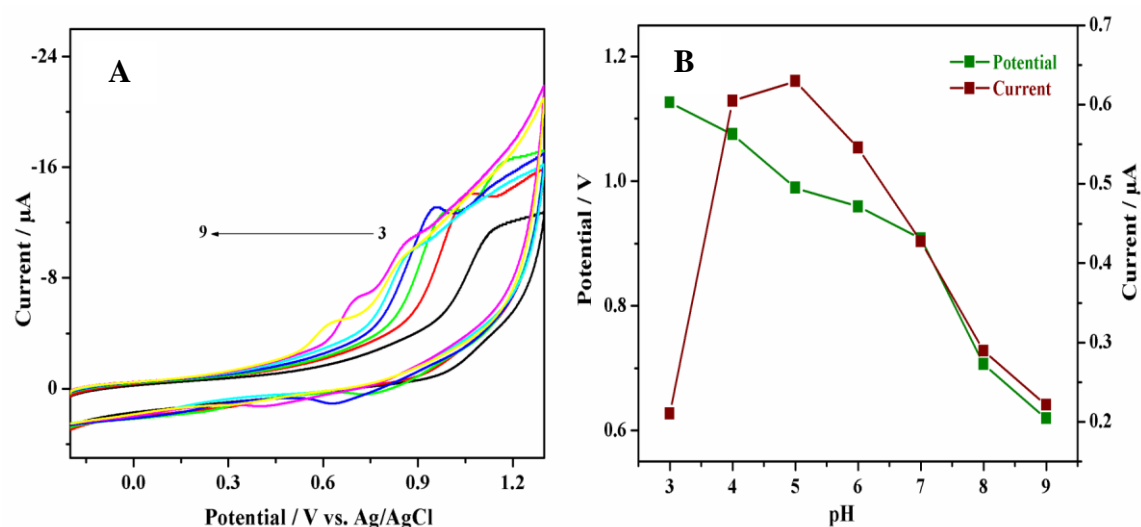
Figure 7. Cyclic voltammograms of 20 μM RPG at bare GCE and ErGO/GCE in B.R. buffer of pH 5.

3.4 Effect of electrolyte pH on electrooxidation of RPG

To characterize the electrochemical properties *viz.*, a number of protons and electrons involved in the electrode process, the effect of pH of supporting electrolyte on the electrochemical response of RPG at ErGO/GCE was investigated. Cyclic voltammograms of RPG (20 μM) in B.R. buffer solution of different pH (3-9) are shown in **Figure 8A**. The peak current of RPG increased gradually in the pH range of 3-5. At pH 6, the peak current decreased with a shift in the peak potential and thereafter the oxidation peak of RPG was noticed to be diminished up to pH 9. A sharper and well-defined peak was noticed in B.R. buffer at pH 5, so pH 5 was maintained throughout the experiment. A negative shift in the peak potential was observed with

an increase in pH, indicating the participation of protons in the electrode process. The plot of E_p versus pH (**Figure 8B**) revealed the linearity in the pH range of 3-9 and the corresponding regression equation is $E_{pa} \text{ (V)} = -0.055 \text{ pH} + 1.345$; $R^2 = 0.988$. The slope obtained (55 mV) was close to the theoretical value of 59 mV pH^{-1} signifying the involvement of an equal number of electrons and protons in the electrode process of RPG [24].

Figure 8. Cyclic voltammograms of $20 \mu\text{M}$ RPG at ErGO/GCE in B.R. buffer of different pH from 3 to 9 (A) and dependence of peak potential and peak current on pH of the solution (B).



3.5 Effect of accumulation time

To study the effect of accumulation time on the electrochemical oxidation of RPG, cyclic voltammograms of RPG were recorded in B.R. of pH 5.0 by varying accumulation time from 0 to 210 s. The peak current of RPG increased gradually with accumulation time from 0 to 150 s, revealing that the surface concentration of RPG increased at ErGO/GCE. Beyond 150 s, a considerable decrease in the peak current was noticed. The decreased peak current was attributed to the surface saturation. Therefore, an accumulation time of 150 s was maintained for further studies.

3.6 Influence of scan rate

Studying the relationship between scan rate and peak current helps in ascertaining the electrochemical mechanism. So, cyclic voltammograms of RPG at different scan rates (10-400 mV s^{-1}) were recorded in B.R buffer (pH 5). As evident from **Figure 9A** and **Figure 9B**, the oxidation peak current of RPG increased with an increase in scan rate with a positive shift in the peak potential. This suggested that the electrode reaction of RPG at ErGO/GCE was diffusion controlled. This was further confirmed by the value of slope (0.5) of $\log I_p$ versus $\log v$ plot (**Figure 9C**) expected for an ideal reaction condition for a diffusion-controlled electrode process [24].

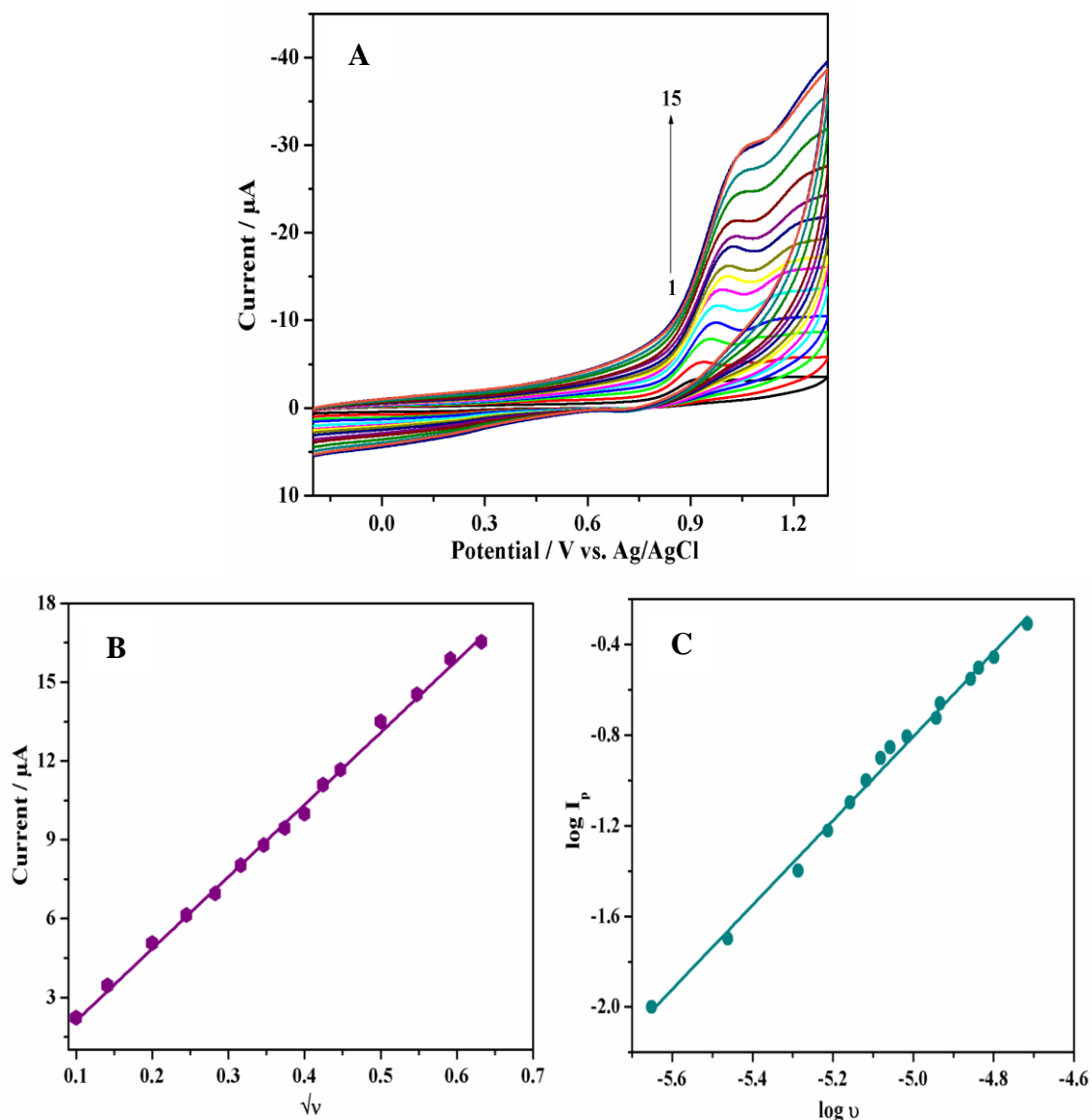
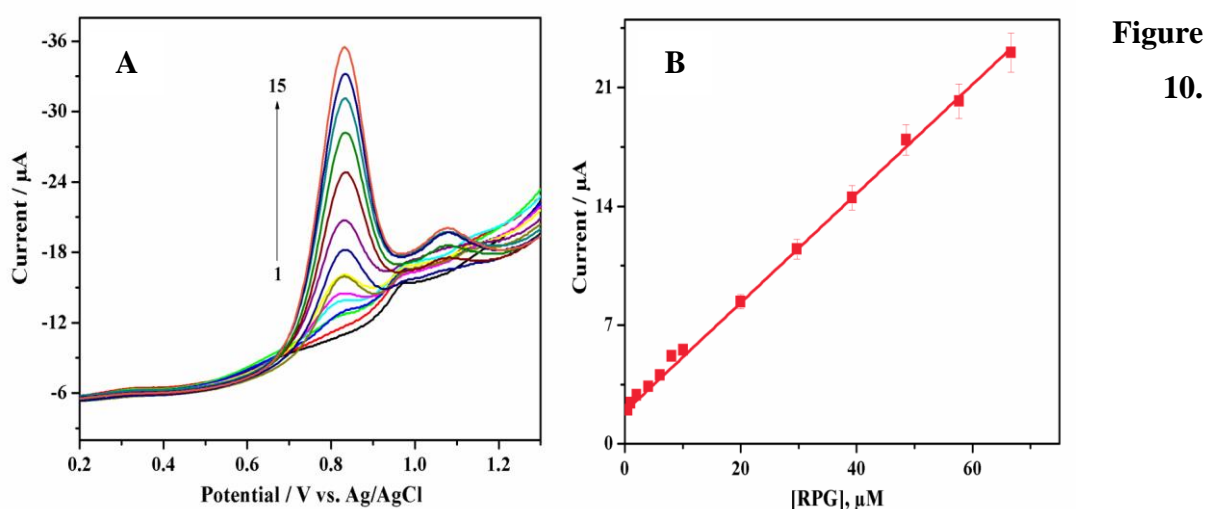


Figure 9. Cyclic voltammograms of 20 μM RPG at ErGO/GCE in B.R. buffer of pH 5 at different scan rates from 10 to 400 mV s^{-1} (A), linear dependence of oxidation peak current of RPG on the square root of scan rate (B) and log-log plot for RPG (C)

3.7 Analytical applications

3.7.1 Calibration curve

Under optimized conditions, the electroanalytical performance of the modified sensor (ErGO/GCE) was examined by differential pulse voltammetric (DPV) and square wave voltammetric (SWV) methods. DPV and SWV responses of different concentrations of RPG at ErGO/GCE are shown in **Figure 10A** and **Figure 11A**, respectively. A linear relationship between the peak current and concentration of RPG in the range of 0.5 -66.7 and 0.1 - 48.5 μM for DPV and SWV methods was noticed respectively, and the same is represented in **Figure 10B** and **Figure 11B**, respectively.



Differential pulse voltammograms for increasing concentrations RPG at ErGO/GCE in B.R. buffer of pH 5 (A) and calibration plot for RPG (B).

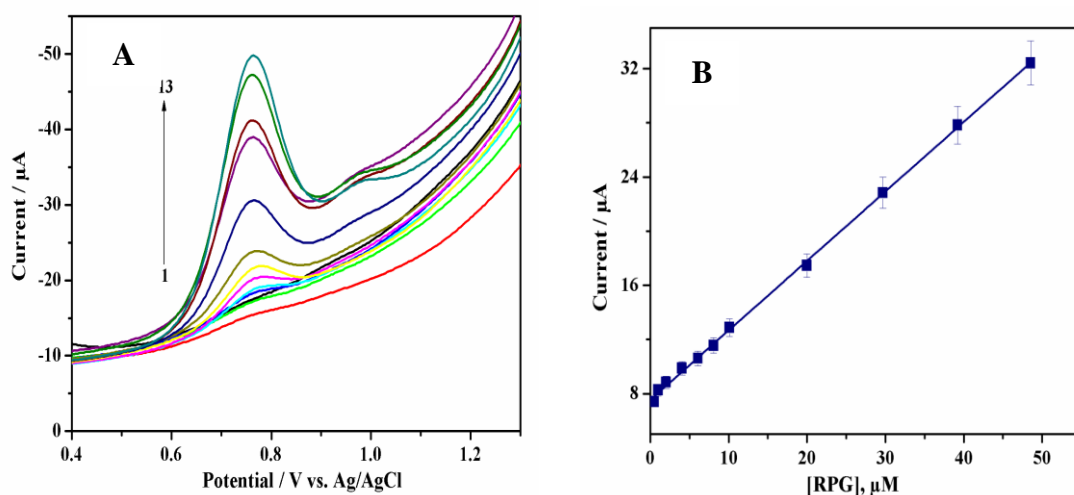


Figure 11. Square wave voltammograms for increasing concentrations RPG at ErGO/GCE in B.R. buffer of pH 5 (A) and calibration plot for RPG (B).

As evident from the figures, the oxidation peak current increased linearly with an increase in the concentration of RPG in the range of 0.5 - 66.7 μM and 0.1 - 48.5 μM for DPV and SWV, respectively. Validation of the procedure for the quantitative determination of RPG was examined by evaluating the limit of detection (LOD) and limit of quantification (LOQ) and are calculated using equations 2 and 3 given below [25];

$$\text{LOD} = 3 s/m \dots\dots\dots (2)$$

$$\text{LOQ} = 10 s/m \dots\dots\dots (3)$$

where s is the standard deviation of the peak current (6 replicates) and m is the slope of the calibration curve. The values of LOD, LOQ and RSD are tabulated in **Table 1**. Low values of LOD and LOQ highlighted the sensitivity of the proposed methods. The inter-day and an intra-day assay of the proposed methods was examined by analyzing 6 replicates of 20 μM RPG by DPV and SWV methods. Low values of RSD indicated the good precision of the methods.

Table 1. Characteristics of the calibration plot for RPG.

Parameter	DPV	SWV
Linearity range, μM	0.5-66.7	0.1-48.5
LOD, μM	0.034	0.020
LOQ, μM	0.9	0.07
Inter-day assay RSD* %	2.98	3.01
Intra-day assay RSD* %	2.87	3.12

*Average of six determination

3.7.2 Analysis of tablets

The utility of the proposed method for the determination of RPG at ErGO/GCE in pharmaceutical formulations is examined by analyzing the content of RPG in commercially available tablets (Eurepa) by DPV method and the corresponding results are summarized in **Table 2**. The reproducibility of the proposed method was evident by their low RSD values. Further, to evaluate the accuracy of the proposed method, recovery studies were performed by

the standard addition method. For this, known quantities of pure RPG were added to known amounts of pre-analyzed formulations and the mixtures were again analyzed as before. The total amount of the drug was then determined and the amount of the added drug was calculated by the difference. A higher recovery value (99.55 %) highlighted the accuracy of the proposed method.

Table 2. Results of analysis of RPG in tablets and recovery studies by DPV method.

Parameters	Eurepa ^a
Amount labeled, mg	2.0
Amount found, mg	1.97
Recovery, %	98.5
RSD ^b , %	2.5
Pure drug added to tablet solution, mg	4.52
Drug found, mg	4.50
Recovery, %	99.55
RSD ^b , %	2.52

^aMarked by Torrent Pharmaceuticals Ltd.

^bAverage of six determinations

3.7.3 Determination of RPG in spiked human urine samples

The application of the DPV method was further established by determining RPG in spiked human urine samples without any pre-treatment. The recovery tests were performed by spiking RPG-free urine with known amounts of RPG. DPVs of these samples were then recorded and a calibration graph was constructed. Later, the concentration of RPG in the urine sample was determined from the calibration graph. The results of the analysis are listed in **Table 3**.

Table 3. Results of analysis of RPG in spiked human urine samples by DPV method.

RPG added, (µM)	n	Amount found, (µM)	Average recovery, (%)	RSD, (%)
2	6	1.97	98.5	2.61
4	6	3.85	96.2	2.48

6	6	5.84	97.3	2.56
---	---	------	------	------

The average recovery was observed to be higher than 96.2 % and the RSD values were less than 3.0 %. These values indicated the accuracy and reproducibility of the results.

4. Conclusions

The present work demonstrates a simple, facile and reproducible method for the fabrication of an electrochemical sensor with reduced graphene oxide. ErGO films were successfully deposited on the surface of GCE by one-step electrochemical reduction and the modified GCE exhibited excellent electrochemical response for the redox of RPG. The fabricated electrode material was characterized by SEM, AFM, XRD and electrochemical techniques. The fabricated ErGO/GCE exhibited excellent electrochemical response towards the oxidation of RPG because of excellent electrical conductivity, strong adsorptive ability and large effective surface area of ErGO/GCE. The proposed sensor exhibited a wide linearity range of 0.5 to 66.7 μM (DPV) and 0.1 to 48.5 μM (SWV) with excellent reproducibility and repeatability. Further, the modified ErGO/GCE was applied for the determination of RPG in pure and spiked human urine samples. Low values of LOD highlighted the accuracy of the proposed methods for the determination of RPG.

References

1. Siddiqui MR, Allothman ZA, Rahman N, Analytical techniques in pharmaceutical analysis: A review, *Arabian Journal of chemistry*, 10 (2017) S1409-21.
2. Uslu B, Ozkan SA, Electroanalytical methods for the determination of pharmaceuticals: a review of recent trends and developments, *Analytical letters*, 44 (2011) 2644-702.
3. Xu Q, Yuan AJ, Zhang R, Bian X, Chen D, Hu X, Application of electrochemical methods for pharmaceutical and drug analysis, *Current Pharmaceutical Analysis*, 5 (2009) 144-55.
4. Smyth WF, Woolfson AD, Drug assays—the role of modern voltammetric techniques, *Journal of clinical pharmacy and therapeutics*, 12 (1987) 117-33.
5. Shao Y, Wang J, Wu H, Liu J, Aksay IA, Lin Y, Graphene based electrochemical sensors and biosensors: a review, *Electroanalysis: An International Journal Devoted to Fundamental and Practical Aspects of Electroanalysis*, 22 (2010) 1027-36.

6. Yang X, Yu X, Heng Y, Wang F, Facile fabrication of 3D graphene–multi walled carbon nanotubes network and its use as a platform for natamycin detection, *Journal of Electroanalytical Chemistry*, 816 (2018) 54-61.
7. Geim AK, Novoselov KS, The rise of graphene, *Nature materials*, 6 (2007) 183-91.
8. Shao Y, Wang J, Engelhard M, Wang C, Lin Y, Facile and controllable electrochemical reduction of graphene oxide and its applications, *Journal of Materials Chemistry*, 20 (2010) 743-8.
9. El-Ries MA, Mohamed GG, Attia AK, Electrochemical determination of the antidiabetic drug repaglinide, *Yakugaku Zasshi*, 128 (2008) 171-7.
10. Whirl-Carrillo M, McDonagh EM, Hebert JM, Gong L, Sangkuhl K, Thorn CF, Altman RB, Klein TE, Pharmacogenomics knowledge for personalized medicine. *Clinical Pharmacology & Therapeutics*, 92 (2012) 414-7.
11. Zhang J, Gao F, Guan X, Sun YT, Gu JK, Fawcett JP, Determination of repaglinide in human plasma by high-performance liquid chromatography–tandem mass spectrometry, *Acta Pharmaceutica Sinica B*, 1 (2011) 40-5.
12. Venkatesh P, Harisudhan T, Choudhury H, Mullangi R, Srinivas NR, Simultaneous estimation of six anti-diabetic drugs—glibenclamide, gliclazide, glipizide, pioglitazone, repaglinide and rosiglitazone: development of a novel HPLC method for use in the analysis of pharmaceutical formulations and its application to human plasma assay, *Biomedical Chromatography*, 20 (2006) 1043-8.
13. Prameela RA, Bala SC, Archana N, Siva TP, Aruna B, Determination of repaglinide in pharmaceutical formulation by HPLC, *J Applied Sci Res*, 5 (2009) 1500-4.
14. Soni LK, Narsinghani T, Jain M, Development and validation of RP-HPLC method for simultaneous estimation of metformin hydrochloride and repaglinide in tablet dosage form, *Journal of liquid chromatography & related technologies*, 35 (2012) 385-92.
15. Jiladia MA, Pandya SS, Estimation of repaglinide in bulk and tablet dosage forms by HPTLC method, *Int J Pharm Pharm Sci*, 1 (2009) 141-4.
16. Gumieniczek A, Berecka A, Hopkała H, Quantitative analysis of repaglinide in tablets by reversed-phase thin-layer chromatography with densitometric UV detection, *JPC- Journal of Planar Chromatography-Modern TLC*, 18 (2005) 155-9.
17. Cijo MX, Basavaiah K, Abdulrahman SA, Vinay KB, Spectrophotometric determination of repaglinide in tablets based on charge-transfer complexation reaction with chloranilic acid and dichloro-dicyano benzoquinone, *Chemical Industry & Chemical Engineering Quarterly*, 17 (2011) 469-76.

18. Kaushal N, Jain S, Tiwary AK, Development of spectrofluorimetric and HPLC methods for in vitro analysis of repaglinide, *Indian journal of pharmaceutical sciences*, 72 (2010) 240-244.
19. El-Ries MA, Mohamed GG, Attia AK, Electrochemical determination of the antidiabetic drug repaglinide, *Yakugaku Zasshi*, 128 (2008) 171-7.
20. Hummers Jr WS, Offeman RE, Preparation of graphitic oxide, *Journal of the american chemical society*, 80 (1958) 1339.
21. Park S, Ruoff RS, Chemical methods for the production of graphenes, *Nature nanotechnology*, 4 (2009) 217-24.
22. Hontoria-Lucas C, López-Peinado AJ, López-González JD, Rojas-Cervantes ML, Martín-Aranda RM, Study of oxygen-containing groups in a series of graphite oxides: physical and chemical characterization, *Carbon*, 33 (1995) 1585-92.
23. Bard AJ, Faulkner LR, Fundamentals and applications, *Electrochemical methods*, 2 (2001) 580-632.
24. Shah A, Diculescu VC, Qureshi R, Oliveira-Brett AM, Electrochemical behaviour of dimethyl-2-oxoglutarate on glassy carbon electrode, *Bioelectrochemistry*, 77 (2010) 145-50.
25. Noureldin HA, Abdel-Aziz AM, Mabrouk MM, Saad AH, Badr IH, Green and cost-effective voltammetric assay for spiramycin based on activated glassy carbon electrode and its applications to urine and milk samples, *RSC Advances*, 13 (2023) 844-52.

Theranostic Applications of Carbon Nanomaterial Modified Sensors: A Promising Future

Nikita Agrawal, Rutesh Savalia and Sanghamitra Chatterjee¹

Department of Chemistry, Institute of Chemical Technology, Matunga, Mumbai 400019, India

1. Introduction

The last few years have witnessed a substantial technological renaissance that boosted the development of nanomaterials which have a great impact on biosensing. The unprecedented properties of carbon nanotubes, fullerenes and graphene have catapulted carbon materials in the hotspot of biomedical research. Of particular interest is the integration of these materials into analytical systems that impact key research areas, in particular: medical diagnostics, multi-modal drug delivery, bio-imaging, environmental monitoring and biocatalytic sensing. The interface of electrochemistry and nanotechnology is a captivating playground for the elemental research and has eventually emerged as a futuristic and sustainable platform.

The globe is currently being swept in an unwavering manner by the Covid-19 pandemic and several countries have factually reported that patients ailing from heart disease, diabetes and hypertension are apparently among the major adversely affected by the coronavirus. Hypertension which can be congruously referred to as the “silent killer” should not be ignored as it is on the prowl in the present scenario. The World Health Organization has recognized hypertension as being the significant cause of cardiovascular mortality and concurrently World Hypertension League identified that there is unawareness prevailing worldwide in more than 50% of the hypertensive population. Onset of stroke, chronic kidney disease, heart failure, myocardial infarction and peripheral arterial disease are instigated by hypertension [1,2]. The prominence of hypertension treatment and the controversies surrounding treatment paradigms have progressed substantially over the period. Drugs which are currently used as antihypertensive include β -blockers, thiazide diuretics, calcium channel blockers, angiotensin II receptor antagonists and angiotensin-converting enzyme inhibitors [3]. Role of calcium antagonist is to operate calcium channels located in cell membrane through voltage to block the influx of calcium ions [4]. One of the antihypertensive calcium channel blockers which is chosen as a coronary vasodilator and improve cardiac function is nifedipine [5].

*Corresponding author. Tel.: +91-22-33611144

Email address: sk.chatterjee@ictmumbai.edu.in (S. Chatterjee)

Nifedipine being an indispensable drug therapy for hypertension acts by relaxing the muscles of heart blood vessels [6]. The drug is also prescribed as an oral tablet to treat cardiovascular disease, angina pectoris and migraine [7,8]. Despite the clinical prominence of nifedipine as a medicament, its overdose can cause manifold ailments which include nausea, vomiting, dizziness, severe constipation, pounding heartbeat, flushing and tachycardia [9,10]. Hence, there is a profound necessity for an apt technique to enumerate the levels of nifedipine in human physiology. Till date, diverse analytical approaches like high-performance liquid chromatography [11], spectrophotometry [12], liquid chromatography in conjunction with UV [13], capillary gas chromatography nitrogen gas detection [14], selected ion monitoring [15] and ultra-performance liquid chromatography–tandem mass spectrometry [16] are devised to detect nifedipine. The disadvantages pertaining to these techniques include high organic solvent usage, time consumption, requisite of skilled experts, temperature-controlled process, pre-treatment of samples and sophisticated instrumentation [17,18]. Conversely, electrochemical analysis has an edge over the conventional techniques with respect to high sensitivity, minimal solvent requirements, simple and inexpensive instrument, fast analysis time and suitable for biological environment [19-21]. Regardless of the advantages of electroanalytical techniques, fewer work has been reported on the electro-oxidation of nifedipine [22-27]. Previous studies utilized differential pulse adsorptive stripping voltammetry, differential pulse voltammetry and cyclic voltammetry (CV) for the determination of nifedipine at varied electrodes. The aforementioned detections comprised of narrow calibration range, high detection limit, low sensitivity and incompatibility with physiological pH. Consequently, there is an evident requirement to develop an electrochemical sensor for the quantifiable and qualitative detection of nifedipine in clinical samples with surpassed analytical parameters.

Fabrication of electrodes with nanomaterials have empowered electrochemists to alter the electrode reactivity and acquire sensitive and selective signals in electrochemical analysis [28-30]. Carbon nanotubes are predominantly used for the sensor modification in which functionalized multiwalled carbon nanotubes (f-MWNTs) have been perceived as an exemplary material due to its fast electron transfer ability and enhanced surface reactivity [31-33]. Due to superior chemical stability, f-MWNTs can undergo the adsorption and desorption reaction without any ensuing deterioration of the structure [34]. The MWNTs are known to contain metallic impurities which provide a facile electrochemical reaction and accelerate the rate of electron transfer [35]. Functionalization of MWNTs with carboxylic group induces remarkable variation in conductivity because of electron-donating or electron-accepting

molecules on their increased surface area [36]. The unification of nanomaterial and nanoparticle has garnered recognition in recent times [37] and zinc oxide (ZnO) is an extensively explored nanoparticle amongst the transition metals for chemical sensing [38,39]. It is endowed with remarkable chemical stability, fast electron transfer capacity, enhanced conductivity and facile preparation mechanism. ZnO nanostructures have an inordinate benefit to an electrochemical reaction because of their large surface area and ameliorated catalytic activity [40,41].

In the present investigation, a novel sensor has been developed utilizing glassy carbon electrode (GCE) fabricated with nanostructured ZnO film in amalgamation with f-MWNTs and chitosan (Chit) as a biocompatible polymer. Square wave voltammetry (SWV) being a potent analytical technique was used for the first time for sensitive detection of nifedipine at physiological pH. The developed protocol was used to selectively detect nifedipine for the first time in the procured urine and serum sample of patients suffering from hypertension and thereby going through medication. The proposed sensor manifested the lowest detection limit and the highest sensitivity for the quantification of nifedipine till date. Hence, the work delineated herein will enable the electrochemical determination of nifedipine in complex biological matrices leading to multifarious clinical applications.

2.1 Structural characterization of sensor

XRD is a vital analytical tool used for the investigation of phase structure and purity of the synthesized compound. The XRD pattern of prepared ZnO nanoparticle shows the diffraction peaks at values corresponding to 31.76, 34.42, 36.25, 47.53, 56.60, 62.86, 66.37, 67.96 and 69.09 which are indexed to (100), (002), (101), (102), (110), (103), (200), (112) and (201) crystal planes respectively. Fig. 1 depicts the XRD pattern obtained for the prepared ZnO nanoparticle which is in accordance with the JCPDS (No. 36-1451) values [42] thereby confirming the formation of ZnO nanoparticles. The surface morphology of the varied sensors was characterized by FEG-SEM images. The FEG-SEM image of f-MWNTs/ZnO/Chit/GCE (Fig. 2) clearly portrayed the uniform distribution of ZnO nanoparticles surrounded by f-MWNTs and chitosan nanocomposite, which augments the facile charge transfer.

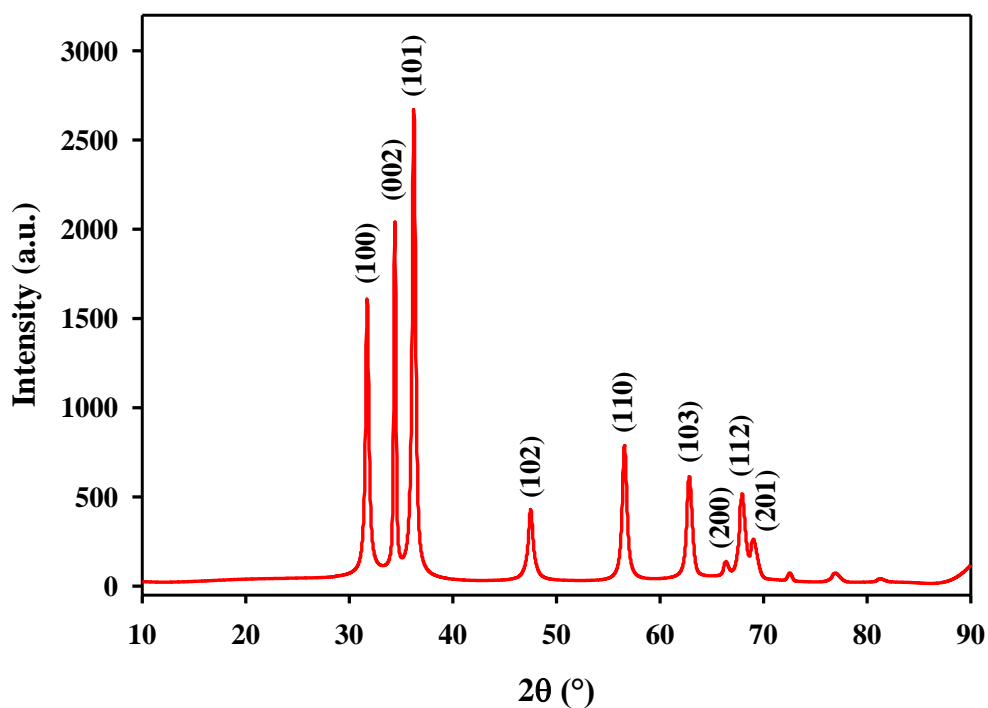


Fig. 1 XRD patterns of synthesized ZnO nanoparticles.

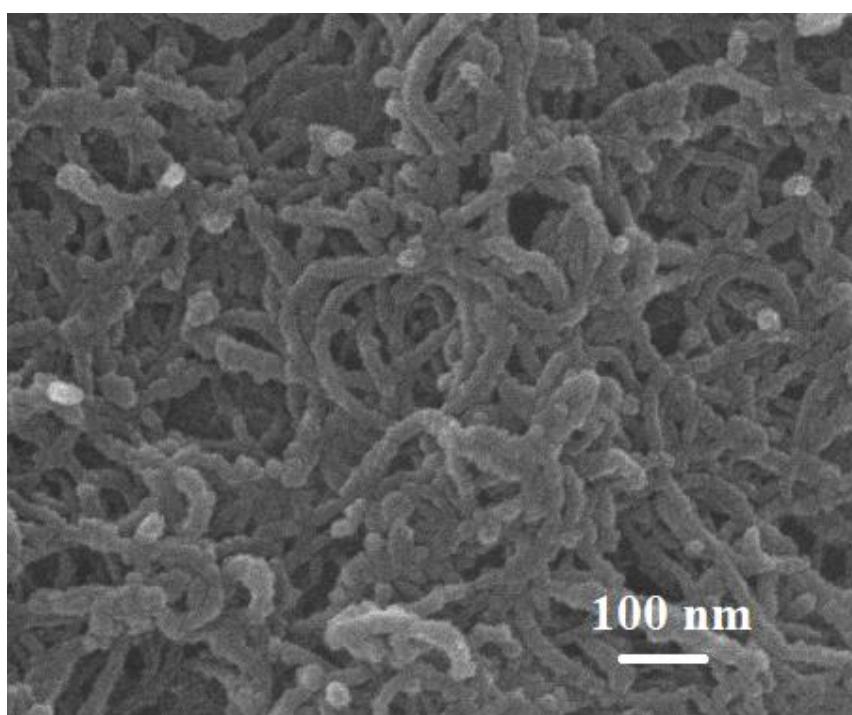


Fig. 2 FEG-SEM image of f-MWNTs/ZnO/Chit/GCE.

2.2 Electroactive surface area of sensors

The working surface area of four different sensors was determined by recording CVs for 1 mM $K_3Fe(CN)_6$ in 0.1 M KCl solution at different scan rates. Randles-Sevcik equation for reversible electrochemical process [43] was applied to determine the electroactive surface area of electrodes which is given as:

$$i_p = 0.446 n^{3/2} F^{3/2} A C D^{1/2} v^{1/2} R^{-1/2} T^{-1/2}$$

where, D denotes diffusion coefficient which is $7.6 \times 10^{-6} \text{ cm}^2 \text{ s}^{-1}$ and n corresponds to the electron transfer value which equals to 1, C is the bulk concentration of $\text{K}_3\text{Fe}(\text{CN})_6$ (mol cm^{-3}), A refers to the surface area of the sensor (cm^2), v is the scan rate (V s^{-1}), F is the Faraday constant, R is the universal gas constant, T is the temperature in Kelvin (298 K) and i_p is peak current. The surface area of bare GCE and ZnO modified GCE was estimated to be 0.020 and 0.092 cm^2 respectively. f-MWNTs modified on the bare substrate was estimated to be 0.173 cm^2 whereas the highest value was obtained for f-MWNTs/ZnO/Chit/GCE. The fabricated sensor with an effective surface area corresponding to 0.218 cm^2 , was almost 11 times more than the bare GCE. This substantial increase in the surface area aids in the enhancement of electroactive sites for the electrochemical oxidation.

2.3 Electrochemical characterization of electrodes

2.3.1 Current density plot

The electrochemical properties of the four different electrodes were investigated by recording current density plot. The related cyclic voltammograms are demonstrated in Fig. 3A which elucidates the current flowing per unit area of the electrodes thereby affirming noteworthy electrochemical property of the developed sensor. The voltammograms were recorded in a solution of 1 mM $\text{K}_3\text{Fe}(\text{CN})_6$ in 0.1 M KCl. The anodic peak was obtained at $\sim 0.274 \text{ V}$ for f-MWNTs/ZnO/Chit/GCE with highest current density of $199 \mu\text{A/cm}^2$ followed by f-MWNTs/GCE with current density corresponding to $106 \mu\text{A/cm}^2$ at $\sim 0.317 \text{ V}$. ZnO/GCE exhibited the anodic peak at $\sim 0.430 \text{ V}$ with current density of $35.65 \mu\text{A/cm}^2$ and least current density value of $7.2 \mu\text{A/cm}^2$ was obtained at $\sim 0.581 \text{ V}$ for bare GCE. The modified electrode with highest current density and lowest potential indicates excellent redox kinetics of the sensor. High current density is generally a less degrading condition than low current density due to the reduced cell voltage. Higher cell voltage can be attributed to fast degradation of the electrode. Thus, the significance of obtaining higher current density at lower potential is that it will lead to enhanced stability and reproducibility of the developed sensor.

2.3.2 Nyquist plot

The EIS study was further performed to ascertain the electrochemical behavior of the different electrodes in respect to their conductivities. The Nyquist plots delineate the interface properties of the sensors by exhibiting differing semicircle diameter which signifies the electron transfer resistance (R_{ct}). Fig. 3B distinctly illustrates that the least and the maximum R_{ct} values were observed for f-MWNTs/ZnO/Chit/GCE and bare GCE respectively. The lowering of the R_{ct} value of the developed sensor in comparison to the other electrodes reveal escalated

conductivity and improved electron transfer rate owing to the synergistic effect of f-MWNTs and ZnO nanoparticles.

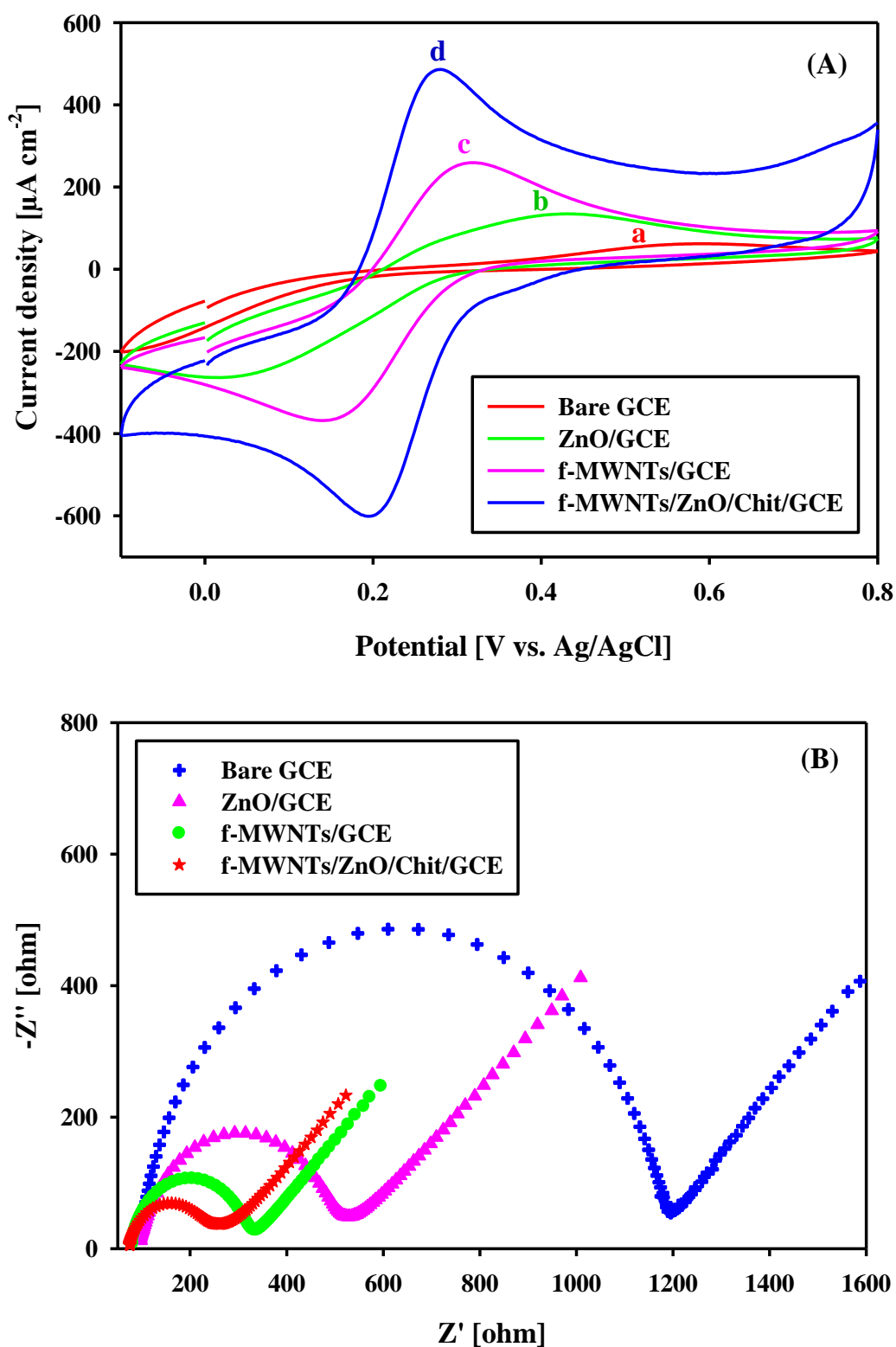


Fig. 3 (A) CVs recorded at scan rate of 25 mVs^{-1} for $1 \text{ mM K}_3[\text{Fe}(\text{CN})_6]$ in 0.1 M KCl solution and (B) Nyquist plots recorded in $1 \text{ mM Fe}(\text{CN})_6^{3-/4-}$ solution containing 0.1 M KCl for different electrodes.

3. Voltammetric behavior of nifedipine

3.1 Cyclic voltammetry

The voltammetric response for 1 μM nifedipine was recorded at bare and modified electrodes in PBS of pH 7.2 at a scan rate of 25 mVs^{-1} as showcased in Fig. 4A. The voltammograms depicted anodic peak at both the electrodes and hence the absence of cathodic peak in the reverse scan indicates the irreversible nature of the oxidation of nifedipine. The f-MWNTs/ZnO/Chit/GCE (curve b) displays the augmentation in oxidative current value corresponding to $10.49 \mu\text{A}$ at a lower oxidation potential of $\sim 840 \text{ mV}$ as compared to that of the bare GCE (curve a) which exhibits the peak current at $0.44 \mu\text{A}$ with high potential of $\sim 904 \text{ mV}$. The substantial enhancement in the current response along with a notable shift of the peak potential at f-MWNTs/ZnO/Chit/GCE gives the insight of the electrocatalytic nature and ameliorated surface area for the electro-oxidation of nifedipine.

3.2 Square wave voltammetry

Square wave voltammetry was employed further for the determination of nifedipine for the first time as it is an efficacious technique with increased sensitivity and lesser background current. Fig 4B demonstrates the voltammograms for 1 μM of nifedipine in PBS of pH 7.2 at four different electrodes. An inconspicuous peak was perceived at bare GCE at $\sim 882 \text{ mV}$ which shifted to lower potentials at ZnO modified GCE ($\sim 860 \text{ mV}$) with an amelioration in the current response. The voltammetric signal at f-MWNTs modified GCE was found to have even higher current response with lower peak potential at $\sim 834 \text{ mV}$. Amongst the four working electrodes, the finest response was acquired at f-MWNTs/ZnO/Chit/GCE exhibiting the oxidation peak potential at $\sim 807 \text{ mV}$. The current signal was ~ 8.3 times incremented in comparison to the bare GCE which can be ascribed due to the integrated electron transfer ability of f-MWNTs and ZnO nanoparticles on the bare substrate. Thus, for further investigations f-MWNTs/ZnO/Chit/GCE employing square wave voltammetry was utilized.

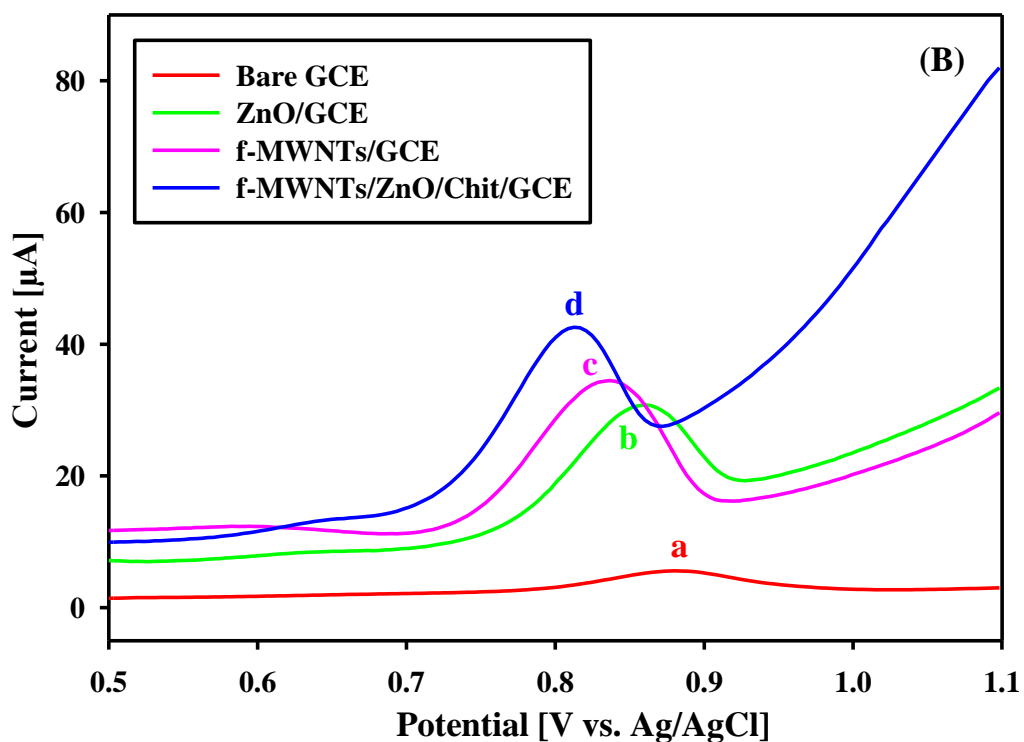
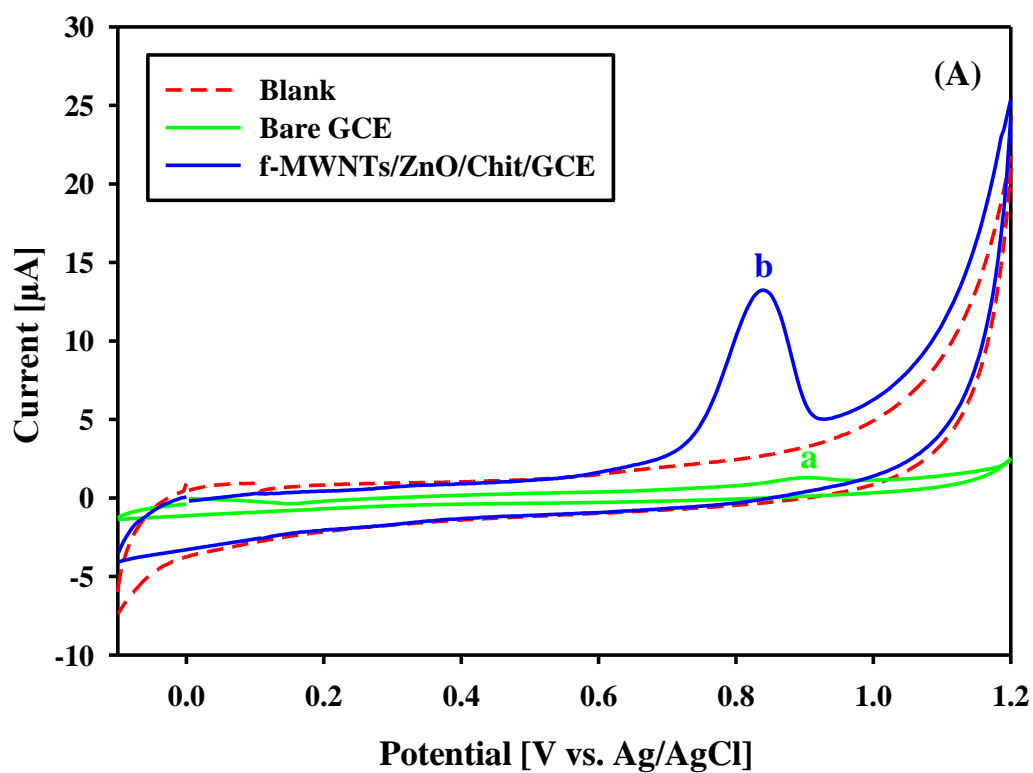


Fig. 4 (A) CVs obtained for 1 μM nifedipine at (a) bare GCE and (b) f-MWNTs/ZnO/Chit/GCE at 25 mVs^{-1} . Voltammetric response recorded in PBS of pH 7.2

(background) at f-MWNTs/ZnO/Chit/GCE (- - -). (B) SWVs obtained for 1 μM nifedipine in PBS of pH 7.2 at 15 Hz at four different electrodes.

4. Optimization of experimental parameters

Electro-oxidation of nifedipine relies significantly on the pH value of the supporting electrolyte. The pH range of 2.0 to 11.0 was examined at a square wave frequency (f) of 15 Hz for 1 μM concentration of nifedipine at f-MWNTs/ZnO/Chit/GCE. With an increase in the pH value, the anodic peak signal of nifedipine was noted to shift to less positive values as displayed in Fig. 5A. The plot of E_p versus pH gives the linear relationship as follows:

$$E_p (\text{pH } 2 - 11) = [-0.0562 \text{ pH} + 1.1922] \text{ V}$$

having correlation coefficient of 0.9967 and slope corresponding to 0.0562 V pH^{-1} . The slope of E_p versus pH gives insight about the number of electrons and protons participating in the reaction mechanism according to Nernstian equation [44]. Thus, from the value of slope it can be inferred that in the oxidation mechanism of nifedipine the number of electrons and protons transferred are the same which is two. The impact of supporting electrolyte on the peak current value for oxidation of nifedipine was also investigated. There was an increase in the current response with increase in the pH till 7.2 (Fig. 5B). Subsequently, a decrease in the current signal was noticed and hence pH 7.2 exhibiting the maximum value of current response was used as the supporting electrolyte for further analysis.

Furthermore, the consequence of f on the current signal as well as the peak potential was studied at pH 7.2 for 1 μM of nifedipine. It was observed in Fig 5C that with an increase in the f the current response increases linearly over the frequency range of 10-100 Hz. The linear relationship obtained from the plot of i_p versus f is as follows:

$$i_p (\mu\text{A}) = 0.59 f + 14.362$$

with correlation coefficient of 0.9963. To investigate the significance of f on the anodic peak value of nifedipine, E_p versus $\log f$ graph was plotted. Fig. 5D displayed that as f increases the peak potential value increases with the linear relationship as:

$$E_p (\text{V}) = 0.0352 \log f + 0.7649$$

with correlation coefficient of 0.9917. This observation of electrochemical oxidation of nifedipine at f-MWNTs/ZnO/Chit/GCE interprets that the process is adsorption controlled and irreversible [45] which is in consonance with the CV investigations.

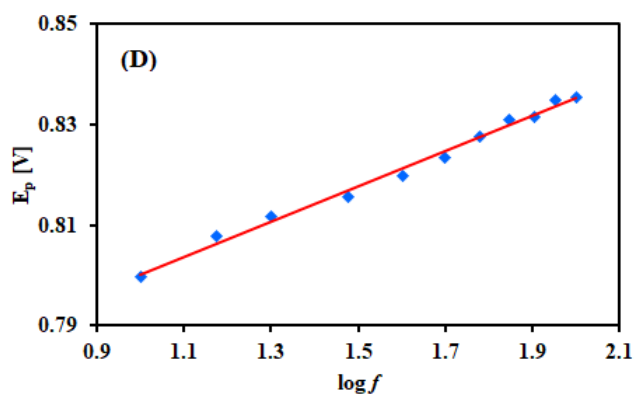
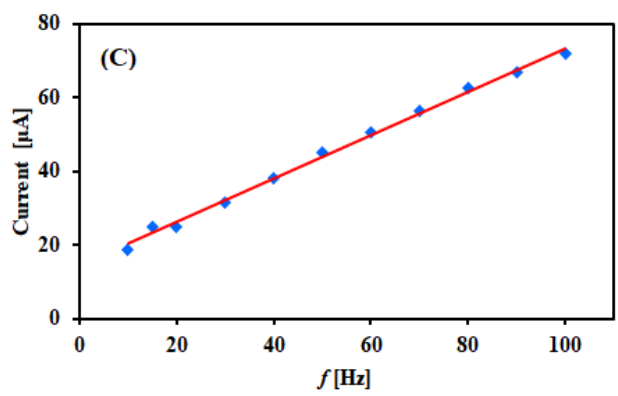
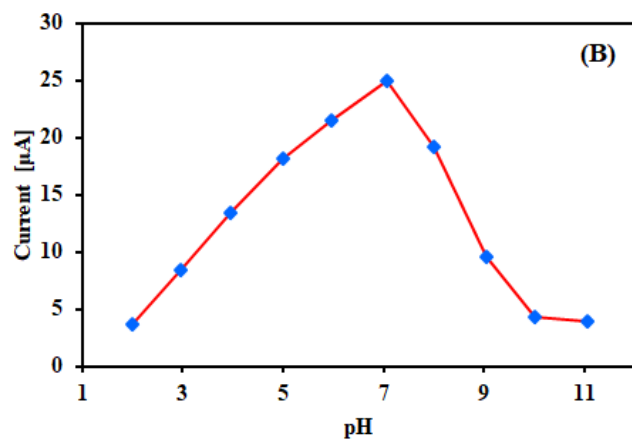
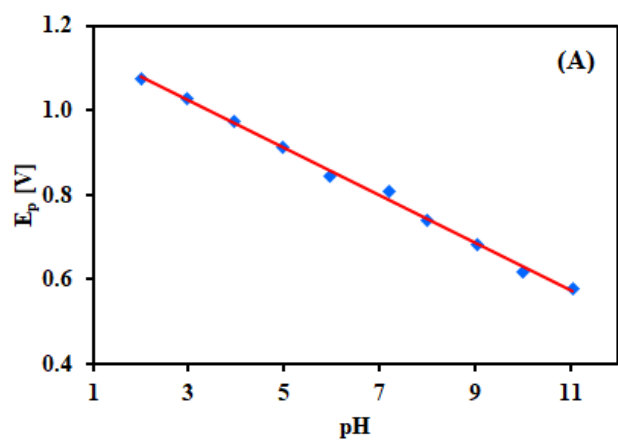


Fig. 5 (A) Observed dependence of peak potential on pH; and **(B)** peak current on pH. **(C)** Effect of square wave frequency on peak current; and **(D)** peak potential for 1 μM nifedipine at f-MWNTs/ZnO/Chit/GCE.

5. Quantification of nifedipine

At f-MWNTs/ZnO/Chit/GCE, nifedipine was quantitatively evaluated by recording square wave voltammograms for varying concentration under optimized conditions. The current response corresponding to the oxidation of nifedipine incremented linearly with increase in the concentration. Fig. 6 shows elevation in peak current values for the increase in nifedipine concentration in the range of 1 nM - 40 μM against the background current. The mentioned calibration range of nifedipine displayed corresponding linear plots with the following regression equations:

$$i_p (\mu\text{A}) = 0.0218 C (\text{nM}) + 2.983 \quad (1 \text{ nM} - 2000 \text{ nM})$$

$$i_p (\mu\text{A}) = 4.3204 C (\mu\text{M}) + 43.502 \quad (4 \mu\text{M} - 40 \mu\text{M})$$

where C is the concentration of nifedipine. The correlation coefficient obtained for the above two equations are 0.9924 and 0.9946 respectively. The sensitivity of the electrode was attained as 21.8 $\mu\text{A} \mu\text{M}^{-1}$. The limit of detection was estimated to be 0.49 nM based on $S/N = 3$ with limit of quantification as 1.64 nM for f-MWNTs/ZnO/Chit/GCE. Table 1 enumerates a comparison of the analytical parameters of the proposed work with the reported literature. It could be patently observed that this work demonstrates the lowest detection limit with augmented sensitivity for the wider linear range.

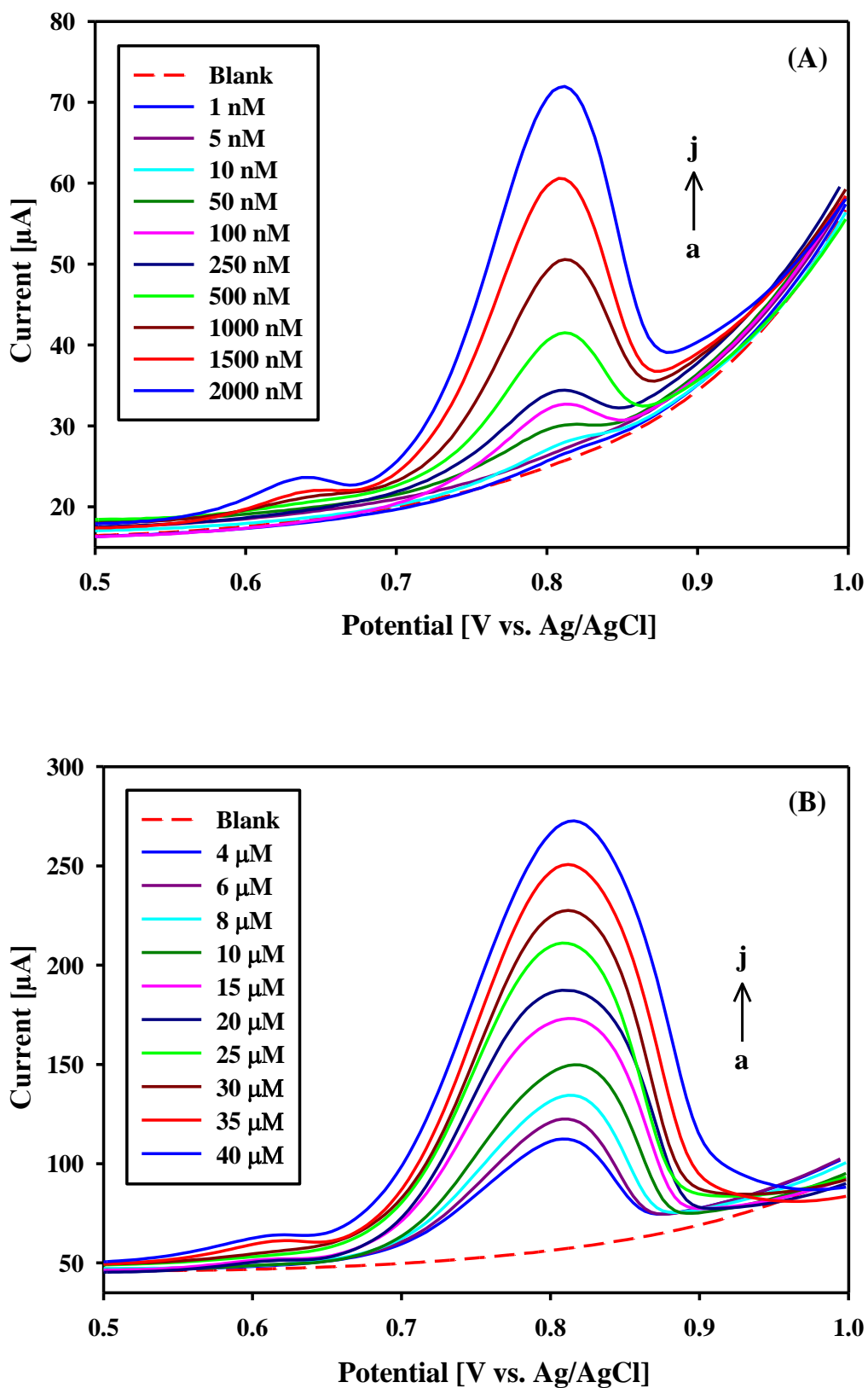


Fig. 6 SWVs recorded at f-MWNTs/ZnO/Chit/GCE for phosphate buffer of pH 7.2 (- -) and increasing concentration of nifedipine (—) from (A) 1 nM to 2000 nM and (B) 4 μM to 40 μM at 15 Hz.

Table 1 Comparison of the f-MWNTs/ZnO/Chit/GCE with the reported sensors for the electrochemical determination of nifedipine.

Technique	Sensor Used	Analytical Range (M)	Limit of Detection (M)	Sensitivity ($\mu\text{A}/\mu\text{M}$)	Reference
DPAdSV	β – cyclodextrin modified carbon nanotube paste electrode	47.7×10^{-9} – 20.0×10^{-6}	14.8×10^{-9}	3.931	22
DPV	Polyvinylpyrrolidone modified carbon paste electrode	75×10^{-9} – 50×10^{-6}	20×10^{-9}	0.698	23
DPV	Boron-doped diamond electrode	3.98×10^{-6} – 107×10^{-6}	612×10^{-9}	0.055	24
DPV	MgO – nanoplatelets modified screen-printed electrodes	0.2×10^{-6} – 104.41×10^{-6}	32×10^{-9}	0.06	25
CV	Polyaniline carboxylic acid functionalized multiwalled carbon nanotubes modified indium-tin-oxide electrode	1.0×10^{-6} – 100×10^{-6}	1000×10^{-9}	0.087	26
DPV	Multi-walled carbon nanotube modified glassy carbon electrode	0.1×10^{-6} – 100×10^{-6}	17×10^{-9}	0.35	27
SWV	f-MWNTs/ZnO/Chit/GCE	1×10^{-9} – 40×10^{-6}	0.49×10^{-9}	21.8	This work

6. Selectivity

To proclaim the selectivity of f-MWNTs/ZnO/Chit/GCE towards nifedipine, SWVs were recorded where the matrix complexes were used as interferents. The peak current response of 1 μ M nifedipine in the presence of prevailing biological metabolites like ascorbic acid, hypoxanthine, L-tryptophan and uric acid was measured. Table 2 depicts the data of insignificant effect of probable interferents present in 50 fold concentration on the electro-oxidation of nifedipine at f-MWNTs/ZnO/Chit/GCE. The tolerance limit of less than ± 5 % for varying concentrations of interfering species was considered for quantitation of nifedipine. The results acquired endorse that the electrochemical detection of nifedipine at f-MWNTs/ZnO/Chit/GCE is unaltered by the interfering species thereby indicating remarkable recognition selectivity.

Table 2 Effect of interferents on the detection of nifedipine.

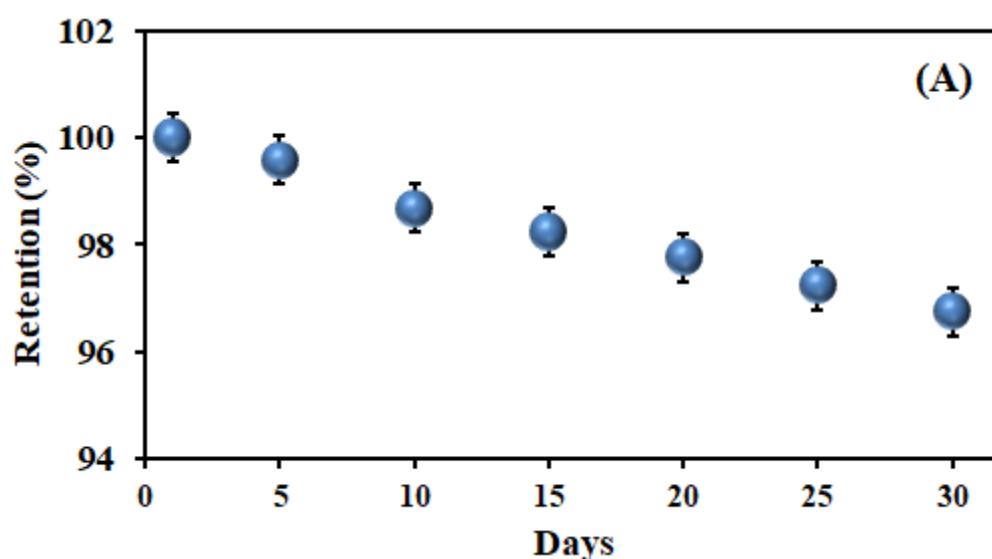
Interferent	Concentration of interferents (μM)	Change in i_p of nifedipine (μA)	Error (%)
Ascorbic Acid	1.00	0.39	1.56
	5.00	1.04	4.17
	10.00	0.93	3.73
	50.00	1.13	4.53
Hypoxanthine	1.00	0.97	3.89
	5.00	0.71	2.85
	10.00	0.94	3.77
	50.00	-0.65	-2.61
L-Tryptophan	1.00	0.63	2.53
	5.00	-0.66	-2.65
	10.00	0.16	0.64
	50.00	0.37	1.48

Uric Acid	1.00	0.30	1.20
	5.00	0.81	3.25
	10.00	1.05	4.21
	50.00	-1.03	-4.13

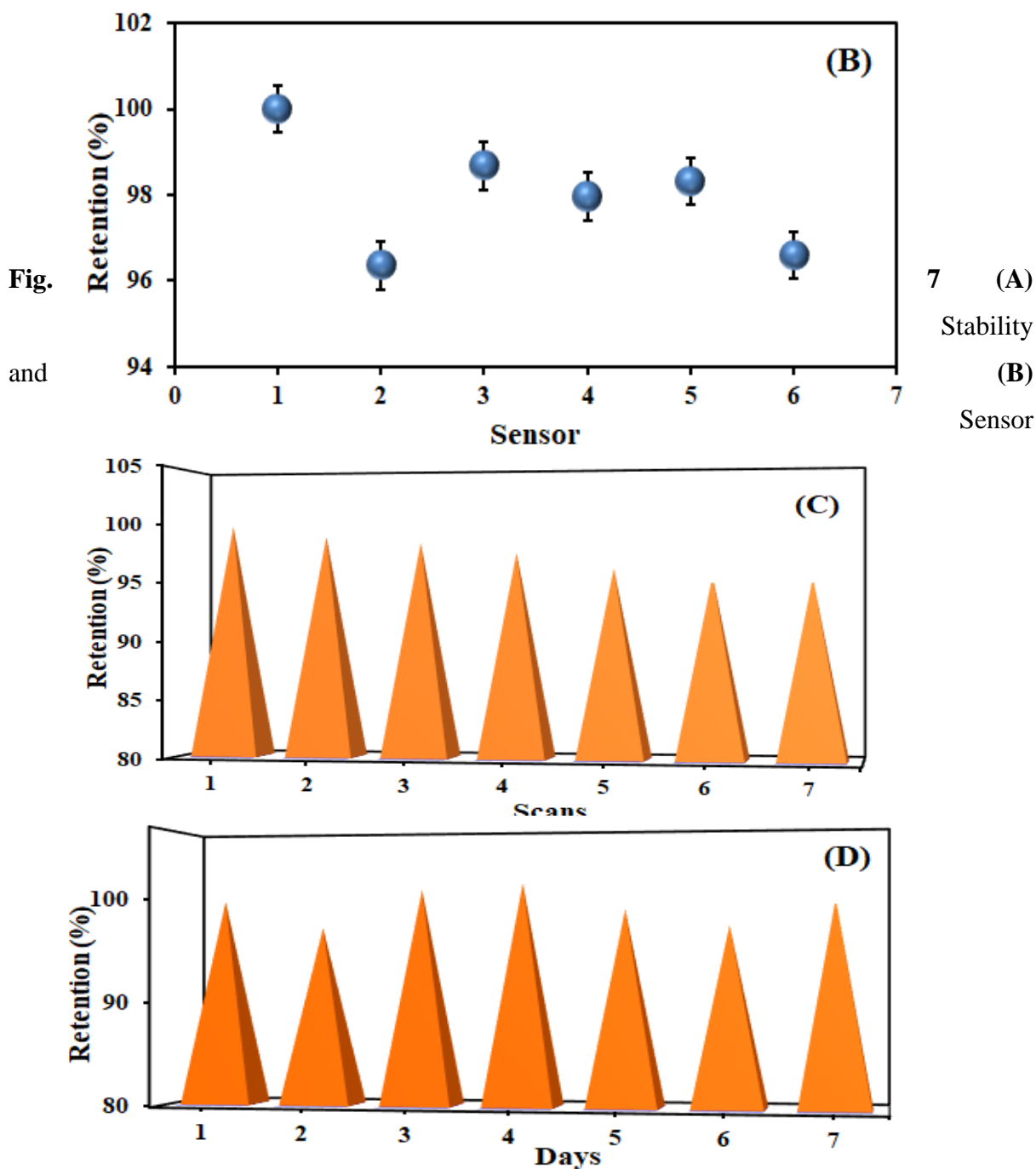
7. Stability and reproducibility of the developed sensor

The stability and reproducibility of the fabricated sensor is an imperative parameter in the view of its applications and viability. SWVs of 1 μ M nifedipine were recorded by storing the f-MWNTs/ZnO/Chit/GCE for 30 days at ambient atmosphere. The current response obtained reveals that there is a minimal variation in the signal value in the span of 30 days (Fig. 7A). The relative standard deviation (RSD) attained for the current response was 1.22 % which manifest worthy stability of the developed sensor.

The reproducibility of the developed electrode was assessed by recording the peak current of fixed concentration of nifedipine at f-MWNTs/ZnO/Chit/GCE under optimized conditions. Six different electrodes with identical modification and almost similar surface area were prepared and tested for reproducibility which demonstrated the RSD of 1.39 % (Fig. 7B). The intra day precision was estimated by performing seven scans of a fixed concentration of the analyte which revealed the RSD of 1.83 % (Fig. 7C). Additionally, inter day reproducibility was calculated by measuring peak current response for seven consecutive days at f-MWNTs/ZnO/Chit/GCE for 1 μ M nifedipine solution (Fig. 7D). The RSD was found to be



1.65 % which is well within the acceptable range. Hence, it can be corroborated that the fabricated sensor possesses the attributes of notable longevity and distinctive reproducibility.



reproducibility of the f-MWNTs/ZnO/Chit/GCE for 1 μ M nifedipine in PBS of pH 7.2. (C) Intra day and (D) Inter day reproducibility of the f-MWNTs/ZnO/Chit/GCE for 1 μ M nifedipine in PBS of pH 7.2.

8. Analytical applications

8.1 Assay of pharmaceuticals

To substantiate the applicability of f-MWNTs/ZnO/Chit/GCE as a promising diagnostic tool, the functioning of the sensor was assessed for the detection of nifedipine in commercially available tablets. To start with, the tablets were weighed and then pulverized finely. Adequate quantity of powdered sample was dissolved in minimum volume of methanol and the solution was made up with double distilled water. Thereafter, SWVs were recorded at f-MWNTs/ZnO/Chit/GCE and the content of nifedipine in the pharmaceutical formulation was calculated utilizing the linear regression equation of calibration curve. The detected values of nifedipine in commercial medicines were found to be close to the claimed values by the proposed methodology as listed in Table 3. Thus, the developed sensor explicitly signify selectivity for nifedipine in drugs without substantial interference of excipients.

Table 3 Determination of nifedipine in pharmaceuticals using f-MWNTs/ZnO/Chit/GCE at pH 7.2.

Sample	Stated content	Detected content	Error (%)
Depine	10.00 mg	9.66 mg	- 3.40
Nicardia	20.00 mg	19.42 mg	- 2.90

8.2 Recovery studies of nifedipine

To perceive the competence of the fabricated sensor it was exerted for the quantitation of nifedipine in real samples like urine and blood serum of normal human. The procured urine samples were diluted 10 times with the PBS of pH 7.2 to reduce the influence of coexisting metabolites in the matrix. The diluted urine sample was subjected to square wave voltammetry at f-MWNTs/ZnO/Chit/GCE which displays the absence of anodic peak signal of nifedipine as can be seen in Fig. 8A (curve a). Subsequently, the urine sample was spiked with varied known amounts of nifedipine from the stock solution which exhibited the oxidation peak of nifedipine at ~ 0.807 V as depicted in Fig. 8A (curves b, c and d). The concentration of the spiked nifedipine was determined using the calibration curve regression equation and the calculated recovery values were within the permissible limits as shown in Table 4. The blood samples obtained were centrifuged in order to segregate the serum followed by 10 times dilution prior

to analysis. Voltammograms were recorded before and after spiking of appropriate concentrations of nifedipine as showcased in Fig. 8B and the calculated acceptable recoveries are listed in Table 4. The results visibly demonstrate satisfactory practicality of the developed sensor.

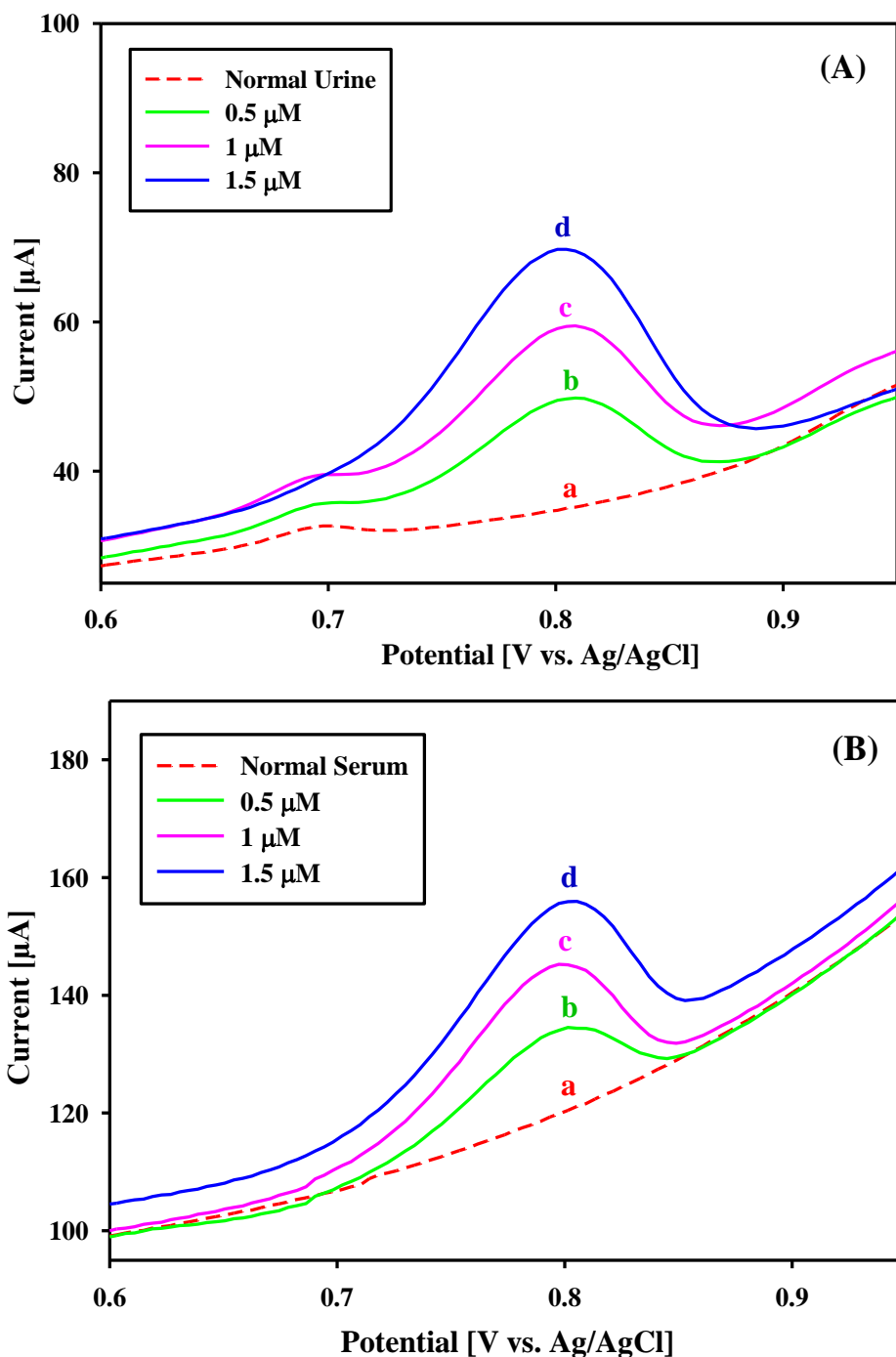


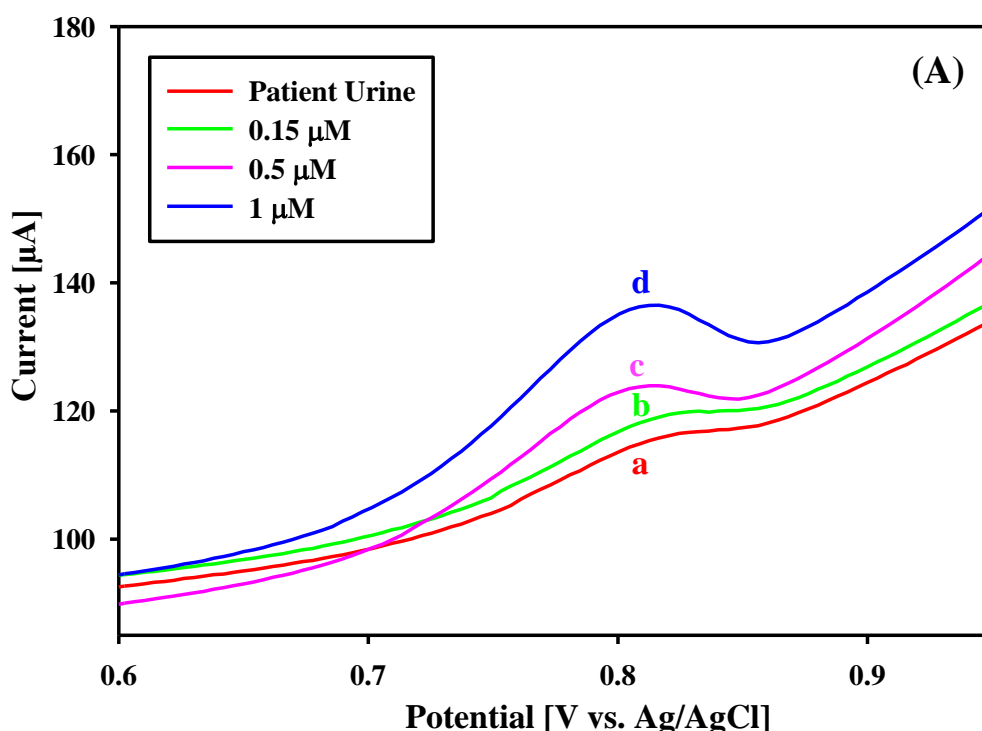
Fig. 8 Voltammograms recorded at f-MWNTs/ZnO/Chit/GCE for (A) normal human urine sample 1 and (B) normal human serum sample 1 before and after spiking different concentrations of nifedipine.

Table 4 Nifedipine concentration in normal human urine and serum samples at pH 7.2 using f-MWNTs/ZnO/Chit/GCE.

	Spiked (μM)	Detected (μM)	Recovery (%)
Normal Human Urine			
Sample 1	0.00	-----	-----
	0.50	0.52	104.00
	1.00	0.98	98.00
	1.50	1.46	97.33
Sample 2	0.00	-----	-----
	0.50	0.51	102.00
	1.00	0.95	95.00
	1.50	1.51	100.67
Normal Human Serum			
Sample 1	0.00	-----	-----
	0.50	0.49	98.00
	1.00	1.01	101.00
	1.50	1.49	99.33
Sample 2	0.00	-----	-----
	0.50	0.51	102.00
	1.00	0.99	99.00
	1.50	1.48	98.67

8.3 Analysis of real samples

Literature survey reveals that till date no one has endeavoured to electrochemically detect nifedipine in human patient biological samples. To affirm the pragmatic application of the developed protocol, the urine and blood serum samples acquired from patients suffering from hypertension were assessed. The samples were assessed after 4 hours of administration of Nicardia tablet containing 20 mg of the drug and SWVs were recorded after appropriate dilution. A distinct oxidation peak corresponding to ~ 0.807 V was attained at f-MWNTs/ZnO/Chit/GCE in both patient urine and serum samples as illustrated in Fig. 9 (curve a). This anodic peak pertaining to the electrochemical oxidation of nifedipine was further validated by spiking manifold known concentrations of the analyte in the real samples as shown in Fig. 9 (curves b, c and d). The increase in the peak current response with an unaltered oxidation potential asserted the recognition selectivity for the sensing of nifedipine. Calibration plot was utilized to calculate the detected concentrations of the analyte in real samples. Table 5 depicts the calculated recoveries which are in the range of 95.13 – 104.47 % and 96.19 – 104.43 % for urine and serum samples respectively. Hence, a realistic application was effectually delineated in physiological pH.



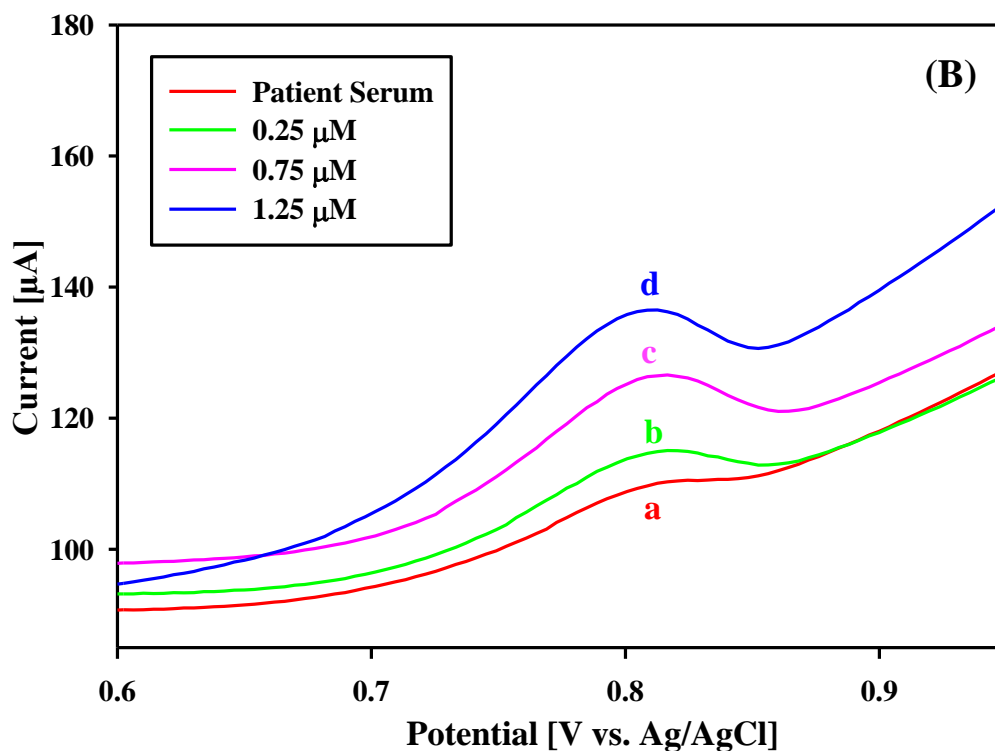


Fig. 9 Voltammograms recorded at f-MWNTs/ZnO/Chit/GCE for (A) patient urine sample 1 and (B) patient serum sample 1 before and after spiking manifold concentrations of nifedipine.

Table 5 Concentration of nifedipine in patient human urine and serum samples at pH 7.2 at f-MWNTs/ZnO/Chit/GCE.

	Spiked (μM)	Detected (μM)	Recovery (%)
Patient Human Urine			
Sample 1	0.00	0.096	-----
	0.15	0.257	104.47
	0.50	0.567	95.13
	1.00	1.087	99.18
Sample 2	0.00	0.085	-----
	0.15	0.244	103.83
	0.50	0.589	100.68

	1.00	1.079	99.45
Patient Human Serum			
Sample 1	0.00	0.203	-----
	0.25	0.436	96.24
	0.75	0.968	101.57
	1.25	1.434	98.69
Sample 2	0.00	0.195	-----
	0.25	0.434	97.53
	0.75	0.909	96.19
	1.25	1.509	104.43

9. Conclusions

Synergistic effect of uniformly distributed ZnO nanoparticle film embedded with f-MWNTs on GCE for the electro-oxidation of nifedipine employing SWV was implemented for the first time. The modification of GCE aided in escalating the electrochemical properties of the bare substrate by diffusion of the analyte inside the porous layers and thereby exhibiting sustained electron mediating behavior. With an upsurge in the conductivity of f-MWNTs/ZnO/Chit/GCE, it manifested a phenomenal sensitivity ($21.8 \mu\text{A } \mu\text{M}^{-1}$) and lowest detection limit (0.49 nM) over a wider linear range from nanomolar to micromolar. The crafted sensor intensely proclaims remarkable selectivity of nifedipine in the presence of biological interferences with realistic reproducibility, long term stability and repeatability. Furthermore, the functionality of the methodology was evinced by applying it to acquire promising results for the quantitation of nifedipine in pharmaceuticals, healthy human urine and serum samples. The developed sensor imparts overt corroboration as a persuasive diagnostic tool by efficaciously detecting nifedipine for the first time in serum and urine sample of people being subjected to antihypertensive medication. Thus, the future perspective of the developed methodology is to be aptly useful for the routine analysis of nifedipine in drug formulations and *in vivo* studies.

Acknowledgements

S. Chatterjee is thankful to the Department of Science and Technology (DST), Govt. of India for the DST INSPIRE Faculty Award [IFA14-CH-155] and research funding. N. Agrawal is grateful to DST INSPIRE for providing the research fellowship. Institute of Chemical Technology (ICT) is acknowledged for providing the research facilities.

References

- [1] R. Guo, X. Hu, Y. Yamada, M. Harada, T. Nakajima, T. Kashihara, M. Yamada, T. Aoyama, Y. Kamijo, Effects of hypertension and antihypertensive treatments on sulfatide levels in serum and its metabolism, *Hypertens. Res.*, 42 (2019) 598.
- [2] Q. Zeng, T. Wei, M. Wang, X. Huang, Y. Fang, L. Wang, Polyfurfural film modified glassy carbon electrode for highly sensitive nifedipine determination, *Electrochim. Acta*, 186 (2015) 465.
- [3] A.V. Chobanian, G.L. Bakris, H.R. Black, W.C. Cushman, L.A. Green, J.L. Izzo, D.W. Jones, B.J. Materson, S. Oparil, J.T. Wright, E.J. Rocella, Seventh Report of the Joint National Committee on Prevention, Detection, Evaluation, and Treatment of High Blood Pressure, *Hypertension*, 42 (2003) 1206.
- [4] C. Lopez-Alarcon, L.J. Nunez-Vergara, J.A. Squella, Voltammetric oxidation of Hantzsch 1,4-dihydropyridines in protic and aprotic media: Relevance of the substitution on N position, *Electrochim. Acta*, 48 (2003) 2505.
- [5] A. Kiriya, A. Honbo, A. Nishimura, N. Shibata, K. Iga, Pharmacokinetic-pharmacodynamic analyses of antihypertensive drugs, nifedipine and propranolol, in spontaneously hypertensive rats to investigate characteristics of effect and side effects, *Regul. Toxicol. Pharmacol.*, 76 (2016) 21.
- [6] P. Sundaresan, R. Karthik, S.M. Chen, J.V. Kumar, V. Muthuraj, E.R. Nagarajan, Ultrasonication-assisted synthesis of sphere-like strontium cerate nanoparticles (SrCeO₃NPs) for the selective electrochemical detection of calcium channel antagonists nifedipine, *Ultrason. Sonochem.*, 53 (2019) 44.
- [7] M. Baghayeri, M. Namadchian, H. Karimi-Maleh, H. Beitollahi, Determination of nifedipine using nanostructured electrochemical sensor based on simple synthesis of Ag nanoparticles at the surface of glassy carbon electrode: Application to the analysis of some real samples, *J. Electroanal. Chem.*, 697 (2013) 53.

- [8] H.J. Wang, C.K. Lu, W.C. Chen, A.C. Chen, Y.F. Ueng, Shenmai-Yin decreased the clearance of nifedipine in rats: The involvement of time-dependent inhibition of nifedipine oxidation, *J. Food Drug Anal.*, 27 (2019) 284.
- [9] S. Laurent, Antihypertensive drugs, *Pharmacol. Res.*, 124 (2017) 116.
- [10] A.G. Ellrodt, M.J. Ault, Calcium-channel blockers in acute hypertension, *Am. J. Emerg. Med.*, 3 (1985) 16.
- [11] L. Logoyda, A HPLC-MS / MS method development and validation for the simultaneous determination of nifedipine and enalapril in human plasma, *Int. J. Appl. Pharm.*, 10 (2018) 35.
- [12] P. Tulasamma, P. Venkateswarlu, Spectrophotometric determination of nifedipine in pharmaceutical formulations, serum and urine samples via oxidative coupling reaction, *Arab. J. Chem.*, 9 (2016) 1603.
- [13] M.V. Vertzoni, C. Reppas, H.A. Archontaki, Sensitive and simple liquid chromatographic method with ultraviolet detection for the determination of nifedipine in canine plasma, *Anal. Chim. Acta*, 573 (2006) 298.
- [14] M.T. Rosseel, M.G. Bogaert, Determination of nifedipine in human plasma by capillary gas chromatography with nitrogen detection, *J. Chromatogr. A*, 279 (1983) 675.
- [15] S. Higuchi, Y. Shiobara, Quantitative determination of nifedipine in human plasma by selected ion monitoring, *Biol. Mass Spectrom.*, 5 (1978) 220.
- [16] D. Wang, K. Jiang, S. Yang, F. Qin, X. Lu, F. Li, Determination of nifedipine in human plasma by ultra performance liquid chromatography – tandem mass spectrometry and its application in a pharmacokinetic study, *J. Chromatogr. B*, 879 (2011) 1827.
- [17] A. Ahmadalinezhad, S. Chatterjee, A. Chen, Synthesis and electrochemical study of nanoporous palladium-cadmium networks for non-enzymatic glucose detection, *Electrochim. Acta*, 112 (2013) 927.
- [18] G. Liu, H. Chen, H. Peng, S. Song, J. Gao, J. Lu, M. Ding, L. Li, S. Ren, Z. Zou, C. Fan, *Biosens. Bioelectron.*, 28 (2011) 308.
- [19] S. Chatterjee, A. Chen, Facile electrochemical approach for the effective detection of guanine, *Electrochem. Commun.*, 20 (2012) 29.
- [20] M. Ahmadi-Kashani, H. Dehghani, A novel selective ternary platform fabricated with MgAl-layered double hydroxide/NiMn₂O₄ functionalized polyaniline nanocomposite deposited on a glassy carbon electrode for electrochemical sensing of levodopa, *Colloids Surf. B*, 194 (2020) 111134.

- [21] R.N. Goyal, S. Chatterjee, A.R.S. Rana, H. Chasta, Application of modified pyrolytic graphite electrode as a sensor in the simultaneous assay of adenine and adenosine monophosphate, *Sens. Actuat. B Chem.*, 156 (2011) 198.
- [22] R.R. Gaichore, A.K. Srivastava, Voltammetric determination of nifedipine using a β -cyclodextrin modified multi-walled carbon nanotube paste electrode, *Sens. Actuat. B Chem.*, 188 (2013) 1328.
- [23] X. Yang, D. Sun, X. Xie, H. Zhang, Sensitive and rapid determination of nifedipine using polyvinylpyrrolidone- modified carbon paste electrode, *Russ. J. Electrochem.*, 50 (2014) 453.
- [24] J. Scremin, E.R. Sartori, Simultaneous determination of nifedipine and atenolol in combined dosage forms using a boron-doped diamond electrode with differential pulse voltammetry, *Can. J. Chem.*, 96 (2018) 1.
- [25] M. Khairy, A.A. Khorshed, F.A. Rashwan, G.A. Salah, H.M. Abdel-Wadood, C.E. Banks, Simultaneous voltammetric determination of antihypertensive drugs nifedipine and atenolol utilizing MgO nanoplatelet modified screen-printed electrodes in pharmaceuticals and human fluids, *Sens. Actuat. B Chem.*, 252 (2017) 1045.
- [26] Q. Wang, R. Zhao, S. Wang, H. Guo, J. Li, H. Zhou, X. Wang, X. Wu, Y. Wang, W. Chen, W. Zhang, A highly selective electrochemical sensor for nifedipine based on layer-by-layer assembly films from polyaniline and multiwalled carbon nanotube, *J. Appl. Polym. Sci.*, 133 (2016) 1.
- [27] B. Mokhtari, D. Nematollahi, H. Salehzadeh, Electrochemical simultaneous determination of nifedipine and its main metabolite dehydronifedipine using MWCNT modified glassy carbon electrode, *J. Mol. Liq.*, 264 (2018) 543.
- [28] C. Yang, M.E. Denno, P. Pyakurel, B.J. Venton, Recent trends in carbon nanomaterial-based electrochemical sensors for biomolecules: A review, *Anal. Chim. Acta*, 887 (2015) 17.
- [29] P. Tarlekar, S. Chatterjee, Enhancement in sensitivity of non-steroidal anti-inflammatory drug mefenamic acid at carbon nanostructured sensor, *J. Electroanal. Chem.*, 803 (2017) 51.
- [30] R. Savalia, S. Chatterjee, Sensitive detection of brucine an anti-metastatic drug for hepatocellular carcinoma at carbon nanotubes – nafion composite based biosensor, *Biosens. Bioelectron.*, 98 (2017) 371.

- [31] M. Deborah, A. Jawahar, T. Mathavan, M.K. Dhas, A.M.F. Benial, Spectroscopic studies on sidewall carboxylic acid functionalization of multi-walled carbon nanotubes with valine, *Spectrochim. Acta A Mol. Biomol. Spectrosc.*, 139 (2015) 138.
- [32] M. Amiri-Aref, J.B. Raoof, R. Ojani, Electrocatalytic oxidation and selective determination of an opioid analgesic methadone in the presence of acetaminophen at a glassy carbon electrode modified with functionalized multi-walled carbon nanotubes: Application for human urine, saliva and pharmaceutical samples analysis, *Colloids Surf. B*, 109 (2013) 287.
- [33] S.S.J. Aravind, S. Ramaprabhu, Chemical noble metal dispersed multiwalled carbon nanotubes immobilized ss-DNA for selective detection of dopamine, *Sens. Actuat. B Chem.*, 155 (2011) 679.
- [34] H. Zhang, J. Ye, Y. Ye, Y. Chen, C. He, Y. Chen, The effect of acid treatment on thermally exfoliated graphite oxide as electrode for supercapacitors, *Electrochim. Acta*, 138 (2014) 311.
- [35] C.E. Banks, A. Crossley, C. Salter, S.J. Wilkins, R.G. Compton, Carbon nanotubes contain metal impurities which are responsible for the “electrocatalysis” seen at some nanotube-modified electrodes, *Angew. Chem. Int. Ed.*, 45 (2006) 2533.
- [36] S. Tursynbolat, Y. Bakytkarim, J. Huang, L. Wang, Ultrasensitive electrochemical determination of metronidazole based on polydopamine / carboxylic multi-walled carbon nanotubes nanocomposites modified GCE, *J. Pharm. Anal.*, 8 (2018) 124.
- [37] R. Savalia, S. Chatterjee, Sensing of sulfasalazine - Cysteine transporter inhibitor with platinum nanoflowers decorated on carbon nanotubes by electrochemical reduction, *Sens. Actuat. B Chem.*, 277 (2018) 39.
- [38] J. Ding, S. Zhu, T. Zhu, W. Sun, Q. Li, Hydrothermal synthesis of zinc oxide-reduced graphene oxide nanocomposites for an electrochemical hydrazine sensor, *RSC Adv.*, 5 (2015) 22935.
- [39] M.B. Wayu, J.E. King, J.A. Johnson, C.C. Chusuei, A zinc oxide carbon nanotube based sensor for In situ monitoring of hydrogen peroxide in swimming pools, *Electroanalysis*, 27 (2015) 2552.
- [40] R. Sha, S.K. Puttapati, V. VSS Srikanth, S. Badhulika, Ultra-sensitive phenol sensor based on overcoming surface fouling of reduced graphene oxide-zinc oxide composite electrode, *J. Electroanal. Chem.*, 785 (2017) 26.
- [41] G. Manasa, R.J. Mascarenhas, B.M. Basavaraja, Sensitively-selective determination of Propyl Paraben preservative based on synergistic effects of polyaniline-zinc-oxide nano-

- composite incorporated into graphite paste electrode, *Colloids Surf. B*, 184 (2019) 110529.
- [42] J. Guo, C. Peng, Synthesis of ZnO nanoparticles with a novel combustion method and their C₂H₅OH gas sensing properties, *Ceram. Int.*, 41 (2015) 2180.
- [43] A.G.M. Ferrari, C.W. Foster, P.J. Kelly, D.A.C. Brownson, C.E. Banks, Determination of the electrochemical area of screen-printed electrochemical sensing platforms, *Biosensors*, 8 (2018) 53.
- [44] Z. Zhang, T. Cserfalvi, M. Gratzl, pH dependent voltammetry at partially oxidized palladium and its potential for voltammetry-based pH sensing, *J. Electroanal. Chem.*, 845 (2019) 1.
- [45] S. Komorsky-Lovric, S. Gagic, R. Penovsky, Voltammetric determination of benzoylecgonine, *Anal. Chim. Acta*, 389 (1999) 219.

Electrochemical sensor applications based on biomass-derived carbon nanomaterials

Shweta J. Malode, Mahesh M. Shanbhag, Nagaraj P. Shetti*

Center for Energy and Environment, School of Advanced Sciences, KLE Technological University, Vidyanagar, Hubballi-580031, Karnataka, India

Corresponding Authors Email:

Nagaraj P. Shetti: npshetti@kletech.ac.in; dr.npshetti@gmail.com

ABSTRACT

In recent years, a growing focus has been placed on using specialized waste biomass as a sustainable, affordable, abundant fuel and material source. By using various dependable waste biomass as a renewable, reasonably priced, and good resource, there is a significant chance to maximize energy output. Thanks to renewable hydrocarbons like biomass, bioenergy, green chemicals, and carbon materials are all made possible. Additionally, sophisticated carbon materials can be produced from biomass. Fuel cells with polymer electrolyte membranes can also support catalysts using carbon sources produced from biomass. The electrochemical and catalytic activity of the sensor is influenced by the surface shape, particularly by the pore volume, surface area, and pore size. In-depth analyses, assessments, and comparisons of the carbon-based materials and composites created from biomass will be made in this paper. Future research fields are recommended for real-world applications, and the accompanying technological challenges are highlighted. Nanocarbon materials are attractive for many electrochemical processes due to their integrated advantages. It is anticipated that the generation of bio-carbon from waste biomass will see a rapid increase in scientific and industry interest in the future years. Biomass-derived carbonaceous nanoparticles have the potential to be used in gas sensors, fuel cells, bioimaging, drug delivery, carbon fixation, and catalysis. This article has discussed these nanoparticles' brand-new and cutting-edge energy storage and conversion capabilities. The remaining challenges, viewpoints, and future research directions are then discussed.

Keywords: Sensors, Biomass, Carbon precursors, Regeneration, Biomass resources, Environmentally friendly

1. Introduction

Recent studies have indicated that biomass, such as waste materials, cereals, landfill gas, wood, and alcohol fuels, can provide significant environmental benefits, such as reducing greenhouse gas emissions. This category contains organic goods made from plants or animals [1]. Three essential components make up biomass: cellulose, lignin, and hemicellulose. In lignocellulosic biomass, cellulose molecules make up 35 to 50% of the material [2,3]. Critical environmental problems are created when agricultural waste and forest residue are frequently burned or thrown outside [4]. Utilizing biomass is the most excellent solution for this issue, which is projected to be a global issue [5]. This method could turn biomass waste into good carbon-based goods for the environment (Fig. 1).

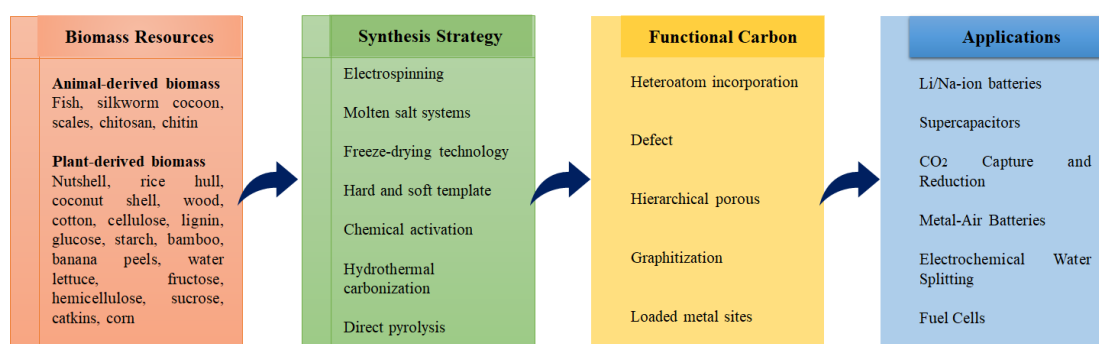


Fig. 1. Applications for porous carbonaceous materials.

Because of its unique qualities, biomass is a reliable substance. Unlike standard materials, it also has a homogeneous structure that reaches the nanoscale [6]. Because of the unique characteristics of biomass, carbon-based products can offer superior qualities. It has been discovered that there is a solid and consistent association between the electrochemical characteristics of porous carbon composites made from biomass and their structural features [7]. For electrochemical applications, porous carbon composites from biomass are extensively researched [8–10]. Recent research suggests that the electrochemical activity of absorbent materials may be enhanced. Recent research has focused on improving the electrochemical efficiency and electrocatalytic training of biomass's readily available carbon molecules. Heteroatom doping is a versatile method for enhancing electrochemical sensing capability. The metal-sulfides promote electrolyte penetration and ion diffusion when joined to carbonaceous biomass materials with interconnecting porous channels.

When nanoparticles are utilized as modifiers, these nanoparticles improve electron transport while also boosting the electrode's sensitivity to various analytes [11–16] (Fig. 2).

The most recent study is thoroughly summarised in this report. Biomass-derived carbonaceous compounds are used in electrochemical sensing. It begins by outlining the steps necessary to transform biomass into carbon molecules. The review focuses on the potential of carbonaceous biomass-derived materials for electrochemical sensing applications. This review emphasizes the right choice of carbon precursors generated by biomass. This separation makes it simpler for readers to evaluate and understand how each of the target analytes stated above is sensed using carbon compounds obtained from biomass.

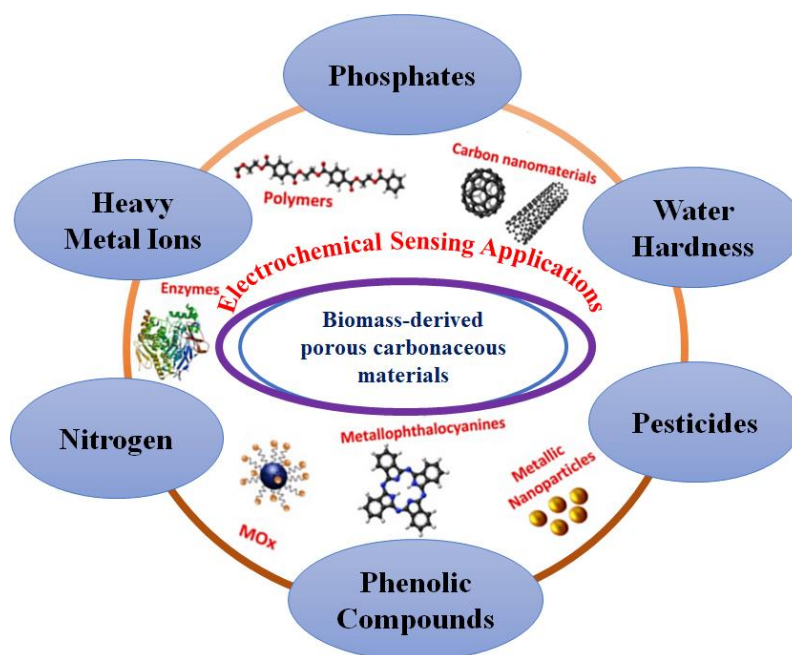


Fig. 2. Porous carbonaceous compounds for electrochemical applications.

Estimates place the production of biomass waste at 10–15 billion tonnes annually. However, most of them are not effectively recycled, especially agricultural wastes, which farmers frequently burn. This reduces the efficiency of biomass by 20% and increases environmental pollution [17]. Biomass is a natural resource that makes up most of nature and is a rich supply of carbon. As a result, biomass waste and carbon-based biomaterials have been employed to produce electricity recently. Carbon materials offer a plethora of uses due to their magnetic properties, including electrocatalytic solid performance, superior structural stability, and low background current [18-21]. Functional materials can be used to solve a variety of environmental and energy issues [22-24]. Supercapacitors and biocarbon are two adsorbents for organic and heavy metal pollutants that have been the subject of extensive research over the past few decades. Despite their apparent importance, there are still opportunities for their use in higher aggregate value technologies, such as sensors and batteries, which have not been

thoroughly explored. Recently, researchers have taken a particular interest in enhancing the crucial properties of biocarbon so that it can function well in these applications.

There is still room for advancement in the production of devices, electrodes, and electrode materials. The industry encounters several challenges, such as high manufacturing costs, adverse environmental effects, and poor efficiency. To enhance material qualities, novel, strong electrode materials must be manufactured or created that are affordable and have high chemical stability—synthetic carbon-based materials. Therefore, creating readily available, durable, and scalable functional materials based on carbon is crucial (Fig. 3).

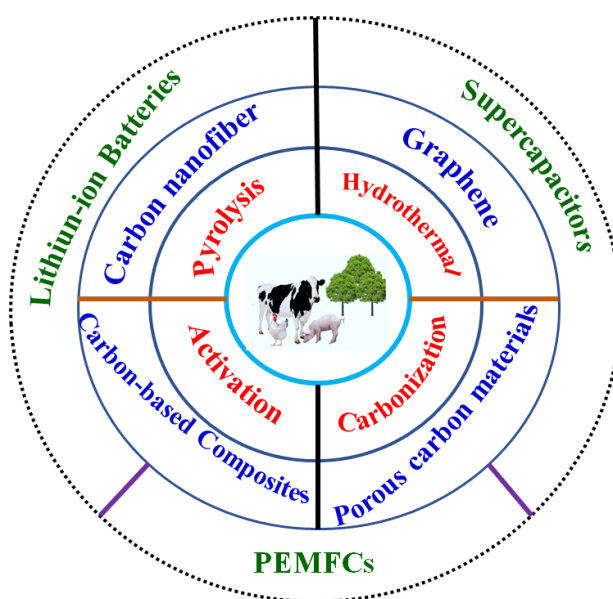


Fig. 3. Potential application of carbon-based materials.

2. Wastes and their effects

Industrial waste and biomass waste are the two different categories of waste materials. Fig. 4 depicts a sample of waste material. In addition to carbon nanotubes, nanosheets, and metallic nanoparticles, scientists have also created NMs from biological and industrial waste. Due to the variety of wastes, researchers have used various pre-treatment techniques in the methodology listed. We have covered several methods for producing the final product following sample preparation.



Fig. 4. Nanomaterials production using industrial wastes.

2.1 Biological Waste (Biowaste)

To develop, grow, and reproduce, plants create primary metabolites [25], but many plant families have secondary metabolites. Secondary metabolites frequently help plants defend themselves against herbivores and other interspecies pests. Additionally capable of reducing and chelating metal ions into nanoparticles are flavonoids, flavones, flavanones, and chalcones. Enols go through tautomeric processes to create reactive hydrogen atoms and nanoparticles known as keto-forms, which can be employed to lower metal ions and reactive hydrogen atoms. Various flavonoids are present in biomass waste formed from fruit residues, which may one day be exploited to make NPs. Through the involvement of biomolecules, a bioreduction process produces metallic nanoparticles. In the presence of redox enzymes and metabolites, many cations are reduced to metallic zerovalent NPs. It is also possible to create metallic nanoparticles of varying sizes using various plant parts.

2.2 Industrial wastes

Batteries, plastics, tyres, and other industrial by-products have all been used to create NMs. A more environmentally beneficial type of recycling might be NM manufactured from various industrial wastes. One of the best methods to handle the massive volume of trash is recycling old lead batteries. In the presence of poly(N-vinyl-2-pyrrolidone), Zhou et al. 2017

[26] employed the thermal breakdown approach to produce submicron-sized lead oxide particles (PVP). PbO and metallic lead were mixed during a three-hour, 350 °C calcination procedure. The submicron region of particle size is decreased by PVP. The procedure produces much dust and SO₂ emissions and consumes energy. High Zn exposure reduces calcium absorption, causing the body's calcium levels to drop. Recycling Zn from Zn-Mn battery waste conserves resources and prevents dangerous chemicals from entering the environment.

Numerous studies have been done on recycling Zn-Mn battery wastes to create various nanomaterials [27]. The solvent can later be recovered by evaporation. Lithium salts are frequently hydrolyzed by water, but they become thermally unstable beyond 80 °C. Thus, the evaporation temperature should stay within that. Different recycling techniques have already been proposed [28]. Non-biodegradable plastic bags, cutlery, and water bottles continue to make up a sizable portion of solid waste. From waste polyethylene terephthalate, multi-walled carbon nanotubes (MWCNT) and nano-channeled ultrafine nanotubes were produced using a novel catalyst- and solvent-free arc discharge method. Around one billion million trash tyres are produced worldwide each year. Tire rubber has been burned or deposited in landfills in massive amounts, which has seriously harmed the ecosystem [29]. Because of this, disposing of tyres in landfills is prohibited in many countries, particularly in Europe [30]. It would be ideal for developing new methods for recycling rubber tyre debris. Tire trash contains a substantial amount of zinc, which leads to the claim that tyres are employed in producing Zn NPs. Broken lead-containing glass may leak some lead if there is acidic leachate in landfills. Therefore, it is not easy to extract all the information from funnel glass using conventional leaching processes.

2.3 Waste-derived NMs

Waste-derived NMs are effective in all their applications, from bioimaging to environmental remediation. Understanding and weighing the adverse effects of nanomaterials is crucial for ecological safety. There needs to be more information on what will occur or how these ENMs will behave after they are introduced into the environment. As more nanotechnology applications are created, more nanoscale materials will enter the waste stream. In contrast to conventional municipal solid trash, nano waste behaves differently. Incineration facilities treat wastes, some of which may contain nanomaterials to an unknown extent. The current frameworks for technology and law are inadequate to handle these nano-waste substances. Some specialists claim ENMs represent a new class of contaminants that must be closely watched throughout the waste-treatment process [31]. Their possible adverse effects on

human health have yet to be fully understood. People appear at risk from threats posed by nano waste, from shallow to potentially harmful hazards at low exposure levels. Given the rapid growth of ENMs in the global market, developing research programs in nanotoxicology is crucial. To create nano waste management, further investigation is required into how NM use affects the environment. Additionally, this might help with cancer and carcinogenesis. Sunscreens' TiO₂ content may be to blame for the brain damage seen in rats, claim Long et al. [32]. CNTs can cause cell senescence, necrosis, and apoptosis in macrophage cell lines. Examining the toxicological effects of ENMs in light of the current circumstances is a great idea to understand or anticipate their environmental impacts correctly. Only a tiny percentage of the ENMs in recycled products will be used again in manufacturing and processing. Because their non-recyclable components will either be landfilled or incinerated, recycling can only sometimes be the ENMs' final destination. Specific characterization techniques must be met to create nano-enabled materials from conventional trash. Examining the data, as mentioned earlier, highlighted the end-of-life nanoproducts' safe-by-design qualities [33]. An analysis of the presence and effects of ENMs in various waste products is shown schematically in Fig. 5.



Fig. 5. ENMs in various waste products and their impact on living systems.

3. Synthesis method

3.1 Waste sample preparation

Pre-treating the material correctly is the initial step in creating NMs from waste. Researchers have developed a range of procedures to prepare samples for testing. Pre-treatment methods are divided into physical, chemical, and combination categories to make them easier to grasp.

3.1.1 Physical pretreatment

Chemicals are not used during the physical preparation process. The conventional and controllable techniques applied to the reactants during biological pre-treatment using a mortar and pestle are milling and grinding. These operations are called "milling" in ball mills, and this straightforward instrument is called "grinding." Ball milling parameters, including duration and energy input, can be managed to provide repeatable outcomes [34]. Ball mills are utilized for particle refining, deagglomeration, and microorganism cracking. Between 0.1 and 1%, energy efficiency was predicted by Ocepec et al. in 1986. Ball mills are used for bench-scale organic chemical synthesis because they mechanically activate solid reactants. Ball milling has also been used as a pre-treatment method to create nanomaterials from industrial wastes.

For instance, Zn NPs were produced utilizing the ball milling technique using scrap tyres from the rubber sector [29]. The discarded tyres were first to cut into 10 cm pieces after the metal wire was removed, and then the particle size was further reduced. The particles were sized down in rolling mills, and the stainless steel was sifted through.

3.1.2 Chemical pretreatment

Chemical pretreatment's main objective is to remove any contaminants from the waste sample that might become soluble by heating or chemical treatment. Strong acid hydrolysis is a standard method for treating waste materials. It involves using concentrated acids such as HNO₃, HCl, and H₂SO₄. The pH of the solution was then kept alkaline by adding an ammonia solution. Li et al. (2016) [35] created -Fe₂O₃ nanoparticles by dissolving waste ferrous sulphate from titanium dioxide in distilled water. Using water for pre-treatment is not necessary to increase the cost of the process by adding hazardous chemicals like ammonia, sulfuric acid, or lime. The price of the actual ingredients must be increased to account for the expense of extracting or neutralizing these compounds. Expanded polystyrene (EPS) can be utilized to create nano- and macroparticles, according to Mangalara et al. [36]. The solution was made by mixing powdered polyvinyl alcohol with water heated to 70°C. Polyvinyl alcohol was dissolved after 6 hours of constant stirring. The production of polystyrene NPs using the emulsification-diffusion process was continued using these samples.

3.1.3 Combined pre-treatment

Chen et al. [37] used physical and chemical processes to recycle waste elm samaras. They collected various dried elm and samara species to make nanosheets. Waste elm samaras were first given a KOH treatment before being baked at 70 °C to dry them. Using NaOH increases pretreatment and chemical costs while also increasing anaerobic digestion efficiency. Pretreatment with alkaline has mild conditions, but it takes longer to react. The addition of oxygen or air to the reaction mixture, in particular, can improve the delignification process for highly lignified materials [37]. The fermentation process can then be inhibited by converting lignin into carboxylic acids. They must therefore be neutralized or obliterated. Oxidation may affect the lignocellulose complex's hemicellulose component.

3.2 Diversity and evolution of electrodes based on biomass-derived carbon

Developing suitable carbonaceous electrode materials for sensing has received the majority of research attention in recent years (carbon quantum dots-CQD). To produce green synthetic carbonaceous materials, biomass was exploited since it is cheap, durable, and diverse. Furthermore, some researchers have been able to explore the potential uses of carbon precursors derived from biomass in electrochemical sensing. Soon, we'll be able to assess how far these fundamental and applied scientific projects have gone. Studies have shown that various bio-wastes are used to create biomass-derived carbonaceous materials. Compared to conventional carbonaceous materials, these materials show excellent activity. The seeds of *Cassia fistula* naturally include Ca, Mg, and K, which function as pore makers and give the seeds a characteristic appearance [38]. Researchers have also studied several biomass precursors because they are readily available and reasonably priced.

In addition, because of their unusually porous architectures, chia seeds, kiwi skin, and almond shells have been suggested as predecessors. The chosen bio-precursor can produce carbon nanoparticles with improved surface shape and customizable porosity. The modifications would improve the carbon electrodes' sensitivity to electrochemical sensing and boost the selectivity of the biomass (Fig. 6).

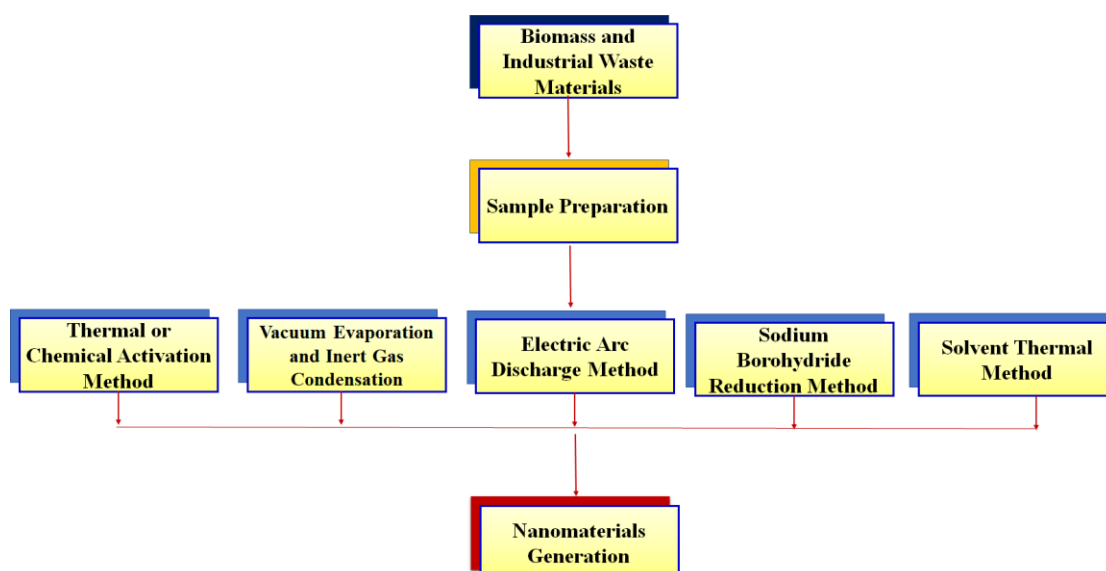


Fig. 6. Methods utilized to produce several nanomaterials from waste materials

4. Biomass-derived porous carbonaceous substances

4.1 Synthesis of carbon compounds

4.1.1 Pyrolysis of Biomass

The main goal of this process is to produce beneficial conjugated carbons. Hemicellulose, lignin, and cellulose are the three primary components of biomass. These materials undergo many chemical processes when they are treated. Between 315 and 400 °C, lignin undergoes pyrolysis, and as the temperature rises, its temperature range widens. This method improves the pore structure of these porous carbons by pyrolyzing them with various precursor activators, including KOH, ZnCl₂, and K₂CO₃ [39,40]. Although the process stages are straightforward to follow, it is challenging to comprehend how the reaction environment works due to its complexity.

4.1.2 Hydrothermal carbonization

This thermochemical method is most frequently used to create porous carbon compounds from biomass. The primary natural resources used as carbon precursors include carbohydrates, agricultural waste, unprocessed plants, and forestry byproducts. The breakthrough in this field occurred in 1913 when Bergius transformed cellulose into a material resembling coal [41]. Various porous and highly surface-area carbonaceous materials are produced with the help of high-temperature HTC. Systematic reviews are provided by Deng et al. (2016) [42] and detail several forms of HTC. This approach is advantageous because it employs less dangerous chemicals, enables temperature-dependent shaping of carbonaceous

materials, and is simple to apply [43,44]. The main disadvantage of HTC is that it produces large carbon particles that shouldn't be used as electrode materials.

4.1.3 Ionothermal Carbonization

The production of porous carbon products from biomass requires using ionic liquids (IL), which are crucial due to their improved thermal stability and low solvent volatility [45]. These properties increase ion transit and make electrode surfaces more active [46]. ITC is an excellent supplementary method since the used solvent (IL) can be recovered and used directly. The use of ILs is advantageous in the production of porous carbonaceous materials. However, the industry cannot use them due to their prohibitive price [47].

4.1.4 Carbonization of Molten Salt

This technique is better than ITC and HTC since those methods require high temperatures to create well-defined pore architectures and strong electroconductivity. MSC is performed warmly and doesn't require aftercare [42]. Because they strongly accelerate activity on lignin, cellulose, and other massive macromolecules, molten salts are used in MSC. The difficulty of MSCs pinpointing the exact course of the mechanism is one of their drawbacks.

4.1.5 Template-assisted synthesis

Template-assisted synthesis can enhance the physical and chemical processes that lead to pore creation by employing templates to induce pore emergence during carbonization. An N-P co-doped mesoporous carbon has been produced by carbonizing an egg yolk using SiO₂ as a rigid template [48]. These complicated templates are challenging to remove after the carbonization procedure because they could alter the material's architecture during the restoration phase. Surfactants and block copolymers are soft templates that are straightforward to withdraw after the carbonization process. One significant disadvantage of the smooth template-assisted synthesis is that it cannot carbonize at high temperatures because the slick template is unstable—the multi-step, expensive template-assisted synthesis process. Biomass pyrolysis and hydrothermal carbonization are the two main methods for generating carbonaceous chemicals from biomass for electrochemical sensors [49].

4.2 Electrochemical sensors applications

4.2.1 Detection of pharmaceutical drugs

Drugs can have positive and negative effects on the host, depending on the medication, dosage, and recipient. Although medicinal drugs are essential to humans, trace levels of dangerous substances shorten their shelf life and reduce efficacy. These hazardous drugs alter

the human body's metabolic pathways in undesirable and occasionally irreversible ways. However, a narcotic overdose may result in medical problems such as liver necrosis and renal failure [50,51]. ZnCl₂ and the KC-designated product were combined for pyrolysis at 700°C. After that, it underwent pyrolysis at 800°C, yielding ZKAKC. The ZKAKC-modified electrode showed more electrocatalytic activity than the other electrodes when the CV plots of the peak current were evaluated. This was because it had the most exceptional value. The surface area was determined using the Randles-Sevcik equation below (1). The formula was often used in published methods to determine the electrode's carbon-modified electrode generated from biomass' electrochemical surface area.

$$I_p = 2.69 \times 10^5 \times A D^{1/2} n^{3/2} v^{1/2} C \quad (1)$$

A schematic representation of the electrochemical uses of bio-carbon nanoparticles is shown in Fig. 7.

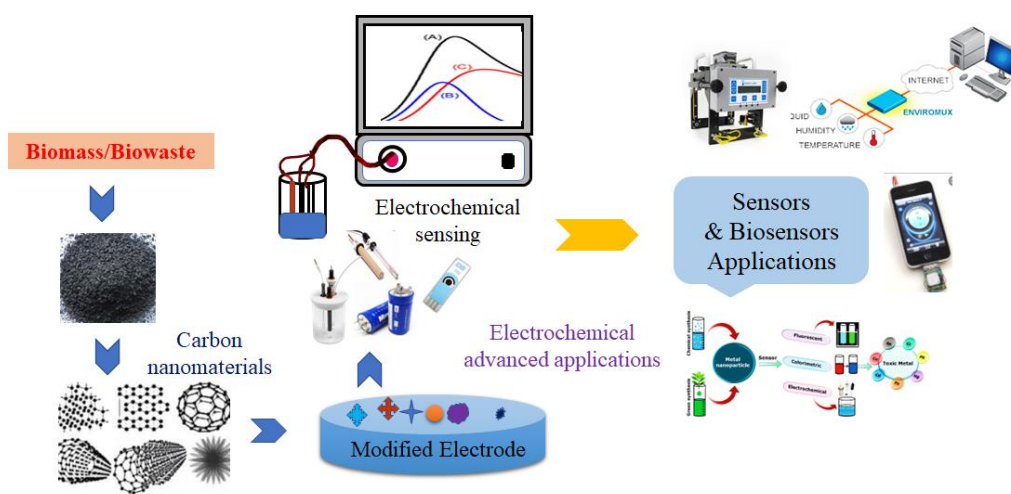


Fig. 7. Application of bio-carbon nanomaterials for electrochemical applications.

4.3.2 Detection of metal ions

Trace amounts of metal ions, often known as heavy metals, are highly hazardous because they have the propensity. Among the many techniques, electrochemical sensing was the most effective way to find these heavy metal ions. Maize powder was used to create the precursor to carbon. KOH and corn powder were combined to form a homogenous suspension in Milli-Q water, which was then baked at 105 °C for 12 hours to dry. In an inert environment using a tube furnace, the product was warmed to 500 °C. At various temperatures, the solution mentioned above underwent complete pyrolysis. The surface morphology and electrochemical characteristics of the electrodes used to detect metal ions are shown in Table 1 [52].

Table 1. Carbon materials comparison based on their electrochemical parameters and surface morphology.

4.3.3 Biomolecule detection

The compounds found in cells and other living things are called biomolecules. They can be of many sizes and types, and they engage in a range of activities. Both enzymatically and non-enzymatically, glucose can be found electrochemically. The bare electrode was subsequently produced by Qu et al. utilizing a drop casting process using nanoflower-shaped porous carbon from roses decorated with cobalt-sulfide (CoS). The rose's porous carbon skeleton had interconnected channels that improved electron and mass transmission. The non-enzymatic method was deemed useless because of its low selectivity (Fig. 8).

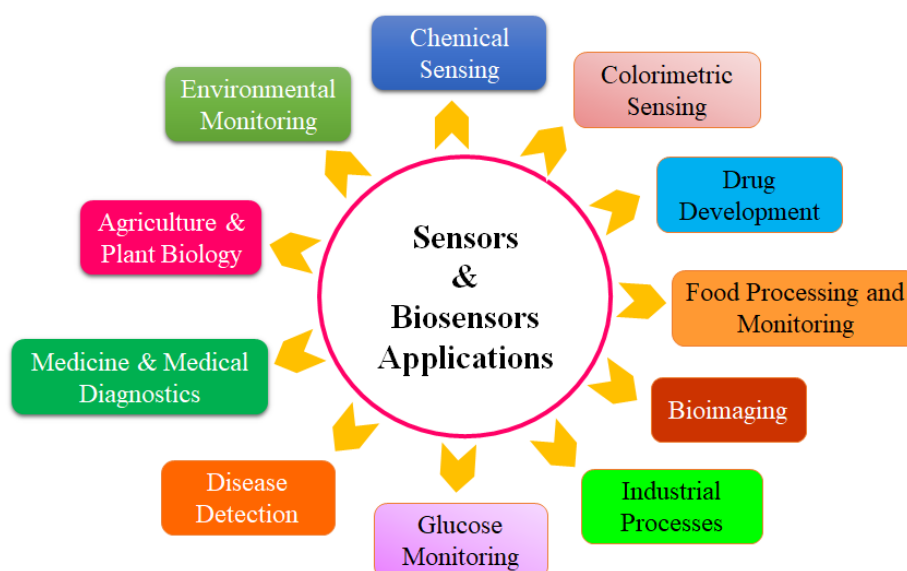


Fig. 8. Applications of biomass-derived carbon nanoparticles in various fields.

4.3.4 Detecting food contaminants

According to the WHO, food additives, due to their detrimental impact on human health, are preferable that food products not include nitrites above-permitted levels [65]. Despite this, nitrosamines, a class of chemicals associated with cancer, are produced from nitrites [66]. Yallappa et al. (2018) [13] made mesoporous carbon nanospheres from Areca nuts using a simple and clean catalytic pyrolysis process. The material's stability, repeatability, and reusability allowed for higher electrochemical performance. The tree bark was heated to temperatures of 700 °C, 800 °C, or 900 °C and carbonized.

Electrode material	Type of analyte		Biomass materials	Synthesis method	Surface properties			Electrochemical parameters			References
					BET surface area (m ² g ⁻¹)	Pore volume (cm ³ g ⁻¹)	BJH pore size (nm)	Linear range (μM)	LOD (M)	Sensitivity (μA μM ⁻¹ cm ⁻²)	
Pt-Re NPs/PAC	Pharmaceutical Drugs	Furazolidine	Cassia fistula fruit	Pyrolysis & Activation	1088	1.03	0.8-3.6	1-299	0.075	5.52	[38]
N, S, P-PC		Chloramphenicol	Elaeagnus gum	Pyrolysis & Hydrothermal carbonization	-	-	-	1-40 50-500	0.01	-	[51]
Bi/PC	Metal ions	Lead Cadmium	Corn powder	Precarbonization & Activation	244.42	0.41	3.-10	0.5x10 ⁶ - 10x10 ⁶ 10x10 ⁶ - 100x10 ⁶	1.72x 10 ⁶ 1.58x 10 ⁶	-	[52]
NPC		Lead	Almond shells	Hydrothermal carbonization & Activation	1075	-	2	2-120	0.7	-	[53]
AC	Bio-molecules	Ascorbic acid (AA) Dopamine (DA) Uric acid (UA)	Pumpkin stem	Hydrothermal carbonization & Activation	793	-	-	- - -	2.3 0.03 0.51	7.6 6.3 6.1	[54]
N-CD	Food Additives	Nitrite	Kiwi and sesame seeds	Pyrolysis	-	-	-	1.2-4.9	0.23	-	[58]
TBAC		Vanillin	Cajeput bark	Pyrolysis & Activation	1234	0.75	4.0	5-1150	0.68	-	[59]
AC	Pollutants	4-Nitrophenol	Mango leaves	Hydrothermal Carbonization & Activation	1555	-	-	1-500	0.16	5.810	[60]
NDC CQD		Bisphenol A Hydrazine	Bamboo fungi Chia seeds	Pyrolysis Hydrothermal Carbonization	1895.5 0.251 x 10 ⁻²	- -	- 2-6	1-50 -	1.068 39.7	- 151.5 x10 ³	[61] [55,56]
PAC/AuNP	Flavonoids	Rutin	Peanut shell	Hydrothermal Carbonization & Activation	2484	1.31	2.68	0.0002-1	2	128.2	[62]
Pt-BPC/CILE		Luteolin	Wheat flour	Hydrothermal Carbonization & Activation	0.434 x 10 ⁻²	-	-	0.008-100	2.6	-	[57]

GPAC		Catechin	Bougainvillea flower	Hydrothermal Carbonization & Activation	1197	0.51	1.72	4-368	0.67	7.2	[63]
OPL-CNP		Butein	Oil palm leaves	Pyrolysis	-	-	-	10-100	7.6	-	[64]

4.3.5 Pollutants detection

Substances made of carbon from biomass have become quite common in the electrochemical detection of these contaminants. Plants and other living things are irreparably harmed by anthropogenic toxins, such as those produced using phenol-based compounds in the chemical and pharmaceutical industries. According to reports, two chemicals can be detected electrochemically: 4-NP and BPA. Madhu et al. (2014) [60] created a biomass-based activated carbon (AC) with remarkably consistent production and beneficial uses. To locate 4-Nitrophenol, this chemical was employed to make an electrode (4-NP).

4.3.6 Detection of flavonoids

The majority of flavonoids have physiological and medicinal effects [67]. Electrodes treated with noble metal nanoparticles exhibit platforms that operate exceptionally well catalytically, transport electrons quickly, and exhibit considerable surface plasmon resonance [68,69]. The modified electrode could detect luteolin at concentrations between 0.008 and 100.0 mmol/L with a linear concentration-response. The biomass-derived carbon source with the most extensive surface area and optimum sensitivity were provided by peanut shells. It is also evident that carbon electrode materials with heteroatom doping and metal nanoparticle distribution have better electrochemical characteristics.

5. CDs-based colorimetric and fluorometric sensors

Many materials exhibit varying capacities for light absorption, reflection, and transmission when exposed to light due to differences in their macroscopic and microscopic composition. Growing interest has been generated by its reasonable pricing, rapid examination, and clear findings [70]. In reality, because most compounds have low extinction coefficients, it is more difficult to discriminate between variations in concentration based solely on color [71]. The highest interest has been shown in CDs as a high-quality carbon nanomaterial type. When creating a CM sensing scheme, they can be used in place of conventional chromogenic agents and combined with additional chromogenic agents to enhance CM sensor performance. When creating dual-response probes, other optical properties of CDs can also be taken into

account to improve the dependability of the sensing system. Pesticide detection via optical and photoelectric colorimetry has grown in importance as a research topic for CDs-based CM sensors in recent years. Utilizing a dispersive liquid-liquid microextraction approach and tri octyl methylammonium chloride as a dispersant agent, a novel absorbance sensor for fenitrothion detection was created in 2017 based on the inherent CM property of CDs. Due to their interaction with fenitrothion, the unmodified CDs enriched in the organic phase recorded enhanced absorption signals that were used to quantify fenitrothion. In contrast to a single response, the results of many signals can be mutually evaluated to provide enhanced accuracy in the CM detection of pesticides. It was easier to identify and determine the increased pesticide dosage because of the more apparent decrease in B, N-CD fluorescence intensity with higher methyl-paraoxon concentrations.

6. Conclusion and future perspectives

Biomass has been converted into biomaterials and sustainable energy alternatives thanks to recent biotechnology, industrial chemistry, engineering, and genetics developments. Biomass-produced materials, composites, and assemblies now have a wide range of new architectures, features, qualities, and uses thanks to nanotechnology. There could be environmental effects from these nanoparticles. Biomass-derived nanoparticles' possible adverse effects on health have not yet been determined. From biomass, absorbent carbon compounds have been made using various techniques. This platform enables the development of portable electrochemical sensors because of its low cost, distinctive structure, environmentally friendly manufacturing methods, and renewable nature. Although there has been much research in this field, there is still room to enhance the development procedure, comprehend how changed electrodes function, and build more reliable, eco-friendly, cost-effective, and selectively modified electrodes.

The continued creation of ONOO—specific fluorescent probes will soon enable more applications in the biochemical and therapeutic sectors. Other response patterns besides those already described will also be looked at to design ONOO- inquiries with better sensitivities and biocompatibilities. The need for improved ONOO- detectors will dramatically rise as other diseases linked to ONOO- are discovered in the coming years. The employment of CD characterization methodologies for blind sensing occasionally occurs due to their incompleteness. There are few comprehensive guides available for CD purification methods. For the creation of optical sensors, CD purification is essential after synthesis. Because of the enormous variety, complex compositions, and distinctive features of CDs, it is more

challenging to make significant purification progress. In the restricted investigation, CDs were heavily utilized in the luminescence mechanism for pesticide detection. Even though phosphorescent and long-lasting CDs are becoming more common, their optical signals are only helpful in steady conditions. Since they are substantially quenched in solutions, optical sensing cannot be fully utilized.

Nanomaterials made from biomass have greatly improved electrochemical sensing properties. However, issues still need to be fixed. Therefore, by conducting additional research in this topic area, it would be able to build mobile electrochemical sensors to identify dangerous contaminants. The popularity of carbon-based electrochemical sensors made from biomass has increased dramatically in recent years. However, these sensors still need to develop into flexible, portable detectors. It might also be improved to produce intelligent, functional machines that would become the norm in this sector.

Our study focused on the most recent advancements in biomass carbon nanoparticles. The key developments in this field and its projected future are listed below. Biomass-derived NMs have demonstrated a favorable response to numerous chemical species' inaccurate sample analysis. It is also challenging to improve selectivity and sensitivity. Recently, scientists have studied how functional groups impact CDs' surfaces. To provide sensitive materials for diverse target detection applications, the nature of CDs may be altered with particular ligands. For instance, a specific probe for detecting glucose was made of CDs modified with boric acid groups. Furthermore, by mixing biomass CDs with other functional materials, the sensing applications of these devices can be increased. Using waste materials also makes it possible to create CDs on a large scale. Additionally, CDs created from biomass have similar performance to CDs created through chemical synthesis that can meet the analysis required in terms of LODs, recoveries, RSDs, and other metrics.

Detecting chemicals and biological agents are essential in medical, industrial, and environmental research. Because of their unique qualities, nanoparticle materials are beneficial for developing new sensors and improving the sensitivity and selectivity of existing ones. It also discusses the recent development of NP-supported electrochemical detecting sensors. They are promising materials for electrochemical sensing due to their advantages over the previously used techniques. An efficient platform is provided by combining traditional procedures that require intricate apparatus and time-consuming protocols. The electrochemical sensors are delicate and prone to error. They can be used simultaneously with numerous analytes. It is common practice to measure biological and environmental analytes using

portable devices. For commercialization, it is essential to develop effective sensors with mass production, system integration, and reusability. This work has highlighted cutting-edge research on NPs generated from biomass and their potential applications in several industries. We briefly addressed the primary production processes for NM and their categorization. It was thoroughly investigated whether NMs made from waste could effectively treat waste and wastewater.

References

- [1] S.H.Y.S. Abdullah, N.H.M. Hanapi, A. Azid, R. Umar, H. Juahir, H. Khatoon, A. Endut, A review of biomass-derived heterogeneous catalyst for a sustainable biodiesel production, *Renewable Sustainable Energy Rev.*, 70 (2017) 1040-1051.
- [2] J.P.H. Wyk, *Biowaste as a Resource for Bioproduct Development, Survival and Sustainability* (2011).
- [3] C.B. Field, M.J. Behrenfeld, J.T. Randerson, P. Falkowski, Primary production of the biosphere: integrating terrestrial and oceanic components, *Science* 281(5374) (1998) 237-240.
- [4] J. Cui, Y. Xi, S. Chen, D. Li, X. She, J. Sun, W. Han, D. Yang, S. Guo, Prolifera-Green-Tide as Sustainable Source for Carbonaceous Aerogels with Hierarchical Pore to Achieve Multiple Energy Storage, *Adv. Funct. Mater.*, 26(46) (2016) 8487-8495.
- [5] D.S. Kosson, H.A. Van der Sloot, T. Eighmy, An approach for estimation of contaminant release during utilization and disposal of municipal waste combustion residues, *J. Hazard. Mater.*, 47(1-3) (1996) 43-75.
- [6] Y. Zhang, X. Liu, S. Wang, L. Li, S. Dou, Bio-nanotechnology in high-performance supercapacitors, *Adv. Energy Mater.*, 7(21) (2017) 1700592.
- [7] J. Cheng, Y. Li, J. Zhong, Z. Lu, G. Wang, M. Sun, Y. Jiang, P. Zou, X. Wang, Q. Zhao, Molecularly imprinted electrochemical sensor based on biomass carbon decorated with MOF-derived Cr₂O₃ and silver nanoparticles for selective and sensitive detection of nitrofurazone, *J. Chem. Eng.*, 398 (2020) 125664.
- [8] Z. Bi, Q. Kong, Y. Cao, G. Sun, F. Su, X. Wei, X. Li, A. Ahmad, L. Xie, C.-M. Chen, Biomass-derived porous carbon materials with different dimensions for supercapacitor electrodes: a review, *J. Mater. Chem. A* 7(27) (2019) 16028-16045.

- [9] B. Dakshayini, K.R. Reddy, A. Mishra, N.P. Shetti, S.J. Malode, S. Basu, S. Naveen, A.V. Raghu, Role of conducting polymer and metal oxide-based hybrids for applications in amperometric sensors and biosensors, *Microchem. J.*, 147 (2019) 7-24.
- [10] S.J. Malode, K. Prabhu, B.G. Pollet, S.S. Kalanur, N.P. Shetti, Preparation and performance of WO₃/rGO modified carbon sensor for enhanced electrochemical detection of triclosan, *Electrochim. Acta*, 429 (2022) 141010.
- [11] S.J. Malode, K.K. Prabhu, N.P. Shetti, Electrocatalytic behavior of a heterostructured nanocomposite sensor for aminotriazole, *New J. Chem.*, 44(44) (2020) 19376-19384.
- [12] S.J. Malode, P.K. Keerthi, N.P. Shetti, R.M. Kulkarni, Electroanalysis of carbendazim using MWCNT/Ca-ZnO modified electrode, *Electroanalysis*, 32(7) (2020) 1590-1599.
- [13] S. Yallappa, M. Shivakumar, K. Nagashree, M. Dharmaprakash, A. Vinu, G. Hegde, Electrochemical determination of nitrite using catalyst free mesoporous carbon nanoparticles from bio renewable areca nut seeds, *J. Electrochem. Soc.*, 165(10) (2018) H614.
- [14] G. Manasa, A.K. Bhakta, J. Bafna, R.J. Mascarenhas, S.J. Malode, N.P. Shetti, An amperometric sensor composed of carbon hybrid-structure for the degradation of aminotriazole herbicide, *Environ. Res.*, 212 (2022) 113541.
- [15] G. Manasa, R.J. Mascarenhas, S.J. Malode, N.P. Shetti, Graphene-based electrochemical immunosensors for early detection of oncomarker carcinoembryonic antigen, *Biosens. Bioelectron.: X* (2022) 100189.
- [16] G. Manasa, R.J. Mascarenhas, N.P. Shetti, S.J. Malode, A. Mishra, S. Basu, T.M. Aminabhavi, Skin patchable sensor surveillance for continuous glucose monitoring, *ACS Appl. Bio Mater.*, 5(3) (2022) 945-970.
- [17] P. Liu, Y. Wang, J. Liu, Biomass-derived porous carbon materials for advanced lithium sulfur batteries, *J. Energy Chem.*, 34 (2019) 171-185.
- [18] E. Paone, T. Tabanelli, F. Mauriello, The rise of lignin biorefinery, *Curr. Opin. Green Sustain. Chem.*, 24 (2020) 1-6.
- [19] W. Tang, Y. Zhang, Y. Zhong, T. Shen, X. Wang, X. Xia, J. Tu, Natural biomass-derived carbons for electrochemical energy storage, *Mater. Res. Bull.*, 88 (2017) 234-241.
- [20] K. Prabhu, S.J. Malode, R.M. Kulkarni, N.P. Shetti, Electro-sensing base for hazardous pesticide 2, 4-DCP and its quantification in real samples at ZnO@ Cu core-shell

- nanoparticles in the presence of cationic surfactant, *Mater. Chem. Phys.*, 278 (2022) 125705.
- [21] K. Prabhu, S.J. Malode, N.P. Shetti, R.M. Kulkarni, Analysis of herbicide and its applications through a sensitive electrochemical technique based on MWCNTs/ZnO/CPE fabricated sensor, *Chemosphere* 287 (2022) 132086.
- [22] F. Zheng, D. Liu, G. Xia, Y. Yang, T. Liu, M. Wu, Q. Chen, Biomass waste inspired nitrogen-doped porous carbon materials as high-performance anode for lithium-ion batteries, *J. Alloys Compd.*, 693 (2017) 1197-1204.
- [23] A. Mishra, A. Mehta, S. Basu, S.J. Malode, N.P. Shetti, S.S. Shukla, M.N. Nadagouda, T.M. Aminabhavi, Electrode materials for lithium-ion batteries, *Mater. Sci. Ener. Technol.*, 1(2) (2018) 182-187.
- [24] K. Prabhu, S.J. Malode, N.P. Shetti, Highly sensitive electrochemical sensor for the detection and quantification of Linuron based on silica gel modified carbon paste electrode, *Environ. Technol. Innov.*, 23 (2021) 101687.
- [25] E. Pichersky, D.R. Gang, Genetics and biochemistry of secondary metabolites in plants: an evolutionary perspective, *Trends Plant Sci.*, 5(10) (2000) 439-445.
- [26] H. Zhou, M. Su, P.-H. Lee, K. Shih, Synthesis of submicron lead oxide particles from the simulated spent lead paste for battery anodes, *J. Alloys Compd.*, 690 (2017) 101-107.
- [27] X. Xiang, F. Xia, L. Zhan, B. Xie, Preparation of zinc nano structured particles from spent zinc manganese batteries by vacuum separation and inert gas condensation, *Sep. Purif. Technol.*, 142 (2015) 227-233.
- [28] C.K. Lee, K.-I. Rhee, Reductive leaching of cathodic active materials from lithium ion battery wastes, *Hydrometallurgy* 68(1-3) (2003) 5-10.
- [29] S. Moghaddasi, A.H. Khoshgoftarmanesh, F. Karimzadeh, R.L. Chaney, Preparation of nano-particles from waste tire rubber and evaluation of their effectiveness as zinc source for cucumber in nutrient solution culture, *Sci. Hortic.*, 160 (2013) 398-403.
- [30] P. Turgut, B. Yesilata, Physico-mechanical and thermal performances of newly developed rubber-added bricks, *Energy Build.*, 40(5) (2008) 679-688.
- [31] M.-A. Marcoux, M. Matias, F. Olivier, G. Keck, Review and prospect of emerging contaminants in waste—Key issues and challenges linked to their presence in waste

- treatment schemes: General aspects and focus on nanoparticles, *Waste Manag.*, 33(11) (2013) 2147-2156.
- [32] T.C. Long, N. Saleh, R.D. Tilton, G.V. Lowry, B. Veronesi, Titanium dioxide (P25) produces reactive oxygen species in immortalized brain microglia (BV2): implications for nanoparticle neurotoxicity, *Environ. Sci. Technol.*, 40(14) (2006) 4346-4352.
- [33] L. Heggelund, S.F. Hansen, T.F. Astrup, A. Boldrin, Semi-quantitative analysis of solid waste flows from nano-enabled consumer products in Europe, Denmark and the United Kingdom—abundance, distribution and management, *Waste Manag.*, 56 (2016) 584-592.
- [34] A. Stolle, T. Szuppa, S.E. Leonhardt, B. Ondruschka, Ball milling in organic synthesis: solutions and challenges, *Chem Soc Rev.*, 40(5) (2011) 2317-2329.
- [35] D. Li, J. Jia, Y. Zhang, N. Wang, X. Guo, X. Yu, Preparation and characterization of Nano-graphite/TiO₂ composite photoelectrode for photoelectrocatalytic degradation of hazardous pollutant, *J. Hazard. Mater.*, 315 (2016) 1-10.
- [36] S.C.H. Mangalara, S. Varughese, Green recycling approach to obtain nano-and microparticles from expanded polystyrene waste, *ACS Sustain. Chem. Eng.*, 4(11) (2016) 6095-6100.
- [37] C. Chen, D. Yu, G. Zhao, B. Du, W. Tang, L. Sun, Y. Sun, F. Besenbacher, M. Yu, Three-dimensional scaffolding framework of porous carbon nanosheets derived from plant wastes for high-performance supercapacitors, *Nano Energy* 27 (2016) 377-389.
- [38] P. Veerakumar, A. Sangili, S.-M. Chen, A. Pandikumar, K.-C. Lin, Fabrication of platinum–rhenium nanoparticle-decorated porous carbons: Voltammetric sensing of furazolidone, *ACS Sustain. Chem. Eng.*, 8(9) (2020) 3591-3605.
- [39] M. Noked, A. Soffer, D. Aurbach, The electrochemistry of activated carbonaceous materials: past, present, and future, *J. Solid State Electrochem.*, 15 (2011) 1563-1578.
- [40] H. Yang, R. Yan, H. Chen, D.H. Lee, C. Zheng, Characteristics of hemicellulose, cellulose and lignin pyrolysis, *Fuel* 86(12-13) (2007) 1781-1788.
- [41] M.-M. Titirici, M. Antonietti, Chemistry and materials options of sustainable carbon materials made by hydrothermal carbonization, *Chem. Soc. Rev.*, 39(1) (2010) 103-116.
- [42] J. Deng, M. Li, Y. Wang, Biomass-derived carbon: synthesis and applications in energy storage and conversion, *Green Chem.*, 18(18) (2016) 4824-4854.

- [43] M.-M. Titirici, M. Antonietti, N. Baccile, Hydrothermal carbon from biomass: a comparison of the local structure from poly-to monosaccharides and pentoses/hexoses, *Green Chem.*, 10(11) (2008) 1204-1212.
- [44] S. Supriya, A. Divyashree, S. Yallappa, G. Hegde, Carbon nanospheres obtained from carbonization of bio-resource: a catalyst free synthesis, *Mater. Today: Proc.*, 5(1) (2018) 2907-2911.
- [45] P. Zhang, Y. Gong, Z. Wei, J. Wang, Z. Zhang, H. Li, S. Dai, Y. Wang, Updating biomass into functional carbon material in ionothermal manner, *ACS Appl. Mater. Interfaces*, 6(15) (2014) 12515-12522.
- [46] Y. Liu, B. Huang, X. Lin, Z. Xie, Biomass-derived hierarchical porous carbons: boosting the energy density of supercapacitors via an ionothermal approach, *J. Mater. Chem. A*, 5(25) (2017) 13009-13018.
- [47] S. Steudte, P. Stepnowski, C.-W. Cho, J. Thöming, S. Stolte, (Eco) toxicity of fluoro-organic and cyano-based ionic liquid anions, *Chem. Comm.*, 48(75) (2012) 9382-9384.
- [48] X. Dong, X. Liu, H. Chen, X. Xu, H. Jiang, C. Gu, Q. Li, S. Qiao, X. Zhang, Y. Hu, Hard template-assisted N, P-doped multifunctional mesoporous carbon for supercapacitors and hydrogen evolution reaction, *J. Mater. Sci.*, 56 (2021) 2385-2398.
- [49] S. Bilge, N.K. Bakirhan, Y.O. Donar, A. Sinag, S.A. Ozkan, E.Ş. Okudan, Green synthesis of carbon based biosensor materials from algal biomass for the sensitive detection of vardenafil, *J. Electroanal. Chem.*, 871 (2020) 114286.
- [50] J.R. Mitchell, R.J. McMurtry, C.N. Statham, S.D. Nelson, Molecular basis for several drug-induced nephropathies, *Am. J. Med.*, 62(4) (1977) 518-526.
- [51] G. Wang, X. Mamat, Y. Li, X. Hu, P. Wang, X. Xin, G. Hu, Highly sensitive electrochemical sensor for the detection of chloramphenicol based on biomass derived porous carbon, *Sci. Adv. Mater.*, 12(3) (2020) 376-382.
- [52] K.M. Zeinu, H. Hou, B. Liu, X. Yuan, L. Huang, X. Zhu, J. Hu, J. Yang, S. Liang, X. Wu, A novel hollow sphere bismuth oxide doped mesoporous carbon nanocomposite material derived from sustainable biomass for picomolar electrochemical detection of lead and cadmium, *J. Mater. Chem. A*, 4(36) (2016) 13967-13979.

- [53] Y. Baikeli, X. Mamat, N. Yalikun, Y. Wang, M. Qiao, Y. Li, G. Hu, Differential pulse voltammetry detection of Pb (ii) using nitrogen-doped activated nanoporous carbon from almond shells, *RSC Adv.*, 9(41) (2019) 23678-23685.
- [54] V. Veeramani, R. Madhu, S.-M. Chen, B.-S. Lou, J. Palanisamy, V.S. Vasantha, Biomass-derived functional porous carbons as novel electrode material for the practical detection of biomolecules in human serum and snail hemolymph, *Sci. Rep.*, 5(1) (2015) 10141.
- [55] R. Sha, S.S. Jones, N. Vishnu, B. Soundiraraju, S. Badhulika, A novel biomass derived carbon quantum dots for highly sensitive and selective detection of hydrazine, *Electroanalysis* 30(10) (2018) 2228-2232.
- [56] T. Sha, X. Li, J. Liu, M. Sun, N. Wang, X. Bo, Y. Guo, Z. Hu, M. Zhou, Biomass waste derived carbon nanoballs aggregation networks-based aerogels as electrode material for electrochemical sensing, *Sens. Actuators B Chem.*, 277 (2018) 195-204.
- [57] J. Liu, H. Cheng, H. Xie, G. Luo, Y. Niu, S. Zhang, G. Li, W. Sun, Platinum nanoparticles decorating a biomass porous carbon nanocomposite-modified electrode for the electrocatalytic sensing of luteolin and application, *RSC Adv.*, 9(58) (2019) 33607-33616.
- [58] K. Li, J. Xu, M. Arsalan, N. Cheng, Q. Sheng, J. Zheng, W. Cao, T. Yue, Nitrogen doped carbon dots derived from natural seeds and their application for electrochemical sensing, *J. Electrochem. Soc.*, 166(2) (2019) B56.
- [59] V. Veeramani, R. Madhu, S.-M. Chen, P. Veerakumar, J.-J. Syu, S.-B. Liu, Cajeput tree bark derived activated carbon for the practical electrochemical detection of vanillin, *New J. Chem.*, 39(12) (2015) 9109-9115.
- [60] R. Madhu, C. Karupiah, S.-M. Chen, P. Veerakumar, S.-B. Liu, Electrochemical detection of 4-nitrophenol based on biomass derived activated carbons, *Anal. Methods*, 6(14) (2014) 5274-5280.
- [61] Y. Xu, W. Lei, Y. Zhang, H. Fan, Q. Hao, S. Gao, Bamboo fungus-derived porous nitrogen-doped carbon for the fast, sensitive determination of bisphenol A, *J. Electrochem. Soc.*, 164(5) (2016) B3043.
- [62] P. Pang, F. Yan, M. Chen, H. Li, Y. Zhang, H. Wang, Z. Wu, W. Yang, Promising biomass-derived activated carbon and gold nanoparticle nanocomposites as a novel electrode material for electrochemical detection of rutin, *RSC Adv.*, 6(93) (2016) 90446-90454.

- [63] V. Veeramani, M. Sivakumar, S.-M. Chen, R. Madhu, H.R. Alamri, Z.A. Alothman, M.S.A. Hossain, C.-K. Chen, Y. Yamauchi, N. Miyamoto, Lignocellulosic biomass-derived, graphene sheet-like porous activated carbon for electrochemical supercapacitor and catechin sensing, *RSC Adv.*, 7(72) (2017) 45668-45675.
- [64] P. Kanagavalli, S. Radhakrishnan, G. Pandey, V. Ravichandiran, G. Perumal Pazhani, M. Veerapandian, G. Hegde, Electrochemical tracing of butein using carbon nanoparticles interfaced electrode processed from biowaste, *Electroanalysis*, 32(6) (2020) 1220-1225.
- [65] A. Üzer, Ş. Sağlam, Z. Can, E. Erçağ, R. Apak, Electrochemical determination of food preservative nitrite with gold nanoparticles/p-aminothiophenol-modified gold electrode, *Int. J. Mol. Sci.*, 17(8) (2016) 1253.
- [66] C. Jo, H. Ahn, J. Son, J. Lee, M. Byun, Packaging and irradiation effect on lipid oxidation, color, residual nitrite content, and nitrosamine formation in cooked pork sausage, *Food Control*, 14(1) (2003) 7-12.
- [67] B. Romano, E. Pagano, V. Montanaro, A.L. Fortunato, N. Milic, F. Borrelli, Novel insights into the pharmacology of flavonoids, *Phytother. Res.*, 27(11) (2013) 1588-1596.
- [68] C.-H. Yen, H.-L. Lien, J.-S. Chung, H.-D. Yeh, Adsorption of precious metals in water by dendrimer modified magnetic nanoparticles, *J. Hazard. Mater.*, 322 (2017) 215-222.
- [69] N.P. Shetti, S.J. Malode, D.S. Nayak, G.B. Bagihalli, S.S. Kalanur, R.S. Malladi, C.V. Reddy, T.M. Aminabhavi, K.R. Reddy, Fabrication of ZnO nanoparticles modified sensor for electrochemical oxidation of methdilazine, *Appl. Surf. Sci.*, 496 (2019) 143656.
- [70] R. Zeng, J. Wang, Q. Wang, D. Tang, Y. Lin, Horseradish peroxidase-encapsulated DNA nanoflowers: an innovative signal-generation tag for colorimetric biosensor, *Talanta* 221 (2021) 121600.
- [71] R. Singh, N. Kumar, R. Mehra, H. Kumar, V.P. Singh, Progress and challenges in the detection of residual pesticides using nanotechnology based colorimetric techniques, *Trends Environ. Anal. Chem.*, 26 (2020) e00086.

Bioelectrochemical Systems: A Versatile Process for Value Addition and Environmental Abatement

Gunda Mohanakrishna

Center for Energy and Environment (CEE), School of Advanced Sciences (SAS), KLE Technological University, Vidyanagar, Karnataka – 580031, India

Corresponding Author: gmohanak@yahoo.com; mohanakrishna.gunda@kletech.ac.in

Abstract

Wastewater generation is ever increasing with time. The diversity of wastewater is also spreading with different emerging industries and changing lifestyles. Wastewater treatment is an energy intensive process, which adds up the production cost respective products. Bioelectrochemical systems (BES) are being evolved as sustainable processes where the organic content present in wastewater can be converted to different energy vectors, that simultaneously treating the wastewater. BES are diverse, which can be classified based on the products delivering through the process. Microbial fuel cells (MFCs) are mostly studied for bioelectricity generation through the action of electrochemical active biofilms on anode, which efficiently treats wide range of wastewaters. Further, the harnessing of electrochemical energy from wastewater treatment was utilized for the hydrogen generation through microbial electrolysis cells (MECs). Most recently, microbial desalination cells and microbial electrosynthesis were emerged for desalination wastewater and CO₂ sequestration respectively. On the whole, BES found efficient over conventional wastewater treatment processes with added benefits such as sustainable and resource recovery.

Introduction

Huge amount of energy and resources are being spent to treat wastewater that costing significant expenses to the industries and urban management authorities. Several novel approaches of environmental management are developing energy-efficient processes or processes with the value addition from the waste/wastewater remediation. Bioelectrochemical systems (BES) are emerging with diverse application which centered with wastewater treatment. BES accomplish significant change in wastewater treatment by considering them as renewable energy-based repository units [1-2]. Microbial fuel cells (MFCs) and microbial

electrolysis cells (MECs) are applications of BES, those are extensively studied with environmental sustainability. BES are hybrid bioelectrochemical processes which accomplish the treatment through the combination of microbial and electrochemical processes. Due to which the treatment efficiency of MFCs is found to superior to conventional biological treatment processes such as activated sludge process, anaerobic digestion and dark fermentation. Conventional treatment processes cannot handle some of the wastewater components, especially dye-based wastewaters, complex organic and inorganic chemicals and wastewaters with toxic organic substances [3-4]. The limitations in conventional biological treatment processes can be attributed to microbial metabolism. On the other hand, existing electrochemical processes also has some limitations in treating this type of waste in terms of energy input and additional waste generation. At this point, BES combines both biological and electrochemical processes for waste remediation along with the energy generation in terms of electricity, hydrogen or other useful chemicals. This multidimensional function of BES has been attracting researchers from chemical engineers, biotechnologists, environmentalists, civil engineers and electrochemists in this field of research.

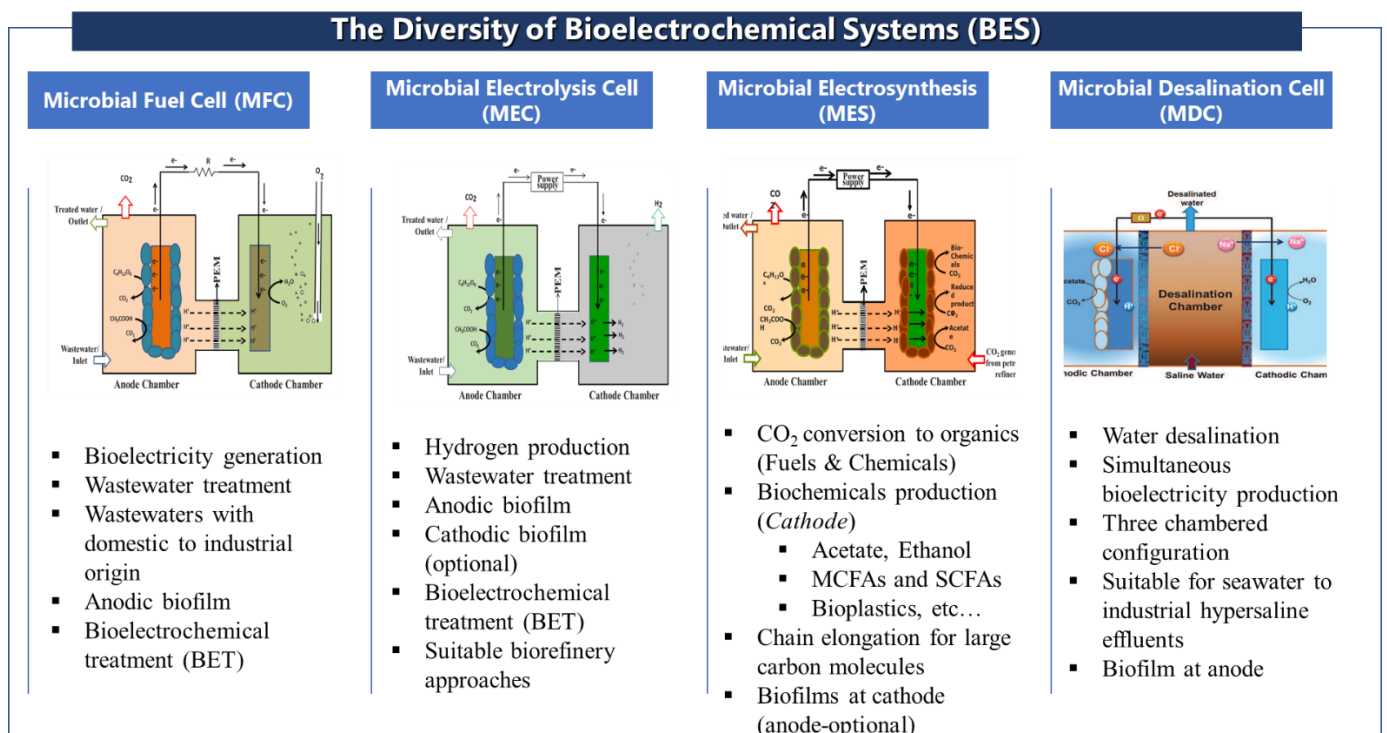


Fig 1. Diverse applications of bioelectrochemical systems and their specific conditions in brief.

Types of bioelectrochemical systems (BES)

Microbial fuel cell (MFC)

In MFC, substrate present in the anodic compartment biologically degrade via electroactive microorganisms (EAMs) as biocatalysts to transform chemical energy stored in organic matter to electrical energy directly via substrate oxidation. An MFC comprises two chambers, anode and cathode, partitioned by a proton exchange membrane (PEM) [5]. In an MFC, microbes remain in anode compartments as biofilms on electrode surface and produce electrons and protons after oxidising an electron donor, usually an organic substrate. The anode is used by the biofilm microbe as the electron acceptor for anaerobic respiration, which receives electrons from the microbe after the electrons have first passed through the microbe's electron transport chain by nicotinamide adenine dinucleotide (NADH) to the terminal electron acceptors and then to the microbe's outer membrane proteins. These microbes produce flavin molecules, or organic compounds based on pteridine, to promote electron transfer to the anode. The electron generated in anode transfer to cathode via external circuit and then combine with oxygen and form a water molecule and proton generated drifted to cathode through PEM (Nafion). These redox reaction in MFC system aids to generate bioelectricity simultaneously treating wastewater and waste remediation. Several sources of substrate include synthetic feed (glucose, sucrose and acetate), wastewater generated from domestic sector and food processing industry. Waste biomasses comprise of lignocellulosic like sugarcane bagasse, wheat strove, rice husk and non-lignocellulosic like microalgal biomass, food waste leachate, activated sludge, sewage water. All these organic substrate acts as a electron donor which is consumed by electrogene and release a external electron in anodic chamber of MFC system [6]. Utilizing these substrates which is cost-effective, all-season availability and biodegradable capability made them a potential substrate for generating bioelectricity. Pretreatment of lignocellulosic biomass is necessary due to its recalcitrant nature, to make an MO capable of efficiently hydrolyse to release fermentable sugar. Microorganism employed in MFC system for electron transfer and electricity generation are electroactive microorganisms i.e., *Geobacter*, *Shewanella*, *Pseudomonas*, and *Rhodospirillum rubrum*. They are iron reducing bacteria among which *Geobacter sulfurreducens* are capable of producing higher power density under optimal temperature condition later these microbe aggregate to form biofilm on anode electrode, act as a electron acceptor. In case if microbes having a high lipid layer such as peptidoglycan and lipopolysaccharide, mediators are required to produce electricity. In mediator-less MFC utilizes anodophiles such as *G. sulfurreducens* and *R. ferrireducens*, microbes which form a biofilm on the surface of anodic electrode and use the anode as their end terminal electron acceptor in their anaerobic respiration [7]. The resistance to the flow of ions in electrolytes and the electron flow

between the electrodes cause Ohmic losses. Ohmic loss in electrolytes is dominant and it can be reduced by shortening the distance between the two electrodes and by increasing the ionic conductivity of the electrolytes. Stirring or bubbling can reduce the concentration gradient in an MFC.

Performance and power generation in MFC system mainly depends on pH, temperature, electrode design, type and concentration of substrate, selection of biocatalyst, HRT, OLR, ionic strength and membrane used in MFC system. pH is one of the vital aspects in MFCs that affects both anodic microbial activities and cathodic reactions. Accumulation of protons would cause anolyte acidification in anodic chamber that results in adverse impact on biofilm, and electrolyte alkalization in the cathode chamber. Hence, reducing pH in the anode chamber due to increased proton concentration results in low power production, which represses the EAMs activation. On the contrary, it causes an increased pH in the cathode chamber that inhibits the oxygen reduction reaction. The use of pH buffers such as phosphate or bicarbonate (pH 7.0) helps to maintain the optimum pH at the anolyte. It was found that an increased anodic pH and optimum operating temperature around 37 °C contribute to increase in current density, increased COD removal and improve the performance of MFC by maximizing the power density. Organic loading rate (OLR) has a significant impact on anodic biofilm based on the characteristics and fermentation of organic waste. Operating the MFC at the higher OLR usually resulted in a decreased Coulombic Efficiency. This indicate the COD removal and current density were significantly affected by increasing OLR, although the performance of MFC decreased when HRT was reduced. The rate of oxidation and reduction of anodic and cathodic half-reactions and charge transfer resistance are governed by the properties of electrode materials, while membranes govern the ion exchange rate and internal resistance of MFC system. Selection of electrode material in MFC should possess good electron conductivity, large surface area and good biocompatibility for microbial adherence. The surface properties of an electrode, such as roughness, porosity, and surface hydrophilicity can affect the formation of biofilm and subsequently derived electric power. MFCs with Pt or Pt-coated cathodes yielded higher power densities than those with graphite or graphite felt cathodes because of highest catalytic activity of Pt, it works in the absence of microbes. Major drawback of using Pt or Pt-black electrodes is that their activities are reduced by the formation of a PtO layer at the electrode surface at positive potentials. Later increased potential can be achieved by using NR & Mn⁴⁺ graphite anode and doping ions like Fe³⁺ and Mn⁴⁺ graphite cathode. The ionic strength of MFC reactor can be enhanced by the addition of NaCl, it rises the

conductivity of anolyte and catholyte. The ideal potentials of MFCs can be calculated by the Nernst equation for these reactions and they range from several hundred mV to over 1000 mV. In MFCs, the reduction of carbon dioxide to methane in the anode compartment consumes electrons, thus decreasing the Coulombic efficiency and lowering the power generation. Also, high concentrations of ammonia are toxic to most exoelectrogenes that power MFC. Therefore, to maximize the electricity recovery from waste biomass and wastewater, future efforts need to be focused on minimizing the negative impacts of methanogenesis and ammonification on MFC performance [8].

MFC-electrosorption is the process of removal of metal, organic pollutant and desalination in wastewater generated from domestic and industrial sectors. The benefit of using this method is it requires low energy, can accumulate more amount of feed with easy electrode regeneration. Migration of charged ions and polar molecule across electrode surface to generate electric field between anode and cathode need a low external voltage around 0.4-1.4 V [9]. The first concept of MFC-electrosorption applied to two single MFCs arranged in sequential manner for removal of phenol on activated carbon fibres in the treatment of an artificial wastewater. The removal of metal ion and contaminant degradation can be achieved by maintaining system at low electrolyte concentration and high pH. MFC- capacitive deionization is another category under MFC which is also called as capacitive deionization (CDI). CDI are being investigated to generate fresh water by removal of ions (deionization) without the requirement of thermal heater and a high-pressure pump subsequently removal of organic pollutants, COD and ammonia can be performed [10]. Water containing low salt concentration about 5 g/L can be effectively achieved by this electrochemical method. Water hydrolysis in the system can be prevented by creating the electric double layer with the voltage lower than 1.4 V. Initially during the treatment process ions are adsorbed on the electrode surface and desorption is done by reversing electrode polarities or short-circuiting. A resistor-capacitor circuit was formed by MFC and CDI among them CDI cell serves as supercapacitor. Compared to pH of electrolyte in MDC (microbial desalination cell) system, MFC-CDI have a stable electrolyte pH. This method shows a promising result for pollutant removal and electricity production without emitting/releasing any secondary pollution.

Microbial electrolysis cell (MEC)

A biological process in which the organic matter is oxidised by microorganisms to produce electrons and protons is called Electrohydrogenesis. The reactor or chamber in which

electrohydrogenesis takes place is referred as microbial electrolysis cell (MEC) where microorganisms are work as biocatalysts. The wastewater or waste are rich in organic matter comprises of abundance in carbohydrates, small amounts of proteins, lipids and nutrients [11-12]. The organic matter in waste is degraded by the microorganisms produces methane and hydrogen. Generally, the MECs are two chambered system which includes anolyte in anodic chamber and catholyte in cathode chamber. The microorganisms that colonize the anode are called as electricigens. The primary driving force for development of MEC is bioelectrochemical energy that generating from wastewater treatment. Electrons generated by bacteria in anode chamber discharge towards cathode through an external circuit while the protons diffuse through the electrolyte to the cathode. To trigger the reduction reaction at cathode to produce hydrogen gas, additional energy is needed. The additional energy depends on the reactor design factors and operational conditions, which is in the range of 0.6 to 1.0 V [13]. This energy can be drawn from renewable energy sources such as solar energy, wind energy, etc. Electroactive biofilm and its activity in association to treat the organics present in wastewater are determining the hydrogen production efficiency. The electrodes and internal resistance are playing key role in coulombic efficiency of overall process.

Microbial desalination cell (MDC)

Application of BES in desalination of saline water and industrial wastewater is found to be a promising technology that utilizes the microbiological energy from the wastewater treatment to drive the ions through ion exchange membranes (IEMs), resulting in desalination. This novel method reduces the electricity requirement for removal of salts. The main feature of the MDC is that exoelectrogenic microorganisms produce electrical potential from the degradation of organic matter, which can then be used to desalinate water by driving ion transport through IEMs [14]. A MDC system, comprise three chamber, desalination chamber situated middle adjacent to it anodic chamber with anion exchange membrane and cathodic chamber with cation exchange membrane is designed. The electrogenic bacteria in biofilm on anodic electrode generate current it mainly influences on this process. When wastewater is used as the source of the organic matter that required for development of potential gradient, the MDC can achieve three goals such as desalination, energy production and wastewater treatment [14]. In anodic compartment bacterial biofilm attached to anodic electrode undergo metabolic process by oxidizing substrate in the anolyte and release external electron through cell membrane into anode, for example, the presence of NaCl in water stream on ionization, the anion (Cl^-) in the desalination chamber migrate to the anode, and the cations (Na^+) migrate to the cathode for

maintaining equilibrium with charge. The water containing high salt concentration results in lower ohmic resistance and higher current density. The current generated in MDC is four times greater in comparison with MFC.

The bioelectrode functions create an electric potential gradient maximum of 1.1 V using acetate as substrate at anode and oxygen reduction reaction at cathode. From the research studies, 11 % and 100 % recorded as minimum and maximum salinity removal efficiencies by MDCs. Above 90 % salinity removals with saline water using 35 g/L NaCl in middle chamber of MDC. On the other hand, high salinity removals always demand for large volume of non-salty water in both anolyte and catholyte chambers, which creates the dilemma for sustainability of the process. Stacked MDCs are showing need of less non salty electrolytes in anode compared to stand alone MDC. Up to 98 % salinity removals were achieved using stacked MDCs consist of five pairs of cells. These results imply that, for practical applications, MDCs are more likely to be used for partial salt removal from seawater. MDCs can also be used for brackish water desalination. Studies using industrial and real field wastewater as organic substrate in anode and buffer as catholyte were showed practical applicability of MDCs at large scale.

Microbial Electrosynthesis (MES)

Bioelectrochemical systems (BESs) are one of the most promising emerging technologies for the reduction of carbon dioxide (CO₂) to multicarbon compounds through biocathodic reactions using specific bacteria or microbial consortia as biocatalysts. This process is termed microbial electrosynthesis (MES) or bioelectrochemical synthesis [15-16]. The is a tremendous research focus on MES by the global research community due to its potential application in the conversion of CO₂ into multicarbon and value-added compounds at the expense of only a minor amount of energy. The advantages of the process also can be stated in terms of CO₂ reduction in the atmosphere and from biofuels and chemicals production causing the emission of GHGs, a low energy input for production, and the use of a renewable and low-cost biocatalyst. The energy required to drive the bioelectrochemical reduction can be generated by renewable energy sources, such as solar cells/photovoltaics, wind power, and geothermal heat. The electrical energy generated from the treatment of wastewater using microbial fuel cells (MFCs) can also be integrated with the MES of multicarbon organic compounds for making the process even more sustainable [17]. The integration of MFCs for energy or biochemicals production by utilizing negative valued waste streams combines integrated wastewater management and energy recovery. This could help solve the energy crisis and environmental pollution simultaneously. Several products, such as acetate, methane, ethanol, butyrate, etc.,

have been produced through MES processes in the lab scale in several proof-of-concept studies, among which acetate is the most studied product to date. Various types of biocatalysts, such as pure cultures, mixed cultures, and enriched cultures, have been used to produce acetate. It was also identified that the reactor configuration, electrode materials, etc., influence the process efficiency. MES also can be integrated with wastewater treatment for biorefinery approach that maximizes the resource recovery [18].

Electroactive biofilms (EAB) and mechanism of electron transfer

The bacteria which involve in generation of electric pulse by oxidation of potential source into electrons are referred as Electrogenic bacteria or electrochemically active bacteria (EAB) [19-20]. The reports of taxonomic profiles of electrode reducing microorganisms like *Proteobacteria* are the dominant phylum that discharges electrons towards anode. According to eight system studies of bacteria, the results shows that 64% of bacteria are belongs to class of α -, β -, γ - and δ -*Proteobacteria* and among these most of them belongs to family *Shewanella* and *Geobacteriaceae*. The complete genome of *Shewanella Oneidensis* has been sequenced in 2002 and subsequently *Geobacter sulfurreducans* in 2003. These two bacteria are efficient in electron transfer mechanism from bacteria to electrode. By understanding the mechanism of electron transfer from microorganism to electrode, the current produced from each BES system is easily calculated. The research investigations show that not only influence substrate selection but also on the manipulation of surface area of electrode. Though the exact mechanism of electron transfer cannot understand but three methods have been proposed for better understanding.

1. Long range electron transfer through electron shuttles
2. Direct electron transfer through outer surface with c-type cytochromes
3. Long range electron transfer via microbial nanowires

Electron transfer mechanism is complex, and proliferation of such conditions depends on various environmental and operational condition adapting for the BES operation. Understanding specific bacterial species and electrochemical and operational conditions will helps in optimizing the BES application with high practical approach in biorefinery.

Conclusions

Multifaceted BES got applications in wastewater treatment, energy generation in terms of hydrogen and bioelectricity and desalination. The applications were also extended in CO₂ reduction to value added products which are ranging from simple organic acids to specialty

chemicals. Specific pollutants related to micronutrients, metals and heavy metals are also showing promising results by BES configuration. MFC, MEC and MDC integration for improved process efficiencies is suitable for the bio-refinery approach. Even though diverse applications of BES were existed with cost effective operational processes, the design and fabrication of such reactors are not found inappropriate when compared to conventional treatment processes. Electrodes and membranes involved in the BES are majorly sharing high expenses in the design. Developing of cost-effective electrodes and membranes need of the hour to be implement with large scale.

References

1. S. Venkata Mohan, G. Mohanakrishna, B. P. Reddy, R. Saravanan, P. N. Sarma, Bioelectricity generation from chemical wastewater treatment in mediatorless (anode) microbial fuel cell (MFC) using selectively enriched hydrogen producing mixed culture under acidophilic microenvironment, *Biochem. Eng. J.*, 39(1) (2008) 121-130.
2. S. Kondaveeti, D. Govindarajan, G. Mohanakrishna, D. Thatikayala, I. M. Abu-Reesh, B. Min, T. M. Aminabhavi, Sustainable bioelectrochemical systems for bioenergy generation via waste treatment from petroleum industries, *Fuel.*, 331 (2023) 125632.
3. A. ElMekawy, H. M. Hegab, G. Mohanakrishna, A. F. Elbaz, M. Bulut, & D. Pant, Technological advances in CO₂ conversion electro-biorefinery: a step toward commercialization, *Bioresour. Technol.*, 215 (2016) 357-370.
4. Y. Guo, J. Wang, S. Shinde, X. Wang, Y. Li, Y. Dai, X. Liu, Simultaneous wastewater treatment and energy harvesting in microbial fuel cells: an update on the biocatalysts, *RSC Adv.*, 10(43) (2020) 25874-25887.
5. G. Mohanakrishna, S. Venkata Mohan, P. N Sarma, Bio-electrochemical treatment of distillery wastewater in microbial fuel cell facilitating decolorization and desalination along with power generation, *J. Hazard. Mater.*, 177(1-3) (2010) 487-494.
6. T. Cai, L. Meng, G. Chen, Y. Xi, N. Jiang, J. Song, M. Huang, Application of advanced anodes in microbial fuel cells for power generation: a review. *Chemosphere*, 248 (2020) 125985.
7. Y. Cao, H. Mu, W. Liu, R. Zhang, J. Guo, M. Xian, H. Liu, Electricigens in the anode of microbial fuel cells: pure cultures versus mixed communities. *Microb. cell factories*, 18 (2019) 1-14.
8. U Schröder, Anodic electron transfer mechanisms in microbial fuel cells and their energy efficiency. *Phys. Chem. Chem. Phys.*, 9 (2007) 2619-2629.

9. Y. Zhang, M. Liu, M. Zhou, H. Yang, L. Liang, T. Gu, Microbial fuel cell hybrid systems for wastewater treatment and bioenergy production: synergistic effects, mechanisms and challenges, *Renewable Sustainable Energy Rev.*, 103 (2019) 13-29.
10. W. Xing, J. Liang, W. Tang, D. He, M. Yan, X. Wang, M. Huang, Versatile applications of capacitive deionization (CDI)-based technologies, *Desalination.*, 482 (2020) 114390.
11. A. Kadier, M. S. Kalil, K. Chandrasekhar, G. Mohanakrishna, G. D. Saratale, R. G. Saratale, P. Sivagurunathan, Surpassing the current limitations of high purity H₂ production in microbial electrolysis cell (MECs): Strategies for inhibiting growth of methanogens, *Bioelectrochem.*, 119 (2018) 211-219.
12. R. Lacroix, E. Roubaud, B. Erable, L. Etcheverry, A. Bergel, R. Basséguy, S. Da Silva, Design of 3D microbial anodes for microbial electrolysis cells (MEC) fuelled by domestic wastewater. Part I: Multiphysics modelling, *J. Environ. Chem. Eng.*, 9(4) (2021) 105476.
13. J. A. Modestra, M. L. Babu, S. Venkata Mohan, Electro-fermentation of real-field acidogenic spent wash effluents for additional biohydrogen production with simultaneous treatment in a microbial electrolysis cell, *Sep. Purif Technol.*, 150 (2015) 308-315.
14. Y. Kim, B. E. Logan, Microbial desalination cells for energy production and desalination, *Desalination.*, 308 (2013) 122-130.
15. G. Mohanakrishna, K. Vanbroekhoven, D. Pant, Impact of dissolved carbon dioxide concentration on the process parameters during its conversion to acetate through microbial electrosynthesis, *React. Chem. Eng.*, 3(3) (2018) 371-378.
16. K. P. Nevin, T. L. Woodard, A. E. Franks, Z. M. Summers, D. R. Lovley, Microbial electrosynthesis: feeding microbes electricity to convert carbon dioxide and water to multicarbon extracellular organic compounds, *MBio.*, 1(2) (2010) e00103-10.
17. L. Jourdin, T. Burdyny, Microbial electrosynthesis: where do we go from here?, *Trends in Biotechnol.*, 39(4) (2021) 359-369.
18. Y. Jiang, H. D. May, L. Lu, P. Liang, X. Huang, Z. J. Ren, Carbon dioxide and organic waste valorization by microbial electrosynthesis and electro-fermentation, *Water Res.*, 149 (2019) 42-55.
19. N. S. Malvankar, Lovley, D. R. Lovley, Microbial nanowires: a new paradigm for biological electron transfer and bioelectronics, *ChemSusChem.*, 5(6) (2012) 1039-1046.
20. C. Liu, L. Ren, B. Yan, L. Luo, J. Zhang, M. K. Awasthi, Electron transfer and mechanism of energy production among syntrophic bacteria during acidogenic fermentation: A review, *Bioresour. Technol.*, 323 (2021) 124637.

Metal/Metal oxide based Hybrid Electrocatalytic Systems for Enhanced Hydrogenation of CO₂ to Formate

Balaji B. Mulik^{ab*}, Ajay V. Munde^a, and Bhaskar R. Sathe^{ac*}

^aDepartment of Chemistry Dr. Babasaheb Ambedkar Marathwada University, Aurangabad 431004, Maharashtra, India.

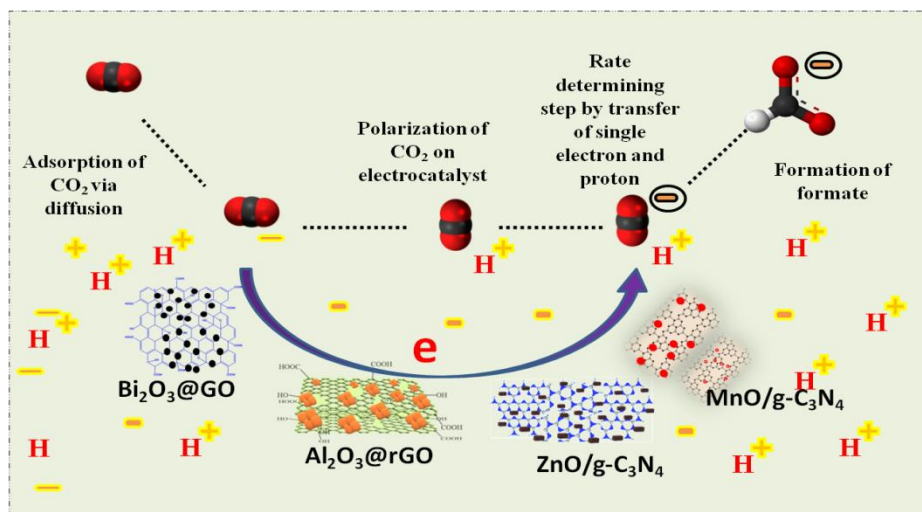
^bDepartment of Basic and Applied Science (Chemistry), MGM University, Aurangabad 431005, Maharashtra, India.

^cDepartment of Nanotechnology, Dr. Babasaheb Ambedkar Marathwada University, Aurangabad 431005, Maharashtra, India.

Corresponding Author: balajimulik70@gmail.com (Dr. Balaji B. Mulik) and bsathe.chemistry@bamu.ac.in (Dr. Bhaskar R. Sathe)

Abstract

Carbon dioxide (CO₂) and global warming challenges and need to be develop electrocatalytic reduction of CO₂ to valuable organic compounds and fuels which significantly contributes to the control of climate change using energy efficient techniques is presently of great importance. Here in this regard we have developed Bi₂O₃@GO, Al₂O₃@rGO, MnO/gC₃N₄ and ZnO@gC₃N₄ electrocatalytic systems. All the electrocatalysts has been characterized by various structural morphological and spectroscopic techniques like XRD, Raman, SEM, TGA, FTIR, TEM and XPS. The electrocatalysts have demonstrated for electrochemical reduction of CO₂ to formate with high Faradic efficiencies by using cyclic voltammetry, linear sweep voltammetry, chronoamperometry and electrochemical impedance spectroscopy (EIS). Additionally, electrocatalysts having higher Faradic efficiency (FE) for formate formation 83, 92, 91 and 69% for Bi₂O₃@GO, Al₂O₃@rGO, ZnO/g-C₃N₄ and MnO₂/g-C₃N₄ nanocomposites respectively. The present methodologies will applicable for industrial scale up and will try to solve the energy and environmental issues.



Schematic: Representation of $\text{Bi}_2\text{O}_3@\text{GO}$, $\text{Al}_2\text{O}_3@\text{rGO}$, $\text{MnO}/\text{gC}_3\text{N}_4$ and $\text{ZnO}@\text{gC}_3\text{N}_4$ based modified electrode for electrochemical hydrogenation of CO_2 to Formate via possible intermediates in aqueous electrolyte.

Introduction

The enlarging worldwide population results in energy crises in current existence. The predominance of the energy comes up from fossil based fuels which have been used for industrialization, transportation and development concern.[1] In practice require to control the emission of greenhouse gases by giving alternative to fossil fuels by buildup a technique for CO_2 reduction and utilization for valuable feedstuff would be maintain a carbon cycle. In due course, on burning of fossil fuels contributes to environmental toxic waste by discharge greenhouse gases such as NO_2 , SO_2 , and CO_2 . Among them CO_2 causes “Global Warming” and having close correlation for change in biodiversity on the planet. [2, 3] Literature, significantly reported various methods for hydrogenation of CO_2 like, photochemical, thermo-steam catalytic, photoelectrochemical, biological and electrochemical, etc. [4, 5] From the above mentioned methods the electrochemical reduction is suitable approach as it is having potential dependent product selectivity like hydrocarbons, acids, alcohols, carbon monoxide, aldehydes, and other products which are having dependent on the experimental conditions like transfer of number of electron and proton, type of supporting electrolyte and type of metal cathode. [6-8]

Although an electrochemical CO_2 reduction has to be carried is extremely complex and vital since of having undistinguished observed potential with hydrogen evaluation reaction (HER),

overpotential required for desired product, complicated electro-kinetics, results in slower rate of CO₂ conversion towards the product and variable product selectivity. [9-11] By taking into account the above concerning problems, the present research community has been devoted to widen or developing a further selective, stable and active nanoelectrocatalyst, having ability to demonstrate selective CO₂ reduction. According to literature lot work has been reported in this area, a number of modified electrodes were tried for significant development of C₁ feedstock's viz., carbon monoxide, formic acid, methanol, formaldehyde, urea and also C₂ to C₃ useful products. From the above, formic acid is essential and precious compound exploited for various chemical industries as a starting material, in fuel cell reactions along with industrial and energy value-added chemicals generation purpose. Literature reflects various electro-catalysts are prepared and reported for formic acid/formate generation as of CO₂ electrochemical reduction. In this line, the cathode material is playing important role for the formate selectivity by the material used in the literature till date including Nobel and transition based metals/metal oxides like Pt, Pd, Ir, Bi, Sn, Pb, Cd, Zn, Mn and Al etc and their hybrids.[12-15]

The aforesaid metal based electro catalysis undergoing high cost, poisonous and required additional cathodic applied potential to catalyses CO₂ through lesser Faradic efficiency (FE). Furthermore, transition based nano-catalysts are interesting with low-cost nanomaterials with a variable oxidation state that makes useful material and used in various electrochemical applications viz., catalysis, sensors, supercapacitors, and alkaline and rechargeable batteries. Several transition metal-based electrocatalysts have been investigated for the selective conversion of CO₂ into formate. For example, Liu et al. reported the selective synthesis of Ni foam modified with MnO₂ to the formation of nanosheets MnO₂ was found be highly active for the electrochemical CO₂ to CO conversion at lower potential and high current density. [16] For example, White and Bocarsly reported indium oxide, hydroxide and pure indium nanoparticles that have can catalyze the electrochemical reductive conversion of CO₂ into formate. Due to their higher surface area and density of surface exposed active sites, the materials at nanoscale unsurprisingly show significantly enhanced activity with respect to their bulk counterparts. Chen and Kanan studied the electrochemical reduction of CO₂ on thin films of Sn/SnO_x electrodes in aqueous NaHCO₃ supporting electrolyte. [17] These SnO_x thin film-based systems displayed 8-fold higher fractional current density and nearly 4-fold greater Faradaic efficiency (FE) for Electrocatalytic hydrogenation of CO₂ as compared with Sn film electrode. [18] While other nanostructured systems, such as Hg-based amalgam, Sn@Bi nanoparticles and Pb and polytetrafluoroethylene electrode have been reported for CO₂

reduction and formate formation, many of them suffer from surface poisoning, higher overpotentials, etc. [19]

Meanwhile, two-dimensional (2D) materials have recently attracted much attention because they enable the dispersion of metal nanoparticles and prevent their aggregation or agglomeration, giving stable heterogeneous nanocatalysts. Graphene oxide (GO) and graphitic carbon nitride (gC_3N_4) are a notable 2D materials that has bonds composed of sp^2 and sp^3 hybridized carbon atoms and a planar network with high mobility of π electrons and N like heteroatom increases the feasibility of electron with electrofility of CO_2 . GO also contains oxygen-based functional groups such as hydroxyls, epoxides and carbonyl groups on its surfaces, which also make GO hydrophilic and dispersible in water. [20-22]

By considering above issues and applicability herein developed $Bi_2O_3@GO$, $Al_2O_3@rGO$, MnO/gC_3N_4 and ZnO/gC_3N_4 electrocatalytic systems. All the electrocatalysts has been characterized by various structural and morphological techniques like XRD, Raman, SEM, TGA, FTIR, TEM and XPS. The electrocatalysts have demonstrated for electrochemical reduction of CO_2 to formate with high Faradic efficiencies. The present methodologies will applicable for industrial scale up and will try to solve the energy and environmental issues.

Experimental

Chemicals

Graphite powder 99.99%, Ethylene glycol (EG) 99.97% (Alfa-Aesar), Sulphuric acid 98%, Nitric acid 78%, $KHCO_3$ (Sigma Aldrich), Bismuth trinitratepentahydrate ($Bi(NO_3)_3(H_2O)_5$), Acetone 99.99%, Triethylamine 99.99% (SD Fine), Carbon dioxide gas 99.99% (Vijay scientific Ltd, India) were procured. All the chemicals were used as received. Aluminium chloride ($AlCl_3$) (Sigma-Aldrich), graphite powder (99.99%, Alfa-Aesar), sulphuric acid (98% Alfa-Aesar), nitric acid (78% Alfa-Aesar), potassium bicarbonate (Sigma-Aldrich), acetone (99.99% Alfa-Aesar), and CO_2 gas (99.99%) and hydrazine hydrate (N_2H_4) (99.99%) (Vijay Scientific Ltd, India). Manganese Chloride ($MnCl_2$) 99.99%, Sodium hydroxide (NaOH) 99.99% (Alfa Aesar), Urea $CO(NH_2)_2$ 99.99%, Citric acid $C_6O_8H_7$ 99.99% (SD Fine chemicals), Potassium bicarbonate $KHCO_3$ (Sigma Aldrich), Nitrogen gas N_2 99.99%, Carbon Dioxide CO_2 gas 99.99% (Vijay Scientific Ltd, India), Zinc sulphate 99.99%, sodium hydroxide 99.99% (Alfa asear), urea 99.99%, citric acid 99.99% (sd fine), potassium bicarbonate (Sigma Aldrich), nitrogen gas 99.99%, carbon dioxide gas 99.99% (Vijay

Scientific Ltd, India). All the chemicals were used of AR grade without further purification. For all synthesis work and electrochemical studies carried out using deionized water.

Synthetic methodologies

In a typical synthesis, initially 50 mL of ethylene glycol (EG) was heated at 110 °C for 30 mins under constant stirring to remove the dissolved oxygen and water molecules from it, thus obtained anhydrous EG was used for further synthesis. Followed to this, 20 mg of GO was added and sonicated in next 3 h for homogeneous dispersion in 50 mL anhydrous EG, on complete dispersion of GO, 10 mM bismuth nitrate (0.014 gm in 50 mL EG) was added dropwise under constant stirring. The reaction mixture was further stirred for 3 h and refluxed for next 6h. The resultant product was cooled to RT and filtered and washed by acetone. This obtained black colored catalyst was dried in the oven at 60 °C for 2 h which results into Bi₂O₃@GO nanocomposite.[23] Synthesize Al₂O₃-rGO, rGO and AlCl₃ were mixed in 1:1 ratio by weight using mortar and pestle. This mixture was kept in a CVD furnace and treated at 600 °C in Ar atmosphere for 2 h, followed by in H₂ atmosphere, for 3 h. MnO₂/g-C₃N₄ nanocomposite was prepared via. a simple solid-phase pyrolysis route. In a typical synthesis, the calculated amount of urea (10 g), citric acid (0.334 g) and manganese chloride anhydrous (0.035 g) were dispersed in a round bottom flask containing deionized water (50 mL). The reaction mixture was further stirred for 2 h, and then it was heated at 80 °C in the oil bath under open air until it dried and became solid material. The obtained solid was calcined at a temperature of 450 °C for the 2 h in the muffle furnace heating rate of 5 °C /min. Also, synthesis of graphitic carbon nitride (g-C₃N₄) without the addition of manganese chloride anhydrous. [24] In a typical synthesis, 10 g urea was taken in round bottom flask (250 mL), into this 0.334 g of citric acid and 0.50 g ZnSO₄ was added followed by 50 mL of deionized water. The reaction mixture was retained for stirring further for (2h) until the solid becomes soluble. The reaction mixture was heated to 80 °C, the solid powder was formed after 2h with constant stirring. The solid form of reaction mixture was calcinated at 550 °C. Formed product has been further well characterized and used for electrochemical studies.

Result and Discussion

Characterization

Transmission Electron Microscopic analysis (TEM)

To determine the exact decoration and size of the hybrid nanomaterials we have demonstrated TEM analysis of $\text{Bi}_2\text{O}_3@\text{GO}$, $\text{Al}_2\text{O}_3@\text{rGO}$, $\text{MnO}/\text{gC}_3\text{N}_4$ and $\text{ZnO}@\text{gC}_3\text{N}_4$ nanoelectrodes. More significantly, to confirm the Bi_2O_3 decoration on GO, we have performed Transmission Electron Microscopy (TEM) analysis as shown in **Fig 1(a)**. The black colored, dense particles of Bi_2O_3 decorated on GO sheet. The mean particle size observed Bi_2O_3 is 1.50 to 2.5 nm with few sheets of the GO which size is having 50 nm. The morphologies and structures of the as-synthesized nanocomposite materials are then studied with TEM. The result is shown in **Fig 1(b)**. The image shows that rGO sheet has a size of ca. ~ 100 nm x 100 nm and it is decorated with Al_2O_3 . The Al_2O_3 particles are quasi-spherical in shape and have average size of 8 ± 0.3 nm. The transmission electron microscopy (TEM) has been carried out to observe the uniform decoration ZnO on $\text{g}/\text{C}_3\text{N}_4$ as shown in **Fig 1(c)**. From figure it has been observed that, the ZnO particle with hexagone size 2 to 10 nm with uniform decorating on $\text{g}-\text{C}_3\text{N}_4$. The pristine $\text{g}-\text{C}_3\text{N}_4$ having dense/aggregated like structure where as dispersion of ZnO hexagones altered structure with more roughed with high surface area. From **Fig 1(d)** The TEM image shows that pure gC_3N_4 having layered structure with average ~ 10 -50 nm in size and soft surface area with aggregated form. In the $\text{MnO}_2/\text{gC}_3\text{N}_4$ nanocomposite, the average size ~ 10 to 50 nm of gC_3N_4 with layered morphology and decoration of MnO_2 having hexagonal like plates were loaded arbitrarily with average size ~ 0.5 to 2 nm nanoparticles clearly seen on the layer of gC_3N_4 . From TEM it has been also demonstrated that the MnO_2 having the interplanar lattice of 0.243 nm between adjacent lattice point. Furthermore, the $\text{MnO}_2/\text{gC}_3\text{N}_4$ composite have more surface area and synergetic effect may be enhanced the electrocatalytic activity.

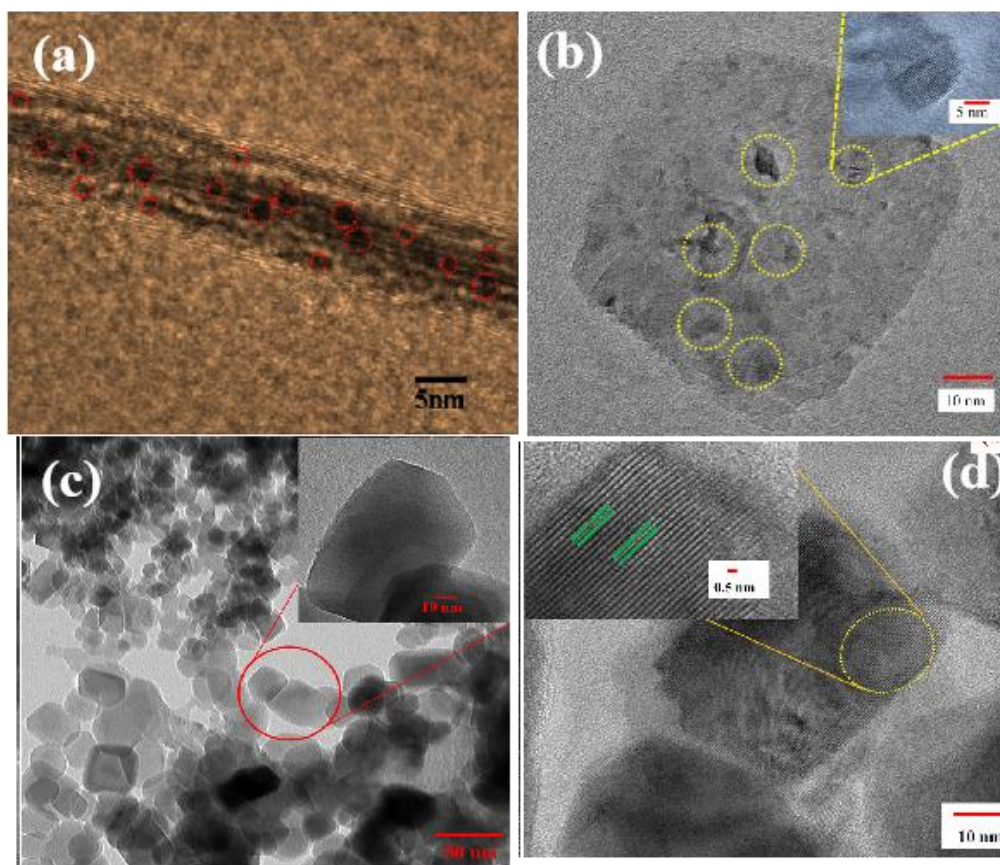


Fig 1. (a) Transmission Electron Microscopy (TEM) of Bismuth oxide ($\text{Bi}_2\text{O}_3\text{GO}$); (b) Transmission electron microscopy (TEM) image of $\text{Al}_2\text{O}_3@\text{rGO}$.; (c) TEM images as synthesized $\text{ZnO}/\text{gC}_3\text{N}_4$; (d) TEM images as synthesized $\text{MnO}_2/\text{gC}_3\text{N}_4$ nanocomposite.

Electrochemical Studies

The electrochemical reduction was carried out between -0.6 to -1.6V by using linear sweep voltammetry (LSV) technique. The cathodic current density for the electrochemical reduction was much higher with lower onset potential for $\text{Bi}_2\text{O}_3\text{-GO}$ than Bi_2O_3 nanoparticles, GO and bare GC. The significant revealed cathodic current for $\text{Bi}_2\text{O}_3\text{-GO}$ comparing with $\text{N}_2\text{-CO}_2$ and without CO_2 , i.e., the current difference between HER and CO_2 reduction conforms the electrochemical reduction of CO_2 on electrocatalyst. Again the current density observed for reduction is high as compared to literature. The onset potential was observed -0.811V vs. RHE as shown in **Fig 2(a)** The electrochemical reduction was increased on $\text{Bi}_2\text{O}_3\text{GO}$ may be due to inter electron transfer from GO to Bi because of the electron donor property of GO. [25]

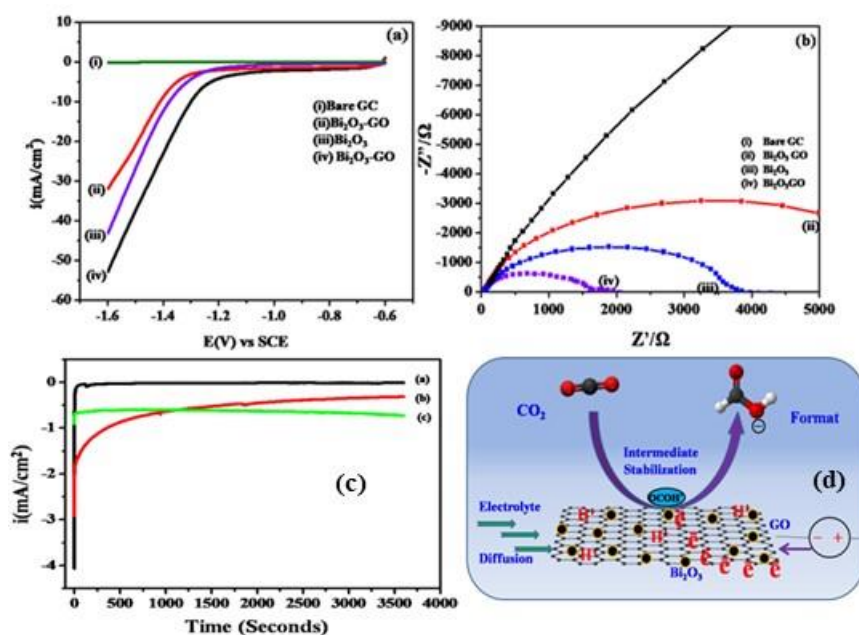


Fig 2: (a) Linear sweep voltammetry shows (i)bare GC; (ii)-GO; (iii)Bi₂O₃GO with N₂; (iv)Bi nanoparticles; (v)Bi₂O₃GO hybrid nanocomposite with N₂CO₂in 0.5M KHCO₃; (b) Nyquist plot of CO₂reduction on (i)-bare GC, (ii) Bi₂O₃GO with N₂, (iii)Bi₂O₃nanoparticles with N₂ CO₂, (iv) Bi₂O₃GOhybrid nanocomposite with N₂CO₂ in 0.5M KHCO₃, (c) Bulk electrolysis of Bi₂O₃@GO at -1.2V, -1.4V and -1.6 V vs SCE in saturated CO₂ in 1 M KHCO₃ (before saturated by N₂ to remove soluble O₂) supporting electrolyte solution and (d) representative schematic presentation of CO₂ reduction.

To know the kinetics of electron transfer at the electrified interface of Bi₂O₃@GO towards CO₂reduction, electrochemical impedance spectroscopy (EIS) was employed. The EIS has been carried out at -1 V v/s RHE for the range of frequency was 0.01 to 1000Hz with N₂and CO₂in KHCO₃electrolyte. Larger the width of semicircle more the resistance (R_{ct}) of charge transfers and vice versa.TheBi₂O₃@GO composite has smaller R_{ct} as compare other three materials, i.e. bare GC, bismuth NPs and Bi₂O₃@GOcomposite without CO₂as shown in **Fig 2(b)**. This concludes the easy path for electron transfer at Bi₂O₃@GOcomposite interface and is in good agreement with the higher current density from LSV for CO₂ reduction (**Fig 2(a)**). The results also conclude the facile electron transfer towards CO₂reduction occurs at -1.0 V v/s RHE on the electrode. Additionally, for the determination of product, we have performed the bulk electrolysis of saturated CO₂in 0.5M KHCO₃ for 3600 sec. at -1.2 (a), -1.4 (b) and -1.6V (c) v/s RHE at different potentials on Bi₂O₃@GO electrocatalyst and are shown in **Fig. 2(c)**. The formate produced at -1.2 (a) 0.000934 mol/lit, -1.4 (b) 0.0013 mol/lit and -1.6 (c) 0.02826 mol/lit V v/s RHE.As potential shifted towards more negative the current density goes on increasing and format production too at under experimental conditions. [26, 27]

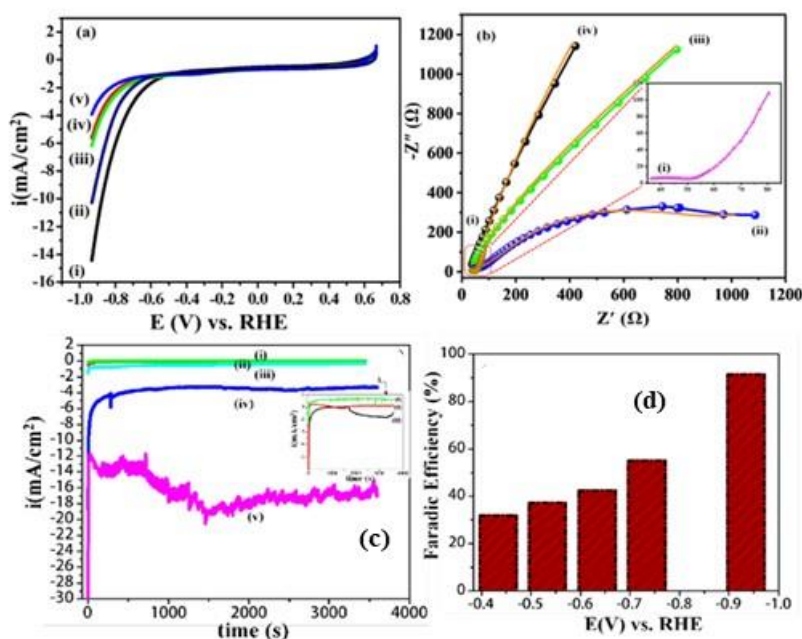


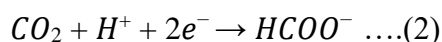
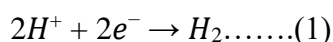
Fig 3. (a) Superimposed LSV curves obtained at a scan rate of 50 mV s^{-1} for electrochemical reduction of CO_2 . Prior to the experiments, the electrolyte is bubbled with N_2 gas (for 30 min) to remove dissolved O_2 , followed by CO_2 gas (for 40 min) to saturate it with CO_2 , except for the control experiment in (ii), in which case only N_2 gas was bubbled. The experiments are done over (i) Al_2O_3 -rGO in KHCO_3 solution (0.5 M) bubbled with N_2 and then CO_2 , (ii) Al_2O_3 -rGO in KHCO_3 solution (0.5 M) saturated only with N_2 gas, (iii) Al_2O_3 bubbled with N_2 and then CO_2 , (iv) rGO saturated with N_2 and then CO_2 , and (v) bare GC in 0.5 M KHCO_3 solution bubbled with N_2 and then CO_2 . (b) Nyquist plots for CO_2 reduction at an applied potential of -0.848 V vs. RHE over (i) Al_2O_3 -rGO hybrid nanocomposite bubbled with N_2 then CO_2 (value Al_2O_3 -rGO hybrid nanocomposite) (ii) Al_2O_3 bubbled with N_2 then CO_2 , (iii) rGO bubbled with N_2 gas then CO_2 , and (iv) bare GC in 0.5 M KHCO_3 bubbled with N_2 and then CO_2 . Bulk electrolysis performed for 3,600 s over (c) Al_2O_3 -rGO at potentials of (i) -0.434 V , (ii) -0.534 V , (iii) -0.634 V , (iv) -0.734 V and (v) -0.934 V vs. RHE in KHCO_3 electrolyte bubbled with N_2 and then CO_2 . (d) The values of FE obtained at applied potentials of -0.434 , -0.534 , -0.634 , -0.734 and -0.934 V vs. RHE are found to be ~ 31.90 , 37.25 , 42.50 , 55.10 and 91.20% , respectively.

Fig 3(b) shows the EIS plots obtained at an applied potential of -0.848 V vs. RHE for (i) Al_2O_3 -rGO hybrid nanocomposite material, (ii) Al_2O_3 , (iii) rGO, and (iv) bare GC in KHCO_3 electrolyte bubbled with N_2 , followed with CO_2 . The results indicate that Al_2O_3 -rGO has the lowest resistivity (with a value of $R_{\text{ct}} = 21.5 \Omega$) compared with Al_2O_3 (with $R_{\text{ct}} = 26.1 \Omega$), rGO (with $R_{\text{ct}} = 28.6 \Omega$) and bare GC (with $R_{\text{ct}} = 58.3 \Omega$). These results indicate that Al_2O_3 -rGO has a relatively greater conductivity and ability to transfer electron during electrocatalytic CO_2 reduction. To examine the stability and the potential of Al_2O_3 -rGO catalyst to reduce CO_2 on a large scale, chronoamperometric (i-t) measurements at different applied potentials using

KHCO₃ solution (0.5 M) as a supporting electrolyte are carried out. The results are displayed in **Fig. 3(c)**. In the experiments, the potential is kept constant for a particular period of time. The changes observed in the electrocatalytic reduction reaction of CO₂ are quantified, based on the product determined by HPLC analysis. It is worth noting here that formate is found to be the product of the electrocatalytic CO₂ reduction reaction. As the potential is shifted towards more cathodic side, the current density of the reaction significantly increases [**Fig. 3(d)**]. [32, 33]

Mechanism:

The electrochemical reduction of CO₂ into formate is having two reductive steps, in both the cases under CO₂ the current increases, the first step corresponding to H₂ generation and second due to both competitive processes corresponding to H₂ generation and CO₂ reduction.



Furthermore, a better comparison, the LSV curves of Al₂O₃-rGO obtained in saturated N₂ gas and in CO₂ gas are overlaid in **Fig. 3(a)**, (i) and (ii). The LSV curves, shown in **Fig. 3(a)**, reveal that the electrochemical reduction of CO₂ over Al₂O₃-rGO takes place at an onset potential of -0.434V vs. RHE. This value is lower as compared with those of the other electrocatalysts, namely, Al₂O₃NPs, rGO, and bare GC, denoted in **Fig. 3(a)**, as (iii), (iv) and (v). Besides, the current density obtained for the former is higher. The higher current density and lower onset potential obtained in CO₂ environment for Al₂O₃-rGO indicate its viability for efficient electrochemical reduction of CO₂. [28-31]

From **Fig. 4(a)**, the behavior of five LSVs corresponding to the different systems has been demonstrated in the potential range of 0.66 to -0.65 V vs. RHE under saturated N₂ followed by CO₂ atmosphere. Amongst this, nanocomposite MnO₂/g-C₃N₄ having the lowest onset potential of -0.14V vs. RHE and a higher current density of ~7 mA/cm². The same nanocomposite with saturated N₂ gas bubbled only; the current and onset potential difference between CO₂ and N₂ confirmed the reduction of CO₂. Again, the current density perceived is lower for MnO₂, g-C₃N₄ and bare GC as correlated with MnO₂/g-C₃N₄. Furthermore, the onset potential and current density were observed in the present system and are more efficient than reports from the literature. The electrocatalytic reduction accompanied due to the synergetic effect and high surface energy of the MnO₂/g-C₃N₄ and easy electron transfer from the

electrode surface to the CO₂ molecule under experimental conditions. In our previous report ZnO decorated g-C₃N₄ heterogeneous catalyst has been used for the electrocatalytic and catalytic hydrogenation of CO₂, as per as potential (i.e. -0.14 V vs. RHE) for formate formation concern the activity observed may be due to the morphology is hexagonal plates with inter-planar lattice for MnO₂. [34- 36]

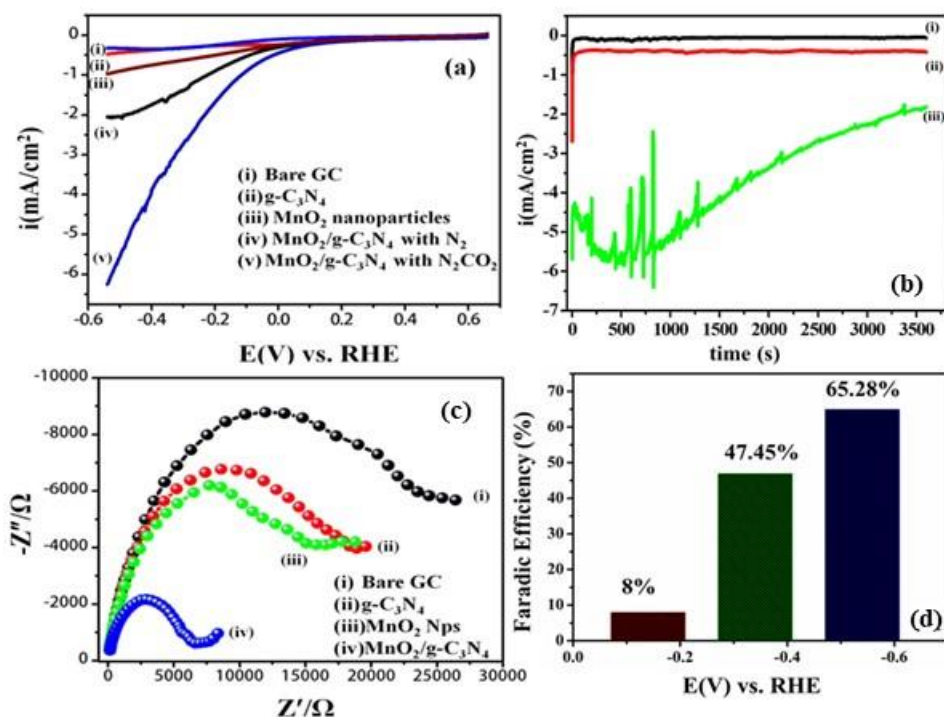


Fig. 4: Superimposed linear sweep voltammogram (LSV) (a) contains (i) bare GC with N₂CO₂, (ii) g-C₃N₄ with N₂CO₂, (iii) MnO₂ nanoparticles (NPs) with N₂CO₂, (iv) MnO₂/g-C₃N₄ with N₂ only and (v) MnO₂/g-C₃N₄ with N₂CO₂. (b) bulk electrolysis at applied potential (i) -0.14 V, (ii) -0.34 V and (iii) -0.54 V vs. RHE; (c) Superimposed Nyquist plot at potential of -0.35 V vs. RHE on working electrode (i) bare GC, (ii) g-C₃N₄, (iii) MnO₂ NPs and (iv) MnO₂/g-C₃N₄ in 0.5 M KHCO₃ under saturated N₂ and CO₂ gas molecules and (d) Faradic efficiency observed 8%, 47.45% and 65.28 % at applied potential, -0.14, -0.34 and -0.54 V vs. RHE respectively.

After confirmation of the reduction of CO₂ based on initial experiments, we have carried out the bulk electrolysis studies and shown in **Fig. 4(b)** for further qualitative and quantitative analysis of reduced products. The saturated CO₂ was containing supporting electrolyte 0.5 M KHCO₃ used for the bulk electrolysis for the time of 3600 sec. at potentials of -0.14, -0.34 and -0.54 V vs. RHE and the obtained product formate is quantified. In i-t (current vs. time) curve the fluctuations has been observed in the graph this is due to interaction between CO₂ molecule on MnO₂/g-C₃N₄ interface with adsorption and product formation after reduction reaction. In

both the step adsorption of CO₂ and desorption of product occurred at electrode interface results in the kinks in the graph. [39, 42]

The electrochemical impedance spectroscopic (EIS) studies were accomplished to depict the electron feasibility at electrode/electrolyte interface during the electrochemical reduction of CO₂. The experiments were performed on a three-electrode system under N₂ followed by CO₂ continuous bubbling in 0.5 M KHCO₃ supporting electrolyte at a potential of -0.35 V vs. RHE from a frequency range of 100 KHz to 0.01 Hz as shown in **Fig. 4(c)**. The semicircle in the Nyquist plot of an electrochemical cell has been shown the direct charge transfer resistance (R_{ct}) values for individual electrocatalysts. The small semicircle indicates easier electron transfer from the electrode (electrocatalyst) to electrolyte at the interface, and less will be the resistance. In contrast, the larger will be the diameter of semicircle, more will be the resistivity in the system. From experimental results exhibited that the MnO₂/g-C₃N₄ nanocomposite is having a small semicircle with resistivity value of 8412.1 Ω whereas, remaining systems showed high resistivity values as 17721.4, 19700.9 and 26407.5 Ω for electrocatalytic systems like MnO₂, g-C₃N₄ and bare GC respectively. The outcome of the Nyquist plot conformed that the MnO₂/g-C₃N₄ is having more feasibility for electron transfer from the surface of the electrode to the CO₂ molecule electro-reduction these result good argument with LSV result. [37, 38]

The MnO₂/g-C₃N₄ nanocomposite has been used for bulk electrolysis and potential-dependent -0.14, -0.34, and -0.54 V vs. RHE, the FE observed are 8, 47.45 and 65.28% respectively. Significantly, it has been noted as an applied potential shifted towards negative the FE increases because at the higher negative potential, the more feasibility of electron and mass transfer results into higher Faradic value and shown in **Fig. 4(d)**. [43]

To examine the electrocatalytic activity of the synthesized material towards the CO₂ reduction on ZnO/C₃N₄ (working electrode), Pt wire counter and SCE as the reference electrodes has been used in potential range of 0.066 V to -0.934V vs. RHE in aqueous 0.5 M KHCO₃ (pH 7.2) supporting electrolyte with a scan rate of 50 mV/s. The pH of the electrolyte after CO₂ saturation was measured and found to be 7.2. Accordingly, linear sweep voltammetric (LSV) measurements were employed to study the conductivity performance and cathodic current profiles are as shown in **Fig. 5(a)**. The electrochemical results demonstrate that the highest current density was observed for the as-prepared ZnO/g-C₃N₄ composite, compared with g-C₃N₄, ZnO and bare GC electrodes respectively. Moreover, the significant current was observed for ZnO/g-C₃N₄ (v) with CO₂ than alone N₂ (iv) purged samples and also

electrocatalyst g-C₃N₄ (iii), ZnO (ii) and bare GC (i) containing KHCO₃ electrolyte. In the electrochemical hydrogenation of CO₂ two reactions are always compete with each other i.e. hydrogen evolution and CO₂ hydrogenation. Additionally, the bulk electrolysis also employed for the stability of as-synthesized ZnO/g-C₃N₄ nanocomposite further product conformation and product efficiency for 3600 sec at three different potentials of -0.504, -0.734 and -0.934 V vs. RHE as shown in **Fig. 5(b)** (i, ii and iii) in 0.5 M KHCO₃ supporting electrolyte solution. It is also observed that as potential goes on increasing the current density also increased. The cathodic current observed was -50 mA/cm² whereas with N₂ -33 mA/cm² the current density difference predominates electrocatalyst is active for CO₂ hydrogenation [44]. The cathodic current enhanced on ZnO/g-C₃N₄ may be due to the inter-electron transfer from ZnO center to CO₂ via. g-C₃N₄ and also the synergetic effect of both the electrocatalyst. The cathodic onset potential observed for the electrochemical reduction was -0.504 V vs. RHE, which is having comparatively low potential as with only saturated N₂ -0.614V vs. RHE. Furthermore, to know the electrode kinetics and different affecting parameters of ZnO/g-C₃N₄ hybrid for CO₂ hydrogenation reactions electrochemical impedance spectroscopy (EIS) was employed and demonstrated in **Fig. 5(c)**. [44-47]

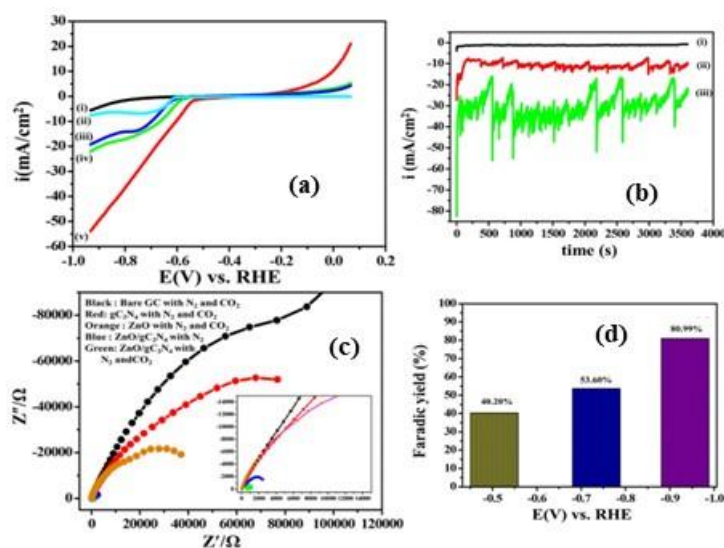


Fig 5. (a) Superimposed linear sweep voltogram (LSV) (i) bare GC with saturated N₂CO₂, (ii) g-C₃N₄ with N₂CO₂, (iii) ZnO nanostructures N₂CO₂, (iv) ZnO/g-C₃N₄ with N₂ only, and (v) ZnO/g-C₃N₄ with N₂CO₂ in 0.5 M KHCO₃ at scan rate 50 mV s⁻¹; Superimposed (b) bulk electrolysis of ZnO/g-C₃N₄ at potential -0.504V (i), -0.734V (ii) and -0.934V (iii) vs. RHE respectively in N₂ saturated and CO₂ in KHCO₃ supporting electrolyte for 3600 s. (c) Nyquist impedance plots: black-bare GC with N₂ CO₂, red- g-C₃N₄ with N₂ CO₂, orange-ZnO with N₂CO₂, blue-ZnO/g-C₃N₄ sheet with N₂CO₂ and green-ZnO/g-C₃N₄ with N₂ and CO₂ in 0.5M KHCO₃ at potential -0.55 V vs. RHE within frequency range

0.01 to 1000 Hz and (d) The Faradic efficiency observed on ZnO/g-C₃N₄ hybrid electrocatalyst at potentials of -0.504 V, -0.734 V and -0.934 V vs. RHE were 40.20%, 53.60% and 80.99% respectively.

The larger the diameter more will be the resistance in charge transfers and vice versa. The electrochemical impedance has been carried out at -0.55V vs. RHE where the range of frequency was 0.01 to 1000 Hz applied with saturated N₂ and followed to CO₂ in KHCO₃ electrolyte. [22-25] The experimental the resistance (R_{ct}) values observed are ~119207.7 Ω, ~76692 Ω, ~2469.6 Ω and ~636 Ω for electrocatalytic systems for bare GC, g-C₃N₄, ZnO and ZnO/g-C₃N₄ respectively. The experimental results evidence proved with CO₂ gas, the more electron feasibility was observed i.e. ZnO/g-C₃N₄ composite having FE values in **Fig 5 (d)**. This is because the rapid electrochemical reduction occurs on ZnO/g-C₃N₄ electrode in CO₂ environment than other electrocatalytic systems.

Conclusion

In summary, we have developed Bi₂O₃@GO, Al₂O₃@rGO, ZnO/g-C₃N₄ and MnO₂/g-C₃N₄ nanocomposite by using simple precipitation followed by the calcination method. The synthesized nanocomposite well characterized by various characterization techniques and used further for electrochemical CO₂ reduction reactions. The proposed electrocatalysts having higher FE for formate formation i.e. 83, 92, 91 and 69% for Bi₂O₃@GO, Al₂O₃@rGO, ZnO/g-C₃N₄ and MnO₂/g-C₃N₄ nanocomposites respectively. The formate generation from CO₂ on this is applicable from industry point of view, as well as for society to reduce environmental pollution concerns.

Acknowledgments

Author BBM are grateful to the University Grant Commission (UGC) New Delhi (India) for SRF Fellowship. BRS is thankful to DST-SERB New Delhi, (India) research project (Ref F.NO.SERB/F/7490/2016-17) and DAE-BRNS, Mumbai (India) research project (Ref F. No. 34/20/06/2014-BRNS/21gs) for financial assistance. We are also thankful to the Department of Chemistry, Dr. Babasaheb Ambedkar Marathwada University, Aurangabad-431004 (MS) India for providing the laboratory facility.

Reference

1. Historical Overview of Climate Change Science, Herve Le Treut (France), Richard Somerville (USA), 2016.

2. Global energy demand rose by 2.3% in 2018, its fastest pace in the last decade, 26 March 2019, by The International Energy Agency.
3. NOAA National Centers for Environmental Information, Global Climate Report - May 2019.
4. T. T. H. Hoang, S. M. J. I. Gold, P. J. A. Kenis, A. A. Gewirth, Nanoporous copper films by additive-controlled electrodeposition: CO₂ reduction catalysis, *ACS Catal.*, 75 (2017) 3313-3321.
5. M. Liu, Y. Yi, L. Wang, H. Guo, A. Bogaerts, Hydrogenation of CO₂ to value-added chemicals by heterogeneous catalysis and plasma catalysis, *Catalysts.*, 9 (2019) 275-279.
6. J. Jang, B. W. Jeon, Y. H. Kim, Bioelectrochemical conversion of CO₂ to value-added product formate using engineered methylobacterium extorquens, *Sci Rep.*, 8 (2018) 7211-7218.
7. D. J. Boston, C. Xu, D. W. Armstrong, F. M. Mac Donnell, Photochemical reduction of carbon dioxide to methanol and formate in a homogeneous system with pyridinium catalysts, *J. Am. Chem. Soc.*, 135 (2013) 16252-16255.
8. T. N. Huan, P. Simon, G. Rousse, I. Genois, V. Artero, M. Fontecave, Porous dendritic copper: an electrocatalyst for highly selective CO₂ reduction to formate in water/ionic liquid electrolyte, *Chem. Sci.*, 8 (2017) 742-747.
9. (a) B. B. Mulik, B. D. Bankar, A. V. Munde, A. V. Biradar, B. R. Sathe, Bismuth oxide-decorated graphene oxide hybrids for catalytic and electrocatalytic reduction of CO₂, *Chem. of Euro. Journal* 26, (2020) 8801-8809; (b) J. Albo, M. Alvarez-Guerra, P. Castano, A. Irabien, *Green Chem.*, Towards the electrochemical conversion of carbon dioxide into methanol, 17 (2015) 2304-2324.
10. (a) D. Saravanakumarn, J. S. S. Lee, N. H. Hur, W. Shin, Electrocatalytic conversion of carbon dioxide and nitrate ions to urea by a titania–nafion composite electrode, *Chem Sus Chem.*, 10 (2017) 3999-4003; (b) A. V. Munde, B. B. Mulik, P. P. Chavan, B. R. Sathe, Enhanced electrocatalytic activity towards urea oxidation on Ni nanoparticle decorated graphene oxide nanocomposite, *Electro. Acta*, 349, (2020) 136386.
11. (a) Q. Lu, F. Jiao, Electrochemical CO₂ reduction: Electrocatalyst, reaction mechanism, and process engineering, *Nano Energy.*, 29 (2016) 439-456; (b) E. V. Kondratenko, G.

- Mul, J. Baltrusaitis, G. O. Larrazábal, J. Peerez-Ramirez, Status and perspectives of CO₂ conversion into fuels and chemicals by catalytic, photocatalytic and electrocatalytic processes, *Energy Environ. Sci.*, 6 (2013) 3112-3135.
12. (a) C. Jia, K. Dastafkan, W. Ren, W. Yanga, C. Zhao, Carbon-based catalysts for electrochemical CO₂ reduction, *Sustain. Energy Fuels.*, 3 (2019) 2890-2906; (b) B. B. Mulik, B. D. Bankar, A. V. Munde, A. V. Biradar, B. R. Sathe, Highly efficient manganese oxide decorated graphitic carbon nitrite electrocatalyst for reduction of CO₂ to formate, *Catalysis Today*, 370 (2021) 104-113
13. (a) S. Ringe, Ezra L. Clark, J. Resasco, A. Walton, B. Seger, A. T. Bell, K. Chan, Understanding cation effects in electrochemical CO₂ reduction, *Energy Environ. Sci.*, 12 (2019) pp. 3001-3014; (b) S. Kaneco, H. Katsumata, T. Suzuki, K. Ohta, High efficiency electrochemical CO₂-to-methane conversion method using methanol with lithium supporting electrolytes, *Energy Fuels.*, 20 (2006) 409-414.
14. T. Zhang, Y. Qiu, P. Yao, X. Li, H. Zhang, Bi-modified Zn catalyst for efficient CO₂ electrochemical reduction to formate, *ACS Sustainable Chem. Eng.*, 7 (2019) 15190-15196.
15. X. Liu, C. Chen, Y. Zhao, B. Jia, A Review on the Synthesis of manganese oxide nanomaterials and their applications on Lithium-ion batteries, *Journal of Nanomaterials.*, 736375 (2013) 1-7.
16. X. Zhang, Z. Zhang, S. Sun, Q. Sun, X. Liu, Hierarchical 3D NiFe₂O₄@MnO₂ core-shell nanosheet arrays on Ni foam for high-performance asymmetric supercapacitors, *Dalton Trans.*, 47 (2018) 2266-2273.
17. Y. Wei, J. Liu, F. Cheng, J. Chen, Mn-doped atomic SnO₂ layers for highly efficient CO₂ electrochemical reduction, *J. Mater. Chem. A.*, 7 (2019) 19651-19656.
18. A. S. Varela, W. Ju, P. Strasser, Molecular nitrogen-carbon catalysts, solid metal organic framework catalysts, and solid metal/nitrogen-doped carbon (MNC) catalysts for the electrochemical CO₂ reduction, *Adv. Energy Mater.*, 8 (2018) 1703614 1-8.
19. G. M. Veith, L. Baggetto, L. A. Adamczyk, B. Guo, S. S. Brown, X.-G. Sun, A. A. Albert, J. R. Humble, C. E. Barnes, M. J. Bojdys, S. Dai, N. J. Dudney, Electrochemical and solid-state lithiation of graphitic C₃N₄, *Chem. Mater.*, 25 (2013) 503-508.

20. (a) J. Safaei, N. A. Mohamed, M. F. M. Noh, M. F. Soh, N. A. Ludin, M. A. Ibrahim, W. N. R. W. Isahak, M. A. M. Teridi, Graphitic carbon nitride (g-C₃N₄) electrodes for energy conversion and storage: a review on photoelectrochemical water splitting, solar cells and supercapacitors, *J. Mater. Chem. A.*, 6 (2018) 22346-22380; (b) T. Thirupathi, K. Ramanujam, Carbon supported g-C₃N₄ for electrochemical sensing of hydrazine, *Electrochem. Energy Technol.*, 4 (2018) 21-31.
21. B. Zhang, T. J. Zhao, W. J. Feng, Polarized few-layer g-C₃N₄ as metal-free electrocatalyst for highly efficient reduction of CO₂, *Nano Res.*, 11 (2018) 2450-2459.
22. W. Wang, Y. Kan, B. Yu, Y. Pan, K. M. Liew, L. Song, Y. Hu, Synthesis of MnO₂ nanoparticles with different morphologies and application for improving the fire safety of epoxy, *Compos. Part A Appl. Sci. Manuf.*, 95 (2017) 173-182.
23. A. Ben-Refael, I. Benisti, Y. Paz, Transient photoinduced phenomena in graphitic carbon nitride as measured at nanoseconds resolution by step-scan FTIR, *Catal. Today.*, 340 (2020) 97-105.
24. (a) M. Sun, T. Lin, G. Cheng, F. Ye, L. Yu, Hydrothermal synthesis of boron-doped MnO₂ and its decolorization performance, *Journal of Nanomaterials*, 175924 (2014) 1-6. (b) L.Feng, Z. Xuan, H. Zhao, Y. Bai, J. Guo, C. Su, X. Chen, MnO₂ prepared by hydrothermal method and electrochemical performance as anode for lithium-ion battery, *NRL* 9 (2014) 290.
25. L. Zhang, X. Hea, X. Xu, C. Liu, Y. Duan, L. Houa, Q. Zhoua, C. Ma, X. Yang, R. Liu, F. Yang, L. Cui, C. Xu, Y. Li, Highly active TiO₂/g-C₃N₄/G photocatalyst with extended spectral response towards selective reduction of nitrobenzene, *Appl Catal B Environ.*, 203 (2017) pp. 1-8;
26. (a) H. Xia, Y. Wang, J. Lin, L. Lu, Hydrothermal synthesis of MnO₂/CNT nanocomposite with a CNT core/porous MnO₂ sheath hierarchy architecture for supercapacitors, *Nanoscale Research Letters*, 7 (2012) 1-6. (b) RP Dighole, AV Munde, BB Mulik, SS Zade, BR Sathe, Melamine functionalised multiwalled carbon nanotubes (M-MWCNTs) as a metal-free electrocatalyst for simultaneous determination of 4-nitrophenol and nitrofurantoin, *N J C.* 46 (2022) 17272-17281

27. Y. Qi, Q. Liang, R. Lv, W. Shen, F. Kang, Z.-H. Huang, Synthesis and photocatalytic activity of mesoporous g-C₃N₄/MoS₂ hybrid catalysts, *R. Soc. Open Sci.*, 5 (2018) 180187.
28. (a) Z. Zhang, J. Huang, M. Zhang, Q. Yuan, B. Dong, Ultrathin hexagonal SnS₂ nanosheets coupled with g-C₃N₄ nanosheets as 2D/2D heterojunction photocatalysts toward high photocatalytic activity, *Appl. Catal. B-Environ.*, 163 (2015) 298-305; (b) B B Mulik, B D Bankar, A V Munde, A V Biradar, T Asefa, BR Sathe, Facile synthesis and characterization of γ -Al₂O₃ loaded on reduced graphene oxide for electrochemical reduction of CO₂, *Sus Energy & Fuels* 6 (2022) 5308-5315
29. M. K. Kesarla, M. O. F. Torres, M. A. A. Ramos, F. O. Chi, C. G. E. Gonzalez, M. Alemand, J. G. T. Torres, S. Godavarthi, Synthesis of g-C₃N₄/N-doped CeO₂ composite for photocatalytic degradation of an herbicide, *J. Mater. Estechnol.*, 8 (2019) 1628-1635.
30. L. Huang, F. Zhang, Y. Li, H. Wang, Q. Wang, C. Wang, H. Xu, H. Li, Chemical reduction implanted oxygen vacancy on the surface of 1D MoO_{3-x}/g-C₃N₄ composite for boosted LED light-driven photoactivity, *J Mater Sci.*, 54 (2019) 5343-5358.
31. J. Wang, C. Li, Z. Yang, D. Chen, Chemical vapor deposition-assisted fabrication of a graphene-wrapped MnO/carbon nanofibers membrane as a high-rate and long-life anode for lithium ion batteries, *RSC Adv.*, 7 (2017) 50973.
32. F. Dong, Z. Zhao, T. Xiong, Z. Ni, W. Zhang, Y. Sun, W. K. Ho, In-situ construction of g-C₃N₄/g-C₃N₄ metal-free heterojunction for enhanced visible-light photocatalysis, *ACS Appl. Mater. Interfaces.*, 5 (2013) 11392-11401.
33. J. Son, D. Song, K. R. Lee, J. I. Han, Electrochemical reduction of CO₂ on Ag/MnO₂ binary catalyst, *J. Environ. Chem. Eng.*, 7 (2019)103212.
34. B. B. Mulik, B. D. Bankar, A. V. Munde, P. P. Chavan, A. V. Biradar, B. R. Sathe, Electrocatalytic and Catalytic CO₂ Hydrogenation on ZnO/g-C₃N₄ Hybrid Nanoelectrodes, *App. Surf Sci.*, 538 (2020) 148120.
35. F. Li, L. Chen, G. P. Knowles, D. R. M. Farlane, J. Zhang, Hierarchical mesoporous SnO₂ nanosheets on carbon cloth: a robust and flexible electrocatalyst for CO₂ reduction with high efficiency and selectivity, *Angew Chem Int Ed Engl.*, 56 (2017) 505-509.

36. V. S. Sapner, P. P. Chavan, B. R. Sathe, 1-Lysine-Functionalized Reduced Graphene Oxide as a Highly Efficient Electrocatalyst for Enhanced Oxygen Evolution Reaction, *ACS Sustainable Chem. Eng.*, 8 (2020) 5524-5533.
37. BB Mulik, AV Munde, RP Dighole, BR Sathe, Electrochemical determination of semicarbazide on cobalt oxide nanoparticles: Implication towards environmental monitoring, *J Ind Eng Chem* 93,(2021) 259-266.
38. (a) S. N. Zhang, M. Li, B. Hua, N. Duan, S. Ding, S. Bergens, K. Shankar, J. L. Luo, A rational design of Cu₂O–SnO₂ core-shell catalyst for highly selective CO₂-to-CO conversion, *Chem Cat Chem.*, 11 (2019) 4147-4153.(b) AV Munde, BB Mulik, RP Dighole, BR Sathe, Urea Electro-Oxidation Catalyzed by an Efficient and Highly Stable Ni–Bi Bimetallic Nanoparticles, *ACS Appl Energy Mat.* 4 (2021) 13172-13182
39. T. Asset, S. T. Garcia, S. Herrera, N. Andersen, Y. Chen, E. J. Peterson, I. Matanovic, K. Artyushkova, J. Lee, S. D. Minter, S. Dai, X. Pan, K. Chavan, S. C. Barton, P. Atanassov, Investigating the nature of the active sites for the CO₂ reduction reaction on carbon-based electrocatalysts, *ACS Catalysis.*, 9 (2019) 7668-7678.
40. B. Zhang, T. J. Zhao, W. J. Feng, Y. X. Liu, H. H. Wang, H. Su, L. B. Lv, X. H. Li, J. S. Chen, Polarized few-layer g-C₃N₄ as metal-free electrocatalyst for highly efficient reduction of CO₂, *Nano Research.*, 11 (2018) 2450-2459.
41. H. Wang, Y. Chen, X. Hou, C. Maa, T. Tan, Nitrogen-doped graphenes as efficient electrocatalysts for the selective reduction of carbon dioxide to formate in aqueous solution, *Green Chem.*, 18 (2016) 3250-3255.
42. Y. Qiu, J. Du, W. Dong, C. Dai, C. Tao, Selective conversion of CO₂ to formate on a size tunable nano-Bi electrocatalyst, *J. CO₂ Util.*, 20 (2017) 328-335.
43. J. H. Koh, D. H. Won, T. Eom, N. K. Kim, K. D. Jung, H. Kim, Y. J. Hwang, B. K. Min, Facile CO₂ Electro-reduction to formate via oxygen bidentate intermediate stabilized by high-index planes of Bi dendrite catalyst, *ACS Catal.*, 7 (2017) 5071-5077.
44. (a) X. Nie, M. R. Esopi, M. J. Janik, A. Asthagiri, Selectivity of CO₂ reduction on copper electrodes: the role of the kinetics of elementary steps, *Angew. Chem. Int. Ed.*, 52 (2013) 2459-2462; (b) Y. F. Zhao, Y. Yang, C. Mims, C. H. F. Peden, J. Li, D. H. J. Mei, Insight into methanol synthesis from CO₂ hydrogenation on Cu(111): Complex reaction network

- and the effects of H₂O, *Catal.*, 281 (2011) 199-211; (c) AV Munde, BB Mulik, RP Dighole, SC Dhawale, LS Sable, AT Avhale, B R Sathe, Bi₂O₃@ Bi nanoparticles for ultrasensitive electrochemical determination of thiourea: monitoring towards environmental pollutants. *Electrochimica Acta* 394, (2021) 139111
45. A. P. Gelbein, Morristown, R. Hansen, W. Caldwell, Hydrogenation Of Carboxylic Acid Compounds To Aldehydes Using MnO₂ On Gamma Aluminaas Catalyst, Patent Number: 4,585,899 United States Patent.
46. (a) Q. Liu, X. Yang, L. Li, S. Miao, Y. Li, Y. Li, X. Wang, Y. Huang, T. Zhang, Direct catalytic hydrogenation of CO₂ to formate over a Schiff-base-mediated gold nano catalyst, *Nat. Commun.* 8 (2017) 1-8. (b) RP Dighole, AV Munde, BB Mulik, BR Sathe, Bi₂O₃ Nanoparticles Decorated Carbon Nanotube: An Effective Nanoelectrode for Enhanced Electrocatalytic 4-Nitrophenol Reduction, *Front. Chem.* 8, (2020) 355.
47. W. H. Wang, Y. Himeda, J. T. Muckerman, G. F. Manbeck, E. Fujita, CO₂ hydrogenation to formate and methanol as an alternative to photo- and electrochemical CO₂ reduction. *Chem. Rev.*, 115, (2015) 12936-12973.

**Designing of photoelectrochemical device towards practical solar water splitting : A
review on recent progress of BiVO₄ photoanodes**

**Ms. Sangeeta Ghosh, Mr. Aditya Poddar, Mr. Himanshu Sekhar Sahoo, Mr.
Swarnendu Baduri, Mr. Debasish Ray, and Dr. Chinmoy Bhattacharya ***

Department of Chemistry, Indian Institute of Engineering Science & Technology (IEST),
Shibpur, Howrah-711103, West Bengal, INDIA

* Email: chinmoy@chem.iests.ac.in, cbhattacharya.besus@gmail.com

Abstract:

The solar-driven photoelectrochemical water splitting process has a tremendous impact, which follows the natural photosynthesis process by converting solar energy into usable forms of chemical energy. The development of a PEC system can convert H₂O to H₂/O₂ or CO₂ to C-based fuels. To obtain the goal for artificial photosynthesis, rate-determining kinetics of the oxygen evolution reaction is considered on a highly efficient photo-anode. BiVO₄ has attracted the attention as a photoanode in the development of the PEC. Owing to an intermediate band gap, the earth-abundant nature of the constituents it is considered as a cost-effective n-type semiconductor for PEC H₂O splitting. The present article elaborates the present status on the progress of BiVO₄-based photoanodes fabrication, with controlling the surface morphology, effects of dopants, different synthesis techniques, co-catalyst, etc. Additionally, unbiased tandem devices of the photo-active systems in the presence of BiVO₄ are also discussed.

Introduction:

Since the industrial revolution, the world's demands have gradually increased daily. To fulfil this, clean renewable resources must be explored to the fullest. Apart from the non-conventional sources of energy and to compete with fossil fuels, a cost-effective means of storing converted energy must be found. To capture and store the limitless solar energy in carbon neutral fashion to prevent the production of any environmental contaminant, and to produce the simplest form of energy hydrogen H₂ and environmental benign oxygen O₂ oxygen (2H₂O + hv → 2H₂ + O₂) by splitting water photoelectrochemical water splitting is classified among the auspicious techniques. The expectation of the community for the foundation of the

future's sustainable energy economy, such as hydrogen, should have cleaner essence possessed by the solar water splitting technology. PEC cells have been proven as a distinguished source to tackle this issue by taking complete advantage of solar energy in meeting sustainable energy goals through an efficient and effective means of hydrogen production that serves as a fuel. A concise chronicle of events concerning the exploitation of some inorganic semiconductors for photo assisted water splitting is adequately demonstrated by Osterloh et al. in their report. In 1955 the foremost monstration step in the domain of Photoelectrochemistry was reported by Brattain et al by exploiting the electrochemical investigation of electrolytic junction of germanium, succeeded by the crucial research of Gerischer, Pleskov and Marcus co-worker. On the other hand, the efficacious operation of water photoelectrolysis in 1971 was brought about by Fujishima and Honda by fabricating PEC cell with TiO₂ nanoparticle semiconductor under illuminating conditions. The momentous work of Fujishima and Honda triggered tremendous number of researchers towards the domain of water photoelectrolysis followed by the groups led by the Gratzel's, Bard's and Nozik., has produced numerous report of great impact on this field. Succeeded by the aforementioned immense works a enormous development has been accomplished in the current time to appraise the conceivable and promising candidate to lead photoelectrochemical water splitting more efficiently. The reported articles display that hydrogen production through PEC inorganic metal oxide based semiconductors in the role of photoanode stand out to be well equipped materials as they owned better durability, electrical properties & ease of tailoring. The two distinguished halves illustrate the electrodictics phenomenon, the evolution of H₂ at photocathode by reducing H₂O and the evolution of O₂ at photoanode/counter electrode by oxidising H₂O as displayed in the below equations.

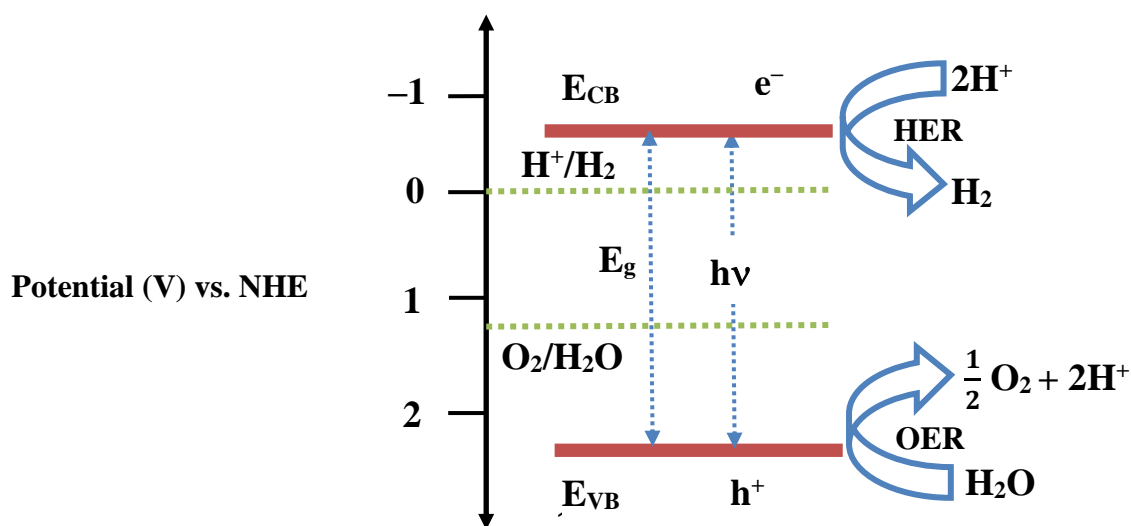
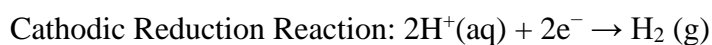
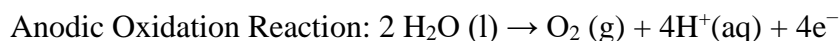


Fig: 1. Oxygen evolution and hydrogen evolution reaction for overall solar water splitting

On illumination, the photoactive material absorbs photon energy greater than its band gap energy and creates excitons (i.e. the photo-generated electron/hole pair). If the semiconductor is of n-type, the photogenerated hole moves to the semiconductor-electrolyte interface to oxidise the water to O₂ molecule and the photogenerated electrons are dragged to the counter electrode (generally Pt in most occasions) by means of external bias to reduce water to H₂. But if the semiconductor is of p-type, due to downward band bending of the interface (semiconductor/electrolyte) the excited electrons are transferred to the semiconductor/electrolyte interface to reduce the water molecule to H₂; on the other hand, the photogenerated holes are dragged to the counter electrode through external bias to oxidise water to O₂. As aforementioned, PEC water splitting technique had few conveniences over the photocatalytic water splitting such as (i) the produced products H₂ and O₂ are need not to be separate as they produced in different chambers; (ii) the recombination of excitons (photogenerated electron/hole pair) are suppressed by self or externally applied bias hence improve the migration of the photogenerated charge to the interface; (iii) conducting substrates were utilized to grow the films, so in future it can be helpful in mass production for industrialization; (iv) importantly like the photocatalytic water splitting it does not demand any external power consumption for stirring. Though they had some challenges, monstrous efforts have been employed to cultivate a convincing model for greater efficacy in water splitting. The photo-driven water splitting is an uphill reaction with positive Gibbs free energy of 237 kJ/mol. To acquire such an amount of energy, the semiconductor should have appropriate band gap energy with proper band alignment so that they can absorb photon (visible light) of sufficient energy to bring out the redox (water oxidation and reduction) reaction. The band gap of the photoelectrodes must be small (~1.5 eV) to absorb an adequate part of the visible region of the solar spectrum. The valance band of the semiconductor should be more positive than the water oxidation potential (1.23 V against NHE at zero pH) to oxidise water into oxygen (O²⁻/O₂) and the conduction band of the semiconductor should be more negative than the water reduction potential (0 V against NHE at zero pH) to reduce water (H⁺/H₂) into hydrogen [1]. Despite that, numerous semiconductors based on inorganic metal oxide employed for the complete water splitting don't own the requirement like desired band gap with proper band alignment and

sufficient durability. Additionally, in PEC methodology, the system experiences energy loss accompanied by the migration and the recombination of photo generated excitons (electron/hole pair) in the semiconductor/electrolyte interface or the bulk solution. Subsequently, for efficacious water splitting, the migration of photogenerated charge, efficient charge separation, and desired band gap with proper band alignment are desirable. Furthermore, the other factors taken into account for the efficiency of overall water splitting are low debye length of the generated charge, better charge absorption through customized surface morphology, size and shape of the semiconductor via involvement of quantum effects, the position of the flat band, the effect of pH, different ions present in the system and charge transfer processes etc. Hence the properties of the photoactive electrodes that owns the efficiency of the PEC water splitting for harvesting limitless solar energy for water splitting. After the pioneering work of Fujishima and Honda employing TiO_2 nanoparticles, several n-type and p-type photocatalysts have been tried for photo assisted water splitting, including main group and transition metals, such as silicon based oxides and carbides, carbon nitride, transition metal based oxide, chalcogenides, metal nitrides respectively. Due to the high chemical durability of neutral and slightly acidic pH, including enough earth-abundance with no toxicity with the legacy of tunable composition, the bismuth-based oxides (n-type semiconductor) are one of the potential aspirants for the solar light-driven water splitting. The crystal of bismuth-based oxide embodied of perovskite unit and is classified among the most enchanting prospect for photo-assisted water splitting due to its well-positioned band gap energy (2.5-2.8 eV), allowing it to absorb nearly 12% of the visible region of the solar spectrum with favourable hole diffusion length of (~150 nm) in contrast with the α - Fe_2O_3 in few nanometres, including superior charge transporting ($12 \text{ cm}^2\text{s}^{-1}\text{V}^{-1}$) property pertaining to TiO_2 ($0.03 \text{ cm}^2\text{s}^{-1}\text{V}^{-1}$). In agreement with the water splitting, the conduction band minima of the semiconductor should be more negative than the water reduction H^+/H_2 potential i.e. 0 V against NHE at zero pH; on the other hand, the valance band maxima should be more positive than the water oxidation O^{2-}/O_2 potential i.e. 1.23 V against NHE at pH 0 [2]. Bismuth oxide consolidates the position of the valance band as the valance band is more positive than the water oxidation potential, but as the coin flip to the position of the conduction band minima, it's not able to reduce water to hydrogen as the conduction band minima are not deep enough situated to overcome the reduction potential. Consequently, bismuth-based oxides in photo-assisted water splitting only produce O_2 not H_2 . Hence to lead the overall water splitting employing bismuth oxide as photo anode it should be united along with a suitable photocathode for the photo-assisted water reduction for the complete fabrication of the PEC device otherwise, the bismuth oxide

photoelectrode is coupled with the counter electrode with an external applied bias to drive the electron to counter electrode to accomplish the water splitting to generate both O₂ and H₂. The upward band bending of the electrode/electrolyte interface made the bismuth oxide the suitable choice to exploit as a photoanode. It's already documented that the theoretical maxima of solar to hydrogen conversion efficiency for bismuth vanadate are about ~4.6% as a PEC tandem device. It's noteworthy that the greater durability of bismuth vanadate in low pH conquers its utility since, in that situation H₂ production is more efficient. Bismuth vanadate is an n-type semiconductor photocatalyst with a direct band gap of 2.48 eV [3]. It absorbs ample visible light and is also used as stable, neutral, nontoxic and relatively cheap electrolyte. The conduction band of the BiVO₄ photocatalyst is composed of mainly V 3d states with small contributions from O 2p and Bi 6p, and the valence band of the BiVO₄ consists of Bi 6s and O 2p. Typically due to the small band gap of the bismuth vanadate, in contrast to TiO₂, provide the former with the privilege to absorb more in the visible region of the solar spectrum on other hand; it portrays a higher stationary photocurrent than Fe₂O₃ owing to enhanced IPCE (incident photon to current conversion efficiency). Consequently, bismuth vanadate is thought to be more appropriate compared to Fe₂O₃ and TiO₂ for applying photoelectrochemical water splitting. Bismuth vanadate as a photocatalyst has gained significant attention towards research due to its high chemical durability. This photocatalyst exists in three phases as mentioned in the following figure which is crystalline - (i) monoclinic phase (ii) scheelite structure with tetragonal phase (iii) zircon structure with tetragonal phase. The monoclinic phase exhibits the highest photocatalytic ability among all the phases as a distortion in the octahedron of VO₄ caused the separation of the negative and positive charges. This led to the generation of an electric field internally and it was productive for making easy separation of the holes and electrons that were photogenerated.

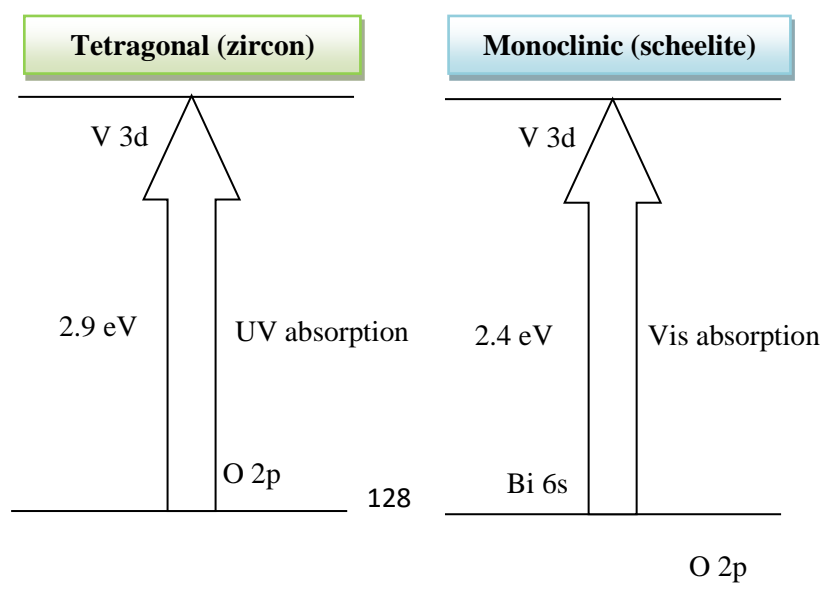


Fig: 2. Band structures of tetragonal BiVO₄ (zircon) and monoclinic BiVO₄ (scheelite)

2. Common synthesis methods to prepare BiVO₄ semiconductors:

There are so many routes that have been proposed to prepare a bismuth vanadate semiconductor. We classify these methods into the electrospinning method, and depending upon phases, they are divided into three major categories; the solid phase technique, the liquid phase technique, and the vapor phase technique. Next, we will demonstrate the technique to fabricate a semiconductor in detail accordingly.

2.1. Electrospinning:

Polymer nanofibers are directly produced by electrospinning technology. This method is especially effective for preparing nanofiber materials. Due to low spinning cost, simple manufacturing equipment, a spacious variation of spinnable materials and a controllable method, it becomes a beneficial technique to harvest different nanofibers comprising organic, organic & inorganic composites and inorganic nanofibers. Cheng et al. synthesized bismuth vanadate nanofiber via electrospinning technique using bismuth nitrate and ammonium meta vanadate as starting material in the presence of citric acid as a chelating agent, [4] the phase junction structure of scheelite, monoclinic and tetragonal phases of electrospun bismuth vanadate were obtained by the controlled heating. The PC activity study reported that the phase junction structure of scheelite - monoclinic and scheelite - tetragonal showed amplified behavior under the irradiation of visible light. R. P. Antony et al. prepared BVO and Mo-doped BVO nanoparticles by the electrospinning process using bismuth nitrate and vanadium acetylacetonate as starting material where ammonium molybdate tetra hydrate is used as the source of molybdenum. [5] The PEC measurements indicate that due to the doping of Mo, the water oxidation photocurrent of BVO increases by four times that of pure semiconductor.

2.2. Solid Phase Technique:

In this method, a precursor is assorted properly and crushed with a specific stoichiometric ratio before calcination at a particular temperature for the product formation without any solvent. This method has some great advantages with simple technique and favorable process, uniformity in particle size, and adjustable force. However, this method's major drawbacks are that the particle's aggregation is facile; the impurities are easily diverse with the product, the ions involved in the oxidation process are also very facile and the powder needs to be fine enough. Li et al. synthesized bismuth vanadate powder by the solid phase technique. [6] The BVO prepared by heating at 500°C showed the best photocatalytic reduction efficiency against Cr (VI).

2.3. Solution Phase Technique:

The solution-phase technique is a well-known example of a wet chemical method. There are many techniques to prepare photocatalytic films/powders using the liquid-phase method. In this section, we have discussed a general overview of several synthesis techniques like the sol-gel technique, the precipitation technique, the liquid deposition technique and the hydrothermal technique or microwave-assisted synthesis technique etc., for the production of BVO photoanodes which have been used in water splitting application.

2.4. Sol-Gel Technique:

The sol-gel method is the most important wet chemical synthetic approach for the preparation of nanoparticles. The construction of the sol and gel is the key factor among all for the synthesis of nanoparticles by the sol-gel method. Drisya et al. prepared TiO₂/BVO nanocomposite via sol-gel method, [7] the composites exhibit significant PC performance under the visible light irradiation; it was also noted that the PC efficiency is increased when percentage of BVO decreased in the nanocomposite. Pookmanee et al. developed bismuth vanadate powder by sol-gel method, [8] from the SEM, XRD study it is observed that the particle size, crystallinity and purity of the sample depend upon the calcined temperature. Wang et al. prepared molybdenum doped BVO by the sol-gel method, which shows enhanced photocatalytic activity than the bare BVO. [9]

2.5. Precipitation or Co-Precipitation Technique:

For synthesizing nanomaterials, the most popular method is the precipitation method, where different chemical components are mixed. The composite prepared by the precipitation technique demonstrated significant light absorption potentiality. It can also promote separating

electrons and holes to improve PC performance. Pérez et al. synthesized BVO powder by surfactant-assisted co-precipitation technique. [10] The PC activity for the photodegradation of RhB of the as-prepared m-BVO in the presence of Pluronic non-ionic surfactants performs a greater activity than the samples synthesized via solid-state reaction. C. Ravidhas et al. fabricated BVO nanostructured powders by co-precipitation process [11] but the limitation of as prepared BVO sample was in its PC activity which may be overcome after the calcination technique. The experimental result shows that the optimized sample prepared at the 450°C has the highest absorption in the visible region. The PC efficiency of BVO, which was prepared by Cruz et al. [12] through the co-precipitation process for the photodegradation of Rhodamine B (RhB) revealed the high capability to bleach the dye solution. Ganeshbabu et al. synthesized bismuth vanadate nanoparticles via chemical precipitation technique. Bismuth vanadate nanoparticles calcined at 400°C exhibit the highest PC performance, as it degrades Methylene blue (MB) dye by about 92.25% within the duration of 120 min. [13]

2.6. Hydrothermal Technique:

It is the most useful technique for the preparation of nanoparticles which is basically an approach of solution-based reaction. In this method, the formation of nanoparticles occurred in a wide temperature range varying from room temperature to very high temperature. Hydrothermal synthesis can produce nanoparticles that are not stable at elevated temperatures. So, pressure is also an important factor for this technique. Lei et al. employed bismuth vanadate photocatalyst via the hydrothermal method; the sample prepared at pH 3 shows the best photocatalytic activity. [14] Again, Chen et al. fabricated bismuth vanadate nanosheet through hydrothermal technique in the presence of bismuth nitrate and ammonium vanadate precursor and in the process sodium dodecyl benzene sulphonate is used for the morphological modification. The improved PC performance of this BVO is mainly attributed to the larger surface area of the nanosheet and higher atomic density of the (010) plane. [15] Similarly, Jiang et al. synthesized bismuth vanadate photocatalyst with various kind of morphologies via hydrothermal method using bismuth nitrate pentahydrate and ammonium metavanadate in the presence or absence of poly (vinyl pyrrolidone), in which the spherical shaped BVO demonstrated the highest photocatalytic activity. [16] J. Yu fabricated BVO nanofibre by this method where the nanofibrous BET surface area was higher than bulk BVO with a surface area of $0.5 \text{ m}^2 \text{ g}^{-1}$. [17] H. Jiang examined the PC performances for degradation of MO using BVO photocatalyst synthesized hydrothermally to achieve improved performance under visible light irradiation. BVO photocatalyst was also prepared by Ran et al. through this approach. [18] The

BVO photocatalyst prepared through hydrothermal techniques, compared to other techniques, revealed improved surface morphological properties of the photocatalyst.

2.7. Microwave-Assisted Synthesis Technique:

A major innovation and a dramatic change were observed through microwave synthesis on the basis of performance for chemical synthesis. It gives the scientist a new opportunity to overcome major drawbacks like conventional heating or time-consuming. For BVO nanomaterials preparation, this technique has enough potential to generate heat selectivity in a suitable solvent. Pookmanee et al. synthesized bismuth vanadate powder through a microwave-assisted synthesis technique. [19] Multi-phase monoclinic and tetragonal structures of BVO were produced by the microwave irradiation of 600-800 W for 4-6 min, and the surface area of BVO powder is in the range of 4.89-15.90 m² g⁻¹. BVO photocatalyst was also developed by Intaphong et al. in microwave-assisted technique with irradiation of 500 W for 2 min, 4 min and 6 min. [20] The best photocatalytic performance is shown for the sample prepared for 4 min. Souza et al. obtained BVO nanoflowers modified with gold nanoparticles through microwave irradiation to increase the photocatalytic efficiency. [21] Another example of BVO heterojunction formation was revealed by Yan et al. through a facial microwave-assisted technique. [22] They explored higher photocatalytic efficiency when tetracycline is degraded due to faster transfer of charges between the heterojunction of the various phases of BVO.

2.8. Electrodeposition:

Electrodeposition is a flexible, low-cost method for fabricating a wide variety of two and three dimensional materials such as coatings and films. Ye et al. synthesized Bi₂O₃/BiVO₄ heterostructure nanospheres via the electrodeposition method followed by annealing. The heterostructure demonstrated a photocurrent of 2.58 mA cm⁻² at 1.2 V vs. Ag/AgCl, which is almost 5 times higher than the pristine BVO. [23] Kong et al. prepared Ni-doped BVO photoanode by the electrodeposition method, where 5% Ni-doped BVO exhibits the highest photocurrent of 2.39 mA cm⁻² at 1.23 V vs. RHE which is about 2.5 times higher than the pure BVO. [24] Cho et al. synthesized W-doped BVO photoanodes by the electrodeposition technique; the photocurrent of W-doped BVO is increased three times than that of pure BVO. [25] A. J. Bard et al. electrodeposited amorphous TiO₂ on W:BVO/F: SnO₂, which results in almost 5.5 times higher water oxidation photocurrent than pure BVO. [26]

2.9. Spin Coating:

It is generally used for the development of nanocomposite film. The smooth deposition of nanomaterials makes the surface of the film uniform through this coating technique. Tayyebi et al. synthesized monoclinic BVO photocatalyst via spin coating followed by calcination method, the photocatalytic activity of monoclinic BVO is increased with an increase in the basicity of the medium. [27] Sitaraman et al. synthesized $\text{WO}_3/\text{BiVO}_4$ heterojunction by spin-coating technique; from the PEC studies, it was evident that the $\text{WO}_3/\text{BiVO}_4$ shows higher photocurrent density (0.64 mA cm^{-2} at 1.23 V vs. RHE) than the bare WO_3 and BiVO_4 . [28] Wang et al. prepared BVO thin film by spin coating followed by annealing, the thin film annealed at higher temperature (500°C - 540°C) shows better PEC performance compared to the others prepared at a lower temperature. [29] Russo et al. synthesized BVO thin film via spin coating technique; from the PEC study, it is evident that the charge transfer kinetics is three times faster than that of the porous film. [30]

3. Strategies for Enhancing PEC Performance:

In order to enhance the PEC water splitting potential, many modifications have been introduced, including the addition of suitable dopants, the development of composites and heterojunctions and the altering surface morphology. In this section, we discussed an overview of the strategies and their principles and provided some examples to explain their applications for the enhancement of the PEC performance of BiVO_4 .

3.1. Heterojunction:

In this section, we will present three different types of heterojunction semiconductor according to their electronic band structure, as presented in Fig.3. In type A, from semiconductor (SC) 1, both photogenerated e^- and h^+ are transferred to SC 2 due to the position of E_{g2} , which is within the E_{g1} . There is no improvement in the photocatalyst due to the charge transformation and accumulation of a semiconductor in this kind of heterojunction. [31] Type B heterojunction consists of the valence band maxima and conduction band minima of SC 1 in lower energy than SC 2. The photogenerated h^+ migrates from SC 2 to SC 1 while the photoexcited e^- moves from SC 1 to SC 2. During the photo-activation process, efficient charge carrier separation occurs if both semiconductors are in suitable contact. [32]

Finally, type C heterojunction forms due to recombination between h^+ from the valence band of SC1 and e^- from the conduction band of SC2. It consists of SC1, which has E_{g1} position

higher in energy than E_{g2} of SC2. An indirect Z scheme, a type C model, can be designed with the help of an appropriate e^- mediator, which could also be quite interesting. Among these three, type B heterojunction semiconductor is the simplest way to extend competent charge transport, enhance light absorption and improve charge carriers' lifetime; we discuss type B in this section.

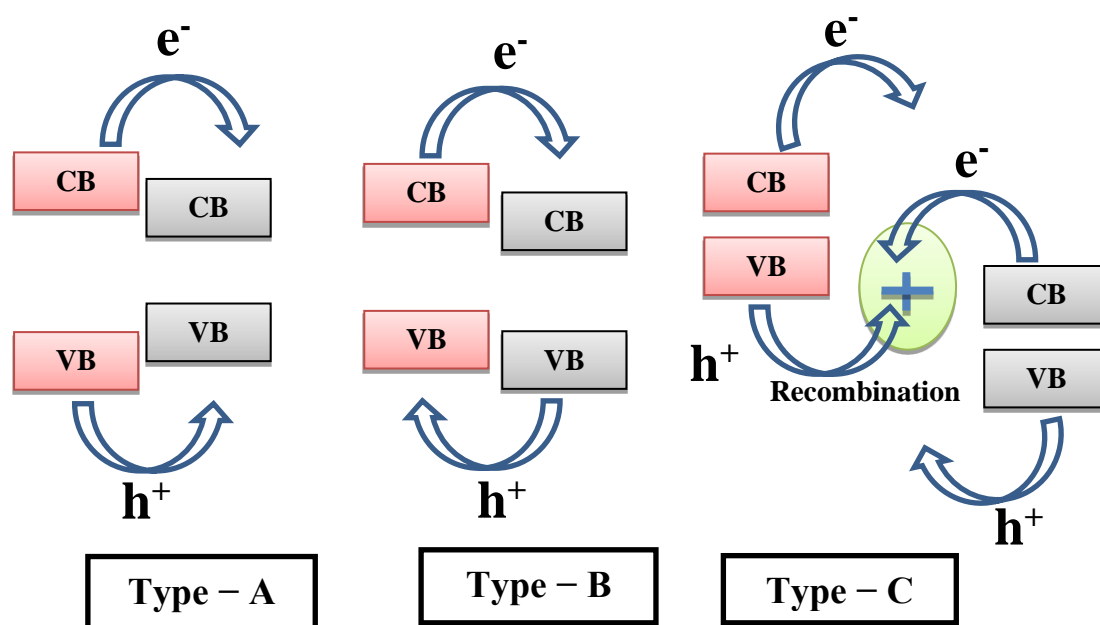


Fig: 3. Construction of the three different types of heterojunction

Regarding BVO, WO_3 is one of the most frequently used semiconductors for type B heterojunction with band gap energy 2.6 eV mainly to split the water molecule. [33] BVO/ TiO_2 is also a promising composite of type B heterojunction semiconductor with similar electronic band configuration to BVO/ WO_3 . The band gap energy of TiO_2 must actively comprise the band gap energy of BVO to form a type A heterojunction due to the suitable band position of the valence band and conduction band where conduction band minima of TiO_2 and BVO are located -0.2 and 0 V, respectively, and valence band maxima are situated at 3.0 and 2.4 V respectively for these two components. It is valid only for single components. However, an interesting feature of the heterojunction must be discussed for the real charge transfer in a composite. Due to the homogenization of the Fermi energy levels, there is a shift in the band gap position of BVO and TiO_2 for the heterojunction. The energy positions of VBM and CBM

are reduced in the case of BVO than those of TiO₂ after the thermodynamic equilibrium in BVO/TiO₂. [34]

Recently researchers are focused on the fabrication of BVO photo-anodes to perceive the progress of the photoelectrochemical study. The bare BVO has many drawbacks such as photoinduced charge carrier recombination, reduced water oxidation kinetics, low charge transportation etc. As a result, the bare BVO is not considered a more impressive photoanode for the water oxidation reaction.

Zhang et al. produced Bi₂O₃/ BVO hetero-structured nanosphere by electro-deposition technique. [35] The PEC studies are done by using a full-arc xenon lamp ($\lambda > 420$ nm) to measure the I_{ph} of Bi₂O₃/BVO (2.58 mA cm⁻² at 1.2 V vs. Ag/AgCl using the same electrolyte. The band gap measurement is also done by UV-Vis absorption spectroscopy the band gap of the Bi₂O₃/BVO sample is calculated at 2.32 eV, which is smaller than the Bi₂O₃ and BVO sample and also the donor density calculation using the Mott-Schottky equation shows the higher donor density of Bi₂O₃/BVO than BVO. An electron beam deposition method was used to develop this ternary heterojunction. After the deposition process, a wet chemical process was employed and during the deposition process, the thickness of WO₃ and SnO₂ layer was varied. The I_{ph} measurement is done by using a three-electrode cell using an Iviumpotentiostat with Pt plate as a counter electrode and Ag/AgCl as a reference electrode and 0.5(M) Na₂SO₃ solution with potassium phosphate buffer solution as an electrolyte, light intensity was maintained at 100 mW cm⁻². Among the various variations that were developed by modifying the thicknesses of the WO₃ and SnO₂ layer, it was observed that the heterojunction SnO₂ 50 nm/ WO₃ 50 nm /BVO exhibited the maximum photocurrent (I_{ph}) of ~2.01 mA cm⁻² (at 1.23 V) under the illumination of visible light from the front and the same heterojunction exhibits a photocurrent of 1.80 mA cm⁻² when visible light was irradiated from the back.

Chong et al. designed n-n heterojunction photoanode V₂O₅/ BVO developed through electro-deposition technique. [36] PEC performance measured by a standard three-electrode assembly using Pt rod is a counter electrode and saturated Ag/AgCl (3M KCl) as a reference electrode in the presence of 0.5 (M) aqueous Na₂SO₄ solution as an electrolyte. The maximum photocurrent for the system appears as 1.53 mA cm⁻² at 1.5 V which is quite higher than that of the individual pristine BVO and V₂O₅ showing I_{ph} of 0.22 and 0.21 mA cm⁻², respectively. Teridi et al. synthesized Se/BVO photoanode via a two-step combination of electrodeposition and an aerosol-assisted chemical vapor deposition technique. The Highest I_{ph} of Se/BVO photoanode is 2.2 mA cm⁻² at 1.3 V vs. SCE [37] which is much higher than that of individual Se and BVO. The enhancement in the I_{ph} is due to the presence of the Se layer which acts as a

hole trapping medium, increases light absorption property and thereby improves the charge separation; all of these effects have been established through DFT simulations study. Stoll et al. fabricated WO₃/BVO on porous titanium substrate via electrochemical anodization of sputtered tungsten layer and BVO layer that was formed via SILAR method. [38]

Parida et al. have prepared In₂S₃/BVO heterojunction through two-step co-precipitation and wet chemical methods. [39] The PEC studies are done by using a 300 W Xe lamp ($\lambda \geq 420$ nm) in the presence of 0.05(M) aqueous AgNO₃ solution. The onset potential of In₂S₃, BVO and In₂S₃/BVO are found to be at -0.49V, -0.59V, -0.42V, respectively and the maximum I_{ph} observed for In₂S₃/BVO heterojunction was found to be 0.269 mA cm⁻² at 1.0 V under visible light illumination which is greater than that of either pure BVO (0.119 mA cm⁻²) or In₂S₃ (0.164 mA cm⁻²). The band gap measurement also shows that the energy gap of In₂S₃/BVO is 1.91eV which is quite smaller than that of pure BVO (2.36 eV) and pure In₂S₃ (2.22 eV).

3.2. Surface morphology:

A significant impact of the interfacial energetic, kinetics and charge transport properties is marked when a polycrystalline semiconductor material shows morphological particulars of the electrode e.g. connectivity, shape, & size of the particles. An effective way to improve the photoelectrochemical properties is to understand and control the morphological aspects of the polycrystalline BVO electrodes. [40]

3.2.1. Shape-dependent or facet-dependent morphologies:

Based on the exposed crystal plane at the interface, photoelectrochemical properties of semiconductor (SC) materials vary significantly. [41] The type of bare facets of metal oxide (MO) based semiconductor influences not only the thermodynamic property e.g. flat band potential, band bending but also kinetic features e.g. catalytic capability significantly. [42] Recently, photoelectrochemical properties of the BVO crystals have been gained a lot of attention due to their various shapes and comparison is also reported. [43]

The synthesis of monoclinic scheelite (m-s) BVO nanoplates with well-defined {001} facets exposed at the surface has been reported by Xi et al. developed through a hydrothermal method. This study shows a feasible approach to improve photo-conversion efficiency by designing nanostructures with appropriate surface facets. The photocatalytic (PC) activity of Rhodamine B for these nanoplates with 400-600 nm width and 20-30 nm thickness was tested for photodegradation. Although the specific surface area of the nanorod sample had thrice superior

(67.5 m²g⁻¹), which was quite higher than that of the nanoplates (21.4 m²g⁻¹), the later demonstrated a better PC performance in comparison with a nanorod shaped sample.

3.2.2. Porous and nanostructured morphologies:

For semiconductor electrodes, the porous structure can also play an important role to reduce e⁻-h⁺ recombination by improving the capacity of the depletion layer, which also employs photoinduced charge carriers. However, by introducing porosity, increasing surface area also achieve contrary effects on charge separation and transportation. As a result, the growth of surface texture, defect sites and grain boundaries are developed with reduced crystallinity. [44] The surface area and morphologies of a photo-electrode must be optimized to utilize the overall net favorable influence.

A modified metal-organic decomposition method was used to prepare porous BVO electrodes by Luo et al. In the high bias zone i.e. 0.9 V vs. RHE, the behavior of porous electrode revealed as one of the foremost performances for water splitting reaction. The electrode/electrolyte junction areas are effectively increased by the resultant electrode which is comprised of 50-200 nm particle size. [45]

A surfactant-assisted (e.g. sodium dodecyl sulfate, SDS) metal-organic decomposition method was also used. Pilli et al. reported that SDS modified electrode achieved a superior I_{ph} in comparison with an electrode developed without any surfactant. The micelles were scattered in the dissolvable solvent and expelled during ignition with the separation of a mesoporous inorganic structure. [46, 47] The observed performance enhancement resulted from the difference in the electrode-electrolyte interfacial area.

Another way to increase the surface area is to synthesize nanowire/nanorod array electrodes. Su et al. reported seed-mediated growth of the BVO where seed layer was put down over any conducting substrate e.g. FTO through the spin coating and the photoanode is heated at 400°C. [48] In a temperature-controlled water bath, the seeded photoanode substrate was then dipped into a solution of BVO to develop a suspension and construct BVO nanowires. Polycrystalline nanowires or nanopyramid arrays of BVO were obtained depending on the solution temperature. The single crystals 1-D nanostructure units confirm superior charge transportation for majority carriers through the wire or via a rod, whereas for the minority carriers' limitation of the travel distance is observed to influence the electrode-electrolyte junction.

Su et al. also investigated a solvothermal technique to deposit a WO₃ nanorod array-based film on a conducting glass material like FTO. A deposition of BVO is then followed by a spin coating technique to prepare WO₃ modified BVO hetero-junction nanorod array films. [49] As

the nanostructured heterojunction having a smaller e^-h^+ recombination rate, the nanorod array of WO_3/BVO heterojunction films exhibited enhanced IPCEs in comparison with the planar WO_3/BVO heterojunction films.

3.3. Doping Approach:

Doping is one of the most intentional tactics to tune the properties of a bulk semiconductor. A pinch of impurities can drastically control the host material's optical and electrical properties drastically. An expected change in the energy or positions of the band edge also occurs depending on the types of doping. Due to the enhancement of $e^- - h^+$ recombination and reduce the bandwidth of the depletion layer, the effect of doping will not always be favorable, as presented in Fig. 4.

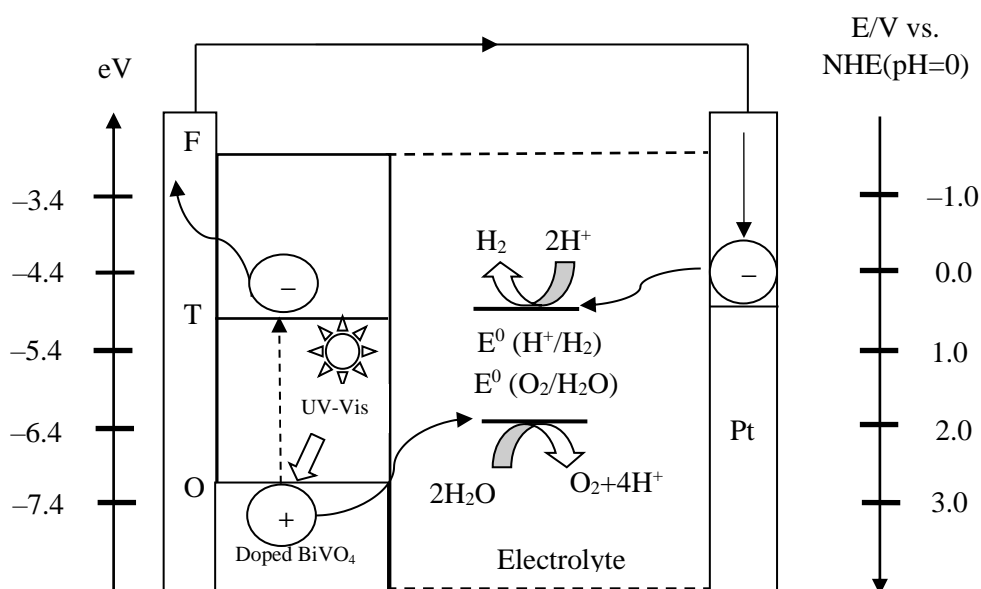


Fig. 4. Plausible water splitting mechanism for doped $BiVO_4$

For a typical BVO photoanode, it can significantly enhance the electronic conductivity, improve photoinduced charge transfer, change the position of band edge to form a new energy level with donor atom to enhance the photon absorption and construct oxygen or vanadium vacancies suitably to enhance photo-induced charge separation. [50, 51] In this section, we focus on the effect of metal in addition to non-metal dopants on BVO photoanodes to enhance the photoelectrochemical performances most significantly.

3.3.1. Doping with Metal

Fischer et al. synthesized Mo-doped BVO thin film in a simple dip-coating method followed by calcination in air. The amount of precursor salt of molybdenum varies to make the sample have a different percentage of Mo doping. The highest I_{ph} of 1.9 mA cm⁻² at 1.23 V vs. RHE was observed for 10% Mo-BVO which is significantly higher than that of the undoped BVO (0.2 mA cm⁻²). [52] The measurement was carried out using a three-electrode cell, with a 150 W white light source adjusted to an intensity of 100 mW cm⁻² 0.1(M) phosphate buffer solution (PBS) was used as an electrolyte at pH 7.3

Zhong et al. developed In³⁺ doped BVO photoanode through the drop-casting method; the photoelectrochemical studies are done by using a three-electrode cell where Pt wire (99.99%), saturated calomel electrode and 0.1(M) Na₂SO₄ (pH6.8) were employed as a counter electrode, reference electrode and electrolyte in the presence of 100 mW/cm² light. The I_{ph} of In³⁺ doped BVO is 1.56 mA cm⁻² at 1.23 V vs. SCE, which is higher than the undoped one. [53] Although the band gap measurement shows both the photoanode had similar band gap, the positive shift of flat band potential (0.12 to 0.16 V) and increase of donor density on doping, as evident from the Mott-Schottky experiment leads to improve photoelectrochemical water oxidation behavior on the modified materials. Zhao et al. [54] also synthesized W doped BVO by simple drop-cast method and compared the PEC performance with pristine BVO. The I_{ph} of pristine BVO is 0.18 mA cm⁻² at 1.23 V vs. RHE which increases to ~ 4 fold upon W doping as a result of enhanced electron density, confirmed by Mott-Schottky analysis. Kong et al. [55] prepared Ni-doped BVO photoanode via an in-situ electrode-position method; PEC studies were carried out using 300 W Xe arc lamp; light source 100 mW cm⁻² and 0.2 (M) Na₂SO₄ solution, as electrolyte. The highest I_{ph} is observed for 5% Ni-doped BVO (2.39 mA cm⁻² at 1.23 V vs. RHE) which is quite higher than pure BVO (0.94 mA cm⁻²); also maximum IPCE of 5% Ni-doped BVO is in 45% within 400-450 nm whereas that of pure BVO is only 25%. The band gap of pure BVO (2.43 eV) is reduced to 2.39 eV with 5% Ni-doped BVO. Sun et al. prepared cobalt-doped BVO photoanode through electrodeposition technique and observed to determine I_{ph} maximum of 3.5 mA cm⁻² at 1.23 V vs. RHE which is almost two times higher than undoped BVO. [56] Ye et al. analyzed the role of various metals like W, B, Pb, Cu, Co, Nb, Ru, Rb, Sn, Zn, Sr, Fe, Ag, Ga, Ir and Ti to identify effective dopants for BVO through using SECM technique under illumination. [57] By using a computer-controlled dispenser, variations of Bi, V and dopant-comprising solutions ratios are monitored on every spot and the arrays of different modified semiconductors were prepared. The arrays were annealed at 500°C in the air to produce photocatalyst oxide. In this study, the dopant concentration range varied from 5-10%. Among all dopants, only W showed an appreciable enrichment of photocurrent and IPCE,

whereas metals like Sn, Rh, Co, Ru, Pd, Ag, Ga, Ir, and Sr exhibited a negative impact on PEC performances of these arrays and the rest showed no perceptible effect. The Mott-Schottky analysis indicated that the carrier density of the W-modified sample was twice the pure one, although the flat band potential did not shift in the -ve direction. XPS analysis results confirmed that the oxidation states of Bi, V, and W atoms were +3, +5, and +6, respectively and the composition ratio of Bi/V/W was established to be 5.1/3.9/1.0 in the optimized semiconductor. Luo et al. studied the consequences as a result of doping of BVO electrodes using various metal ions such as W, La, Sr, Zr, Mo, Ta, Ti, Zn, Si, Ag which have been developed by the process of metal-organic decomposition. The photocurrent (I_{ph}) got enhanced due to doping, specifically with W^{6+} or Mo^{6+} ion. [58] The BVO samples were modified by addition of 3 (wt%) Mo and this modification led to tremendous enhancement in photocurrent along with that there was a significant increase in IPCE in seawater as there had been oxidation of Cl^- in the presence of light. The presence of Mo^{6+} ion inside the sites of V^{5+} was observed by analysing the Raman spectra of the samples that had been modified.

From the slope of Mott-Schottky plots and the enhancement in carrier density, the role of Mo as a dopant was confirmed, although the shift in flat band potential was negligible. The surface electrochemical performance was further improved for Mo-doped BVO. Mo-rich segregations i.e. MoO_x , could act as recombination centers on the surface. [59] In the reaction mixture, the amount of dopants added to produce doped BVO differs to some extent from the quantity of dopants that are actually implemented into the host arrangement. Here, on the surface, impurity phases can be formed by residual dopant ions or at the borders of the host molecule, which is so small that common characterization techniques like XRD or EDX can't detect it. A facile charge transportation or charge separation can be acquired in the presence of these impurity phases. Hence the effect of unincorporated dopants would be maximized to ensure the removal of impurity phases.

Modified BVO structure with co-dopants of Mo and W exhibited better performance in comparison with any one of Mo or W doped BVO. [60] Park et al. demonstrated that BVO photoanode with co-dopants 2 at% Mo and 6 at% W performed more upgraded activity in comparison with the bare or only W modified BVO. The addition of Mo to the W-doped BVO sample indicates twice the carrier density compare to only the W-doped sample, as measured through Mott-Schottky analysis. A structural change occurs for Mo/W-doped as well as W-doped BVO from monoclinic scheelite to tetragonal scheelite phases, which was revealed by XRD analysis.

Another interesting feature was also reported from DFT calculations which indicate that the substitution of V by W & Mo revealed the the dopant serves as superficial donor atoms to increase the carrier density in BVO. The tetragonal scheelite structure has to be considered as a developed symmetry than the monoclinic scheelite structure. In this study, there was no further discussion about the relationship between the changes in crystal structure with the change in any photoelectrochemical properties. The W/Mo-doped BVO and W-doped BVO have a similar band gap compared to the bare one, confirmed by IPCE spectrum analysis at 500 nm. This experiment shows better photoactivity of W & Mo doped BVO over W doped BVO in the presence of low intense monochromator.

An increase in carrier density with a lowering slope of the Mott-Schottky plots was again confirmed. Band gap remains unchanged after the addition of Mo or W metal as well this flat band potential remains unchanged in the -ve direction with increasing the carrier density. From these studies, it is evident that modification of Mo and W become quite popular owing to their unique effects, whose addition is more facile and no further improvement in I_{ph} with the increase in the doping level of either Mo or W compared to co-doping of Mo and W. To identify the specific and synergistic effect of Mo & W, further studies need to be performed to understand the modified BVO systems.

3.3.2. Doping with Non-metal

Phosphorous, non-metal constituent was also incorporated into BVO through the urea-precipitation method as reported by Jo et al. [61] where a small fraction of VO_4^{3-} oxoanions was replaced by PO_4^{3-} oxoanions. In the host structure, the incorporation of PO_4^{3-} oxoanions, which were added as a phosphorous precursor, caused shifts in the XRD peaks, indicating an increase in cell parameters. The band gap energy is also increased slightly (~0.01-0.04 eV) in the UV-visible absorption spectrum region. The electrophoretic deposition of $Bi(VO_4)_{0.998}(PO_4)_{0.002}$ achieved a better performance to generate an appreciably higher photocurrent compared to the pure BVO electrode. The charge transfer resistance of BVO remarkably decreases upon the addition of PO_4^{3-} , as indicated by the EIS measurements.

The authors also established that the reduction in charge transfer resistance and increase in the charge carrier density could result from P doping indicated through DFT calculations. An internal electric field is created due to different P-O and V-O bond lengths during the charge rearrangement all over the dopant to impose the lattice strain.. It may achieve a significant advantage in separating $e^- - h^+$ pairs, resulting in improved photoelectrochemical properties.

3.4. Co-catalyst:

Gamelin et al. [62] synthesized Co-Pi modified tungsten doped bismuth vanadate photoanode which demonstrates a low onset potential of 0.31 V vs. RHE at pH 8. Liu et al. [63] synthesized a CoOOH-over layer coated coral-like BVO photoanode which also has a low onset potential of 0.2 V vs. RHE, a maximum I_{ph} of 4.0 mA cm^{-2} at 1.23 V vs. RHE. Pilli et al. synthesized Co-Pi catalyst modified Mo doped BVO which shows I_{ph} of 1.0 mA cm^{-2} at 1.0 V vs. Ag/AgCl. [64] Nam et al. synthesized W-Mo doped BVO photoanode modified with iron oxy-hydroxide electrocatalyst via a two-step process drop-casting followed by photo-assisted electro-deposition, the co-catalyst modified doped BVO photoanode attained at least two-fold higher I_{ph} (at 0.3 V vs. Ag/AgCl) than that of the doped BVO photoanode. [65]

4. Conclusion:

The photoelectrochemical performance towards the water splitting reaction, using the Bismuth Vanadate as a photo electrode, has been discussed in this article The photocatalyst Bismuth Vanadate has been proven as a distinguished and promising candidate as an effective semiconductor. The presence of low band gap makes this photocatalyst quite recognisable to researchers. This article mainly focuses on the various synthetic routes of this photocatalyst, the effects of altering surface morphology, doping with metals and non-metals and developing heterojunctions for improving the PEC performance of the semiconductor and its efficiency towards the extraction of renewable energy from the sun. This review also highlights the possibilities of enhancing the ability of the semiconductor by imposing restrictions on the recombination of the holes and electrons that have been generated under the illumination of visible light. As the bismuth vanadate-based photocatalysts are effective in working under irradiation of visible light, these photocatalysts will gain much more fame in the near future when the time comes for extraction of renewable energy from solar energy.

5. Acknowledgement:

The author SG sincerely acknowledges the Department of Science & Technology, Government of India, for financial support (vide reference no. SR/WOS-A/CS-10/2018, dated 02.01.2019) under DST-Women Scientist Scheme - A (DST-WOS-A) to carry out this work. Financial support through the sponsored project grant of the Govt. of India from DST (Sanction Order No. DST/INT/SL/P-33/2021, dt. 08-10-2021) to the Department of Chemistry, IEST, Shibpur are gratefully acknowledged. The present work was also financially supported by CSIR (File no. 01(2876)/17/EMR-II, 02.05.2017) to the Department of Chemistry, IESTS.

References:

- [1] S. Ghosh, P. Hajra, D. Sariket, D. Ray, S. Baduri, C. Bhattacharya, Modifications of BiVO₄ semiconductors for oxidation of water and detoxification of organic wastes: photoelectrochemical applications of semiconductors, IGI Global, 2022, pp. 1-28.
- [2] S. Ghosh, D. Laha, P. Hajra, D. Sariket, D. Ray, S. Baduri, H. S. Sahoo, C. Bhattacharya, Development of transition metal incorporated bismuth-based oxide semiconductors as potential candidates for solar assisted water splitting applications, ChemElectroChem, 2023 (Article DOI: 10.1002/celec.202201062).
- [3] P. Hajra, S. Kundu, A. Maity, C. Bhattacharya, Facile photoelectrochemical water oxidation on Co²⁺-adsorbed BiVO₄ thin films synthesized from aqueous solutions, Chem. Eng. J., 374 (2019) 1221-1230.
- [4] J. Cheng, J. Feng, W. Pan, Enhanced Photocatalytic Activity in Electrospun Bismuth Vanadate Nanofibers with Phase Junction, ACS Appl. Mater. Interfaces, 7 (2015) 9638-9644.
- [5] R. P. Antony, P. S. Bassi, F. F. Abdi, S. Y. Chiam, Y. Ren, J. Barber, J. S. ChyeLoo, L. H. Wong, Electrospun Mo-BiVO₄ for efficient photoelectrochemical water oxidation: Direct evidence of improved hole diffusion length and charge separation, ElectrochimicaActa, 211 (2016) 173-182.
- [6] J. Li, Y. Chen, C. Chen, S. Wang, Solid-phase synthesis of visible-light-driven BiVO₄ photocatalyst and photocatalytic reduction of aqueous Cr(VI), Bulletin of Chemical Reaction Engineering & Catalysis, 14, (2019) 336-344.
- [7] K. T. Drisya, M. S. López, J. J. R. Ramírez, J. C. D. Álvarez, A. Rousseau, S. Velumani, R. Asomoza, A. Kassiba, A. Jantrania & H. Castaneda, Electronic and optical competence of TiO₂/BiVO₄ nanocomposites in the photocatalytic processes, Scientific Reports, 10 (2020) 13507.
- [8] P. Pookmanee, S. Kojinok, R. Punthaeod, S. Sangsricharan, S. Phanichapat, Preparation and characterization of BiVO₄ powder by the sol-gel method. Ferroelectrics, 456 (2013) 45-54.
- [9] G. L. Wang, L. W. Shan, Z. Wu, L.M. Dong, Enhanced photocatalytic properties of molybdenum-doped BiVO₄ prepared by sol-gel method, J. Alloys Comp., 36 (2017) 129-133.
- [10] U.M. G. Pérez, S. S. Guzmán, A. M. d. I. Cruz, J. Peral, Selective synthesis of monoclinic bismuth vanadate powders by surfactant-assisted co-precipitation method: study of their electrochemical and photocatalytic properties, Int. J. Electrochem. Sci, 7 (2012) 9622-9632.
- [11] C. Ravidhas, A. J. Josephine, P. Sudhagar, A. Devadoss, C. Terashima, K. Nakata, A. Fujishima, A. M. E. Raj, C. Sanjeeviraja, Facile synthesis of nanostructured monoclinic bismuth vanadate by a co-precipitation method: Structural, optical and photocatalytic properties, Materials Science in Semiconductor Processing, 30 (2015) 343-351.

-
- [12] A. M. d. I. Cruz, U.M. G. P. rez, Photocatalytic properties of BiVO₄ prepared by the co-precipitation method: degradation of rhodamine B and possible reaction mechanisms under visible irradiation, *Materials Research Bulletin*, 45 (2010) 135-141.
- [13] M. Ganeshbabu, N. Kannan, P. S. Venkatesh, G. Paulraj, K. Jeganathan D. Mubarak Ali, Synthesis and characterization of BiVO₄ nanoparticles for environmental applications, *RSC Adv.*, 10 (2020) 18315-18322.
- [14] B. X. Lei, L. L. Zeng, P. Zhang, Z. F. Sun, W. Sun, X. X. Zhang, Hydrothermal synthesis and photocatalytic properties of visible-light induced BiVO₄ with different morphologies, *Advanced Powder Technology*, 25 (2014) 946-951.
- [15] L. Zhang, D. Chen, X. Jiao, Monoclinic structured BiVO₄ nanosheets: hydrothermal preparation, formation mechanism, and coloristic and photocatalytic properties, *J. Phys. Chem. B*, 110 (2006) 2668-2673.
- [16] H. Jiang, H. Dai, X. Meng, L. Zhang, J. Deng, Y. Liu, C. T. Au, Hydrothermal fabrication and visible-light-driven photocatalytic properties of bismuth vanadate with multiple morphologies and/or porous structures for Methyl Orange degradation, *Journal of Environmental Sciences*, 24 (2012) 449-457.
- [17] J. Yu, A. Kudo, Hydrothermal synthesis of nanofibrous bismuth vanadate, *Chemistry Letters*, 34 (2005) 850-851.
- [18] R. Ran, J. G. McEvoy, Z. Zhang, Synthesis and optimization of visible light active BiVO₄ photocatalysts for the degradation of RhB, *Int. J. Photoenergy*, 2015, 612857.
- [19] P. Pookmanee, P. Longchin, W. Kangwansupamonkon, R. Puntharod, S. Phanichphant, Microwave-assisted synthesis bismuth vanadate (BiVO₄) powder, *Ferroelectrics*, 455 (2013) 35-42.
- [20] P. Intaphong, A. Phuruangrat, and P. Pookmanee, Synthesis and characterization of BiVO₄ photocatalyst by microwave method, *Integrated Ferroelectrics*, 175 (2016) 51-58.
- [21] J. S. Souza, F. T. H. Hirata, P. Corio, Microwave-assisted synthesis of bismuth vanadate nanoflowers decorated with gold nanoparticles with enhanced photocatalytic activity, *J. Nanopart. Res.*, 35 (2019) 1-9.
- [22] M. Yan, Y. Yan, Y. Wu, W. Shi, Y. Hua, Microwave-assisted synthesis of monoclinic-tetragonal BiVO₄ heterojunctions with enhanced visible-light-driven photocatalytic degradation of tetracycline, *RSC Adv.*, 5 (2015) 90255-90264.
- [23] K. H. Ye, X. Yu, Z. Qiu, Y. Zhu, X. Lu, Y. Zhang, Facile synthesis of bismuth oxide/bismuth vanadate heterostructures for efficient photoelectrochemical cells, *RSC Adv.*, 5 (2015) 34152.
- [24] D. Kong, J. Qi, D. Liu, X. Zhang, L. Pan, J. Zou, Ni-doped BiVO₄ with V⁴⁺ species and oxygen vacancies for efficient photoelectrochemical water splitting, *Trans. Tianjin Univ.*, 25 (2019) 340-347.

-
- [25] S. K. Cho, H. S. Park, H. C. Lee, K.M. Nam, A. J. Bard, Metal doping of BiVO₄ by composite electrodeposition with improved photoelectrochemical water oxidation, *J. Phys. Chem. C*, 117 (2013) 23048-23056.
- [26] D. Eisenberg, H. S. Ahn, A. J. Bard, Enhanced photoelectrochemical water oxidation on bismuth vanadate by electrodeposition of amorphous titanium dioxide, *J. Am. Chem. Soc.*, 136 (2014) 14011-14014.
- [27] A. Tayyebi, T. Soltani, B. K. Lee, Effect of pH on photocatalytic and photoelectrochemical (PEC) properties of monoclinic bismuth vanadate, *J. Colloid Interface Sci.*, 534 (2019) 37-46.
- [28] S. R. Sitaaraman, M. I. Shanmugapriyan, K. Varunkumar, A. N Grace, R. Sellappan, Synthesis of heterojunction tungsten oxide (WO₃) and Bismuth vanadate (BiVO₄) photoanodes by spin coating method for solar water splitting applications, *Mater. Today: proceedings*, 45 (2021) 3920-3926.
- [29] L. Shi, S. Zhuo, M. Abulikemu, G. Mettela, T. Palaniselvam, S. Rasul, B. Tang, B. Yan, N. B. Saleh, P. Wang, Annealing temperature effects on photoelectrochemical performance of bismuth vanadate thin film photoelectrodes, *RSC Adv.*, 8 (2018) 29179-29188.
- [30] S. Hernández, G. Gerardia, K. Bejtkab, A. Finaa, N. Russo, Evaluation of the charge transfer kinetics of spin-coated BiVO₄ thin films for sun-driven water photoelectrolysis, *Appl. Catal. B*, 190 (2016) 66-74.
- [31] M. R. Gholipour, C. T. Dinh, F. Beland and T.O. Do, Nanocomposite heterojunctions as sunlight-driven photocatalysts for hydrogen production from water splitting, *Nanoscale*, 7 (2015) 8187-8208.
- [32] S.J.A Moniz, S.A. Shevlin, D.J. Martin, Z. X. Guo and J. Tang, Visible-light driven heterojunction photocatalysts for water splitting - a critical review, *Energy. Environ Sci.*, 8 (2015) 731-759.
- [33] I. Fujimoto, N. Wang, R. Saito, Y. Miseki, T. Gunji and K. Sayama, WO₃/BiVO₄ composite photoelectrode prepared by improved auto-combustion method for highly efficient water splitting, *Int. J. Hydrog. Energ.*, 39 (2014) 2454-2461.
- [34] J. Sun, X. Li, Q. Zhao, M. O. Tadé and S. Liu, Quantum-sized BiVO₄ modified TiO₂ microflower composite heterostructures: efficient production of hydroxyl radicals towards visible light-driven degradation of gaseous toluene, *J. Mater. Chem. A*, 3 (2015) 21655-21663.
- [35] K. H. Ye, X. Yu, Z. Qiu, Y. Zhu, X. Lu and Y. Zhang, Facile synthesis of bismuth oxide/bismuth vanadate heterostructures for efficient photoelectrochemical cells, *RSC Adv.*, 5 (2015) 34152-34156.
- [36] C. S. Yaw, Q. Ruan, J. Tang, A. K. Soh, M. N. Chong, A Type II n-n staggered orthorhombic V₂O₅/monoclinic clino bisvanite BiVO₄ heterojunction photoanode for photoelectrochemical water oxidation: fabrication, characterisation and experimental validation, *Chem. Eng. J.*, 364 (2019) 177-185.
- [37] S. N. F. M. Nasir, H. Ullah, M. Ebadi, A. A. Tahir, J. S. Sagu, and Md. A. M. Teridi, New insights into Se/BiVO₄ heterostructure for photoelectrochemical water splitting: a combined experimental and DFT study, *J. Phys. Chem. C*, 121 (2017) 6218-6228.

-
- [38] T. Stoll, G. Zafeiropoulos, I. Dogan, H. Genuit, R. Lavrijsen, B. Koopmans and M.N. Tsampas, Visible-light-promoted gas-phase water splitting using porous $\text{WO}_3/\text{BiVO}_4$ photoanodes, *Electrochem. Commun.*, 82 (2017) 47-51.
- [39] B. Baral, S. Mansingh, K. H. Reddy, R. Bariki, and K. Parida, Architecting a double charge-transfer dynamics $\text{In}_2\text{S}_3/\text{BiVO}_4$ n-n isotype heterojunction for superior photocatalytic oxy tetracycline hydrochloride degradation and water oxidation reaction: Unveiling the association of physicochemical, electrochemical, and photocatalytic properties, *ACS Omega*, 5 (2020) 5270-5284.
- [40] K.S. Choi, Shape effect and shape control of polycrystalline semiconductor electrodes for use in photoelectrochemical cells, *J. Phys. Chem. Lett.*, 1 (2010) 2244-2250.
- [41] P. A. M. Hotsenpiller, J. D. Bolt, W. E. Farneth, J. B. Lowekamp and G. S. Rohrer, Orientation Dependence of Photochemical Reactions on TiO_2 Surfaces, *J. Phys. Chem. B*, 102 (1998) 3216-3226.
- [42] H. G. Yang, C. H. Sun, S. Z. Qiao, J. Zou, G. Liu, S. C. Smith, H. M. Cheng and G. Q. Lu, Anatase TiO_2 single crystals with a large percentage of reactive facets, *Nature*, 453 (2008) 638-641.
- [43] G. Xi and J. Ye, *Chem. Commun.*, Synthesis of bismuth vanadate nanoplates with exposed {001} facets and enhanced visible-light photocatalytic properties, 46 (2010) 1893-1895.
- [44] S. P. Berglund, D. W. Flaherty, N. T. Hahn, A. J. Bard and C. B. Mullins, photoelectrochemical oxidation of water using nanostructured BiVO_4 films, *J. Phys. Chem. C*, 115 (2011) 3794-3802.
- [45] W. Luo, Z. Yang, Z. Li, J. Zhang, J. Liu, Z. Zhao, Z. Wang, S. Yan, T. Yu and Z. Zou, Solar hydrogen generation from seawater with a modified BiVO_4 photoanode, *Energy Environ. Sci.*, 4 (2011) 4046-4051.
- [46] S. K. Pilli, T. E. Furtak, L. D. Brown, T. G. Deutsch, J. A. Turner and A. M. Herring, Cobalt-phosphate (Co-Pi) catalyst modified Mo-doped BiVO_4 photoelectrodes for solar water oxidation, *Energy Environ. Sci.*, 4 (2011) 5028-5034.
- [47] S. K. Pilli, T. G. Deutsch, T. E. Furtak, J. A. Turner, L. D. Brown and A. M. Herring, Light induced water oxidation on cobalt-phosphate (Co-Pi) catalyst modified semi-transparent, porous $\text{SiO}_2\text{-BiVO}_4$ electrodes, *Phys. Chem. Chem. Phys.*, 14 (2012) 7032-7039.
- [48] J. Su, L. Guo, S. Yoriya, and C. A. Grimes, Aqueous growth of pyramidal-shaped BiVO_4 nanowire arrays and structural characterization: Application to photoelectrochemical water splitting, *Cryst. Growth Des.*, 10 (2009) 856- 861.
- [49] J. Su, L. Guo, N. Bao and C. A. Grimes, Nanostructured $\text{WO}_3/\text{BiVO}_4$ heterojunction films for efficient photoelectrochemical water splitting, *Nano Lett.*, 11 (2011) 1928-1933.
- [50] W. Zhang, F. Wu, J. Li, D. Yan, J. Tao, Y. Ping and M. Liu, Unconventional relation between charge transport and photocurrent via boosting small polaron hopping for photoelectrochemical water splitting, *ACS Energy Lett.*, 3 (2018) 2232-2239.
- [51] A. J. Rettie, H. C. Lee, L. G. Marshall, J. F. Lin, C. Capan, J. Lindemuth, J. S. McCloy, J. Zhou, A. J. Bard and C. B. Mullins, Combined charge carrier transport and photoelectrochemical

characterization of BiVO₄ single crystals: Intrinsic behavior of a complex metal oxide, *J. Am. Chem. Soc.*, 135 (2013) 11389-11396.

[52] M. Rohloff, B. Anke, S. Zhang, U. Gernert, C. Scheu, M. Lerch and A. Fischer, Mo-doped BiVO₄ thin films - high photoelectrochemical water splitting performance achieved by a tailored structure and morphology, *Sustainable Energy Fuels*, 1 (2017) 1830-1846.

[53] X. Zhong, H. He, M. Yang, G. Ke, Z. Zhao, F. Dong, B. Wang, Y. Chen, X. Shia and Y. Zhou, In³⁺-doped BiVO₄ photoanodes with passivated surface states for photoelectrochemical water oxidation, *J. Mater. Chem. A*, 6 (2018) 10456-10465.

[54] X. Zhao, J. Hu, S. Chen, and Z. Chen, An investigation on the role of W doping in BiVO₄ photoanodes used for solar water splitting, *Phys. Chem. Chem. Phys.*, 20 (2018) 13637-13645.

[55] D. Kong, J. Qi, D. Liu, X. Zhang, L. Pan, J. Zou, Ni-doped BiVO₄ with V⁴⁺ species and oxygen vacancies for efficient photoelectrochemical water splitting, *Trans. Tianjin Univ.*, 25 (2019) 340-347.

[56] G. Liu, F. Li, Y. Zhu, J. Lia and L. Sun, Cobalt doped BiVO₄ with rich oxygen vacancies for efficient photoelectrochemical water oxidation, *RSC Adv.*, 10 (2020) 28523-28526.

[57] H. Ye, J. Lee, J. S. Jang and A. J. Bard, Rapid screening of BiVO₄-based photocatalysts by Scanning Electrochemical Microscopy (SECM) and studies of their photoelectrochemical properties, *J. Phys. Chem. C*, 114 (2010) 13322-13328.

[58] W. Luo, Z. Yang, Z. Li, J. Zhang, J. Liu, Z. Zhao, Z. Wang, S. Yan, T. Yu and Z. Zou, Solar hydrogen generation from seawater with a modified BiVO₄ photoanode, *Energy Environ. Sci.*, 4 (2011) 4046-4051.

[59] W. Luo, Z. Li, T. Yu and Z. Zou, Effects of surface electrochemical pretreatment on the photoelectrochemical performance of Mo-doped BiVO₄, *J. Phys. Chem. C*, 116 (2012) 5076-5081.

[60] H. S. Park, K. E. Kweon, H. Ye, E. Paek, G. S. Hwang and A. J. Bard, Factors in the metal doping of BiVO₄ for improved photoelectrocatalytic activity as studied by scanning electrochemical microscopy and first-principles density-functional calculation, *J. Phys. Chem. C*, 115 (2011) 17870-17879.

[61] W. J. Jo, J. W. Jang, K. J. Kong, H. J. Kang, J. Y. Kim, H. Jun, K. P. S. Parmar and J. S. Lee, Phosphate doping into monoclinic BiVO₄ for enhanced photoelectrochemical water oxidation activity, *Angew. Chem. Int. Ed.*, 51 (2012) 3147.

[62] D. K. Zhong, S. Choi, and D. R. Gamelin, Near-complete suppression of surface recombination in solar photoelectrolysis by "Co-Pi" catalyst-modified W:BiVO₄, *J. Am. Chem. Soc.*, 133 (2011) 18370-18377.

[63] F. Tang, W. Cheng, H. Su, X. Zhao, and Q. Liu, Smoothing surface trapping states in 3D coral-like CoOOH-wrapped-BiVO₄ for efficient photoelectrochemical water oxidation, *ACS Appl. Mater. Interfaces*, 10 (2018) 6228-6234.

[64] S. K. Pilli, T. E. Furtak, L. D. Brown, T. G. Deutsch, J. A. Turner and A. M. Herring, Cobalt-phosphate (Co-Pi) catalyst modified Mo-doped BiVO₄ photoelectrodes for solar water oxidation, *Energy Environ. Sci.*, 4 (2011) 5028-5034.

[65] E. Jin Joo, G. Park, J. S. Gwak, J. H. Seo, K. Y. Jang, K. H. Oh and K. M. Nam, Efficient photoelectrochemical water oxidation by metal-doped bismuth vanadate photoanode with Iron oxyhydroxide electrocatalyst, *J. Nanomater.*, 2016, 1827151.

EIHE 2023

Patron

A. K. Mohanty (Director, BARC)

Advisory Committee

A. K. Tyagi (BARC)	J. Srivastava (HWB)
S. Kannan (BARC)	P. D. Naik (HBNI)
T. K. Ghanty (BARC)	V. Kain (BARC)
P. Vadgama (UK)	S. Manohar (BARC)
S. M. Yusuf (BARC)	S. K. Aggarwal (Mumbai)
K. T. Shenoy (BARC)	Shigeru Amemiya (USA)
R. Katakya (U.K)	M. Opallo (Poland)
P. Mukherjee (BRIT)	P. K. Mohapatra (BARC)
S. Mitra (IITB)	R. Tewari (BARC)
Awadhesh Kumar (BARC)	T. Pradeep (IITB)
F. Marken (UK)	S. Carsten (UK)
C. M. A. Brett (Portugal)	P. Balaya (Singapore)
G. Wittstock (Germany)	S. K. Haram (Pune)
D. Koley (USA)	S. Sampath (IISc)
A. R. Hillman(UK)	A.M.O. Brett (Portugal)

EIHE 2023

Organizing Committee

Chairman: A. K. Tyagi & P. D. Naik

C. N. Patra (Vice- Chair)

S. K.Guin (Ireland)

A. K. Satpati (Convener)

S. Shendage (Vaze College)

Kothandaraman R. (Co-convener)

N. P. Shetti (Belgaon)

M. K. Dey (Secretary)

R. K. Singhal (BARC)

P. K. Mishra (Jt.Secretary)

R. J. Mascarenhas (Bengaluru)

V. T. Aher (Treasurer)

S. Basu (CSIR-IMMT/IITD)

S. Sahoo (Jt. Treasurer)

C. Bhattacharya (IEST)

A. K. Tripathi (BARC)

S. Kumar (NCCCM)

A. Mukhopadhaya (IITB)

T. V. Krishnamohan(BARC)

S. Prasad(USA)

S. A. Kumar (BARC)

J. Kumar (BARC)

S. D. Kumar (BARC)

Subir K Ghosh (BARC)

T. N. Narayanan (TIFRH)

M. K. Sharma (BARC)

V. S.Tripathi (BARC)

S. Manna (BARC)

B. R. Sathe (Aurangabad)

EIHE 2023

Members of Accommodation, Transport, Catering & Hall management Committee

N. Raje

K. K. Swain

S. K. Gupta

H. Basu

J. R. Kale

M. Ghosh

H. Parab

R. G. Dalavi

B. B. Kalekar

B. N. Singh

Sweta Singh

Abhishek Sharma

P. S. Remya Devi

N. Ajith

S. S. Pawar

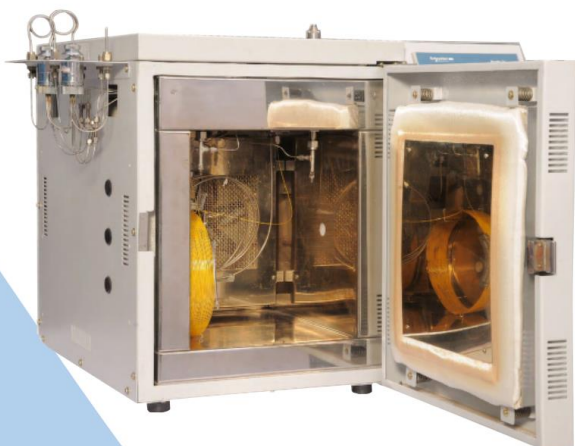
P. Bhaye

Applications

- ◆ Petrochemical Industries
- ◆ Refinery & Fertilizer Industries
- ◆ Agricultural Sector
- ◆ Industrial Chemicals
- ◆ Environmental Analysis
- ◆ Defense, Space & Atomic Energy
- ◆ Flavors
- ◆ Solvent Analysis
- ◆ Trapped & Free Gases
- ◆ Pharmaceutical
- ◆ Food Analysis
- ◆ Testing Laboratories

Configurations

Can be configured to OLGC, TOGA, RGA, NGA & can be coupled with MS, Head Space Autosampler & Automatic Liquid Sampler



High Performance Detectors

- ◆ Flame Ionization Detector (FID)
- ◆ Thermal Conductivity Detector (TCD)
- ◆ Ionization Detector (PDHID / DID/ ADID)
- ◆ Micro Thermal Conductivity Detector (MTCD)
- ◆ Electron Capture Detector (ECD) & Other Specific Detectors





Phadke Instruments Pvt. Ltd.

Distributors of Scientific Research Instruments

Phadke Technologies

PhadkeSTAT Indigenously Developed Potentiostat

- PhadkeSTAT 20 Full Scale Current 20 mA to 200nA
- PhadkeSTAT 2: USB Powered HandHeld Potentiostat
- Phadkage: Faraday Cage for Shielding in Low Current Applications



Complete Range of Electrochemical Cells and Electrodes.
RRDE Rotating Ring-Disk Electrode.
Spectroelectrochemical System



Compact USB Powered Potentiostats for Biosensor Research using Screen Printed Electrodes



- Full Range of Electrochemical Instrumentation with Cells and Electrodes
- Polarographic Analyzer with HMDE, RDE and Solid Electrodes
- Electrogravimetry System



- Full Range of Water and Soil Analysis Systems
- BOD/COD/TOC Analyzers
- Multiparameter Environmental Titration System



- ESR Spectrometer
- Scanning Electron Microscope
- BET Surface Area and Pore Size Distribution Analyzer
- Helium Pycnometer



- Photoelectric Spectrometer with LEDs and Xenon Lamp
- IMPS/IMVS System for Dye Sensitized Solar Cells
- Scanning Kelvin Probe



Screen Printed Electrodes for biosensor Applications



Glove Box for Experiments in Inert Atmosphere



Planetary Ball Mill
Transparent Glove Box



Ion Chromatograph



Ambient Air Monitoring System



Spin Coater

Email: sales@phadkeinstruments.com

Contact No: 022 4970 9352

Laboratory & Scientific Instruments



Nitrogen Evaporator
50, 25, 08 Samples



48, 96 & 144 SPE Positive Pressure Processor



100, 150 & 144 Sample Evaporator



LCMS / LCMSMS Nitrogen Generator



Nitrogen Gas Generator & Nitrogen Plant



Nitrogen Air & Hydrogen Combination Generator for GC TOC



Hydrogen Gas Generator



HPLC Column Washing Pump (4 Column)



Probe Sonicator / Ultrasonic Processor



Multifunctional Ultrasonic Cleaner



Ultrasonic Bath with Chiller



Sterility Testing Manifold (3 Branch & 6 Branch)



Stomacher Blender / Paddle Bag Mixer



Manual Hydraulic Press for FTIR & XRF (15 to 40 tons)



KBr Die Set for Pallet Making Sizes 3mm to 75mm available



Gas Purification & Control Panel



Cylinder Regulator & Line Regulators



Gas, Oil / LPG Gas Sampling Cylinder



Gas Distribution Panel



Auto Gas Change Over / Mechanical-Auto Gas Change Over



An ISO 9001:2015 Certified Company



INTRODUCTION

We introduce ourselves as one of the Leading Dealers, Importers & Stockiest of Laboratory Glasswares, Chemicals & Scientific Instruments, ESTABLISHED SINCE 1952, an if you give us a chance by registering your firm in your Vendor's list and send us your Regular Valued Enquiries, from time to time, we assure you to give you our most competitive rates, backed by our services, for the available items.

We specialize and maintain regular stock of the following items

- Quartz and Silica tubes, rods, wools, boats, beakers, crucibles, plates, disc, etc
- All sizes of Agate Mortar & Pestles, Basins, etc
- All sizes of Laboratory Teflon materials, Silicon tubings
- High Purity Alumina wares such as crucibles, tubes, trays, boats, etc
- Quartz Single and Double distillation apparatus
- Digital balances (Analytical, Top-loading, Industrial, etc)
- Silver & Platinum Paste
- High purity metals such as: Platinum, tungsten, tantalum, molybdenum in the form of foils, wires powders etc.
- Chemicals / Solvents /Speciality Chemicals / Biochemicals / Kits / Antibodies

We also deal in the following:

- All types of Laboratory Instruments such as Ovens, Incubators, Hot Plates, pH Meters, Ultrasonic baths, Water Baths, Water Stills, Gas Flow Meters, BOD Incubators, Furnaces, Constant Temperature Water Baths, Microscopes, Karl Fisher Apparatus, Autoclaves, Gas Generators, KBR Hydraulic Press, Portable & Oil-sealed Vacuum Pumps
- All types of Imported Instruments such as Spectrophotometers, Viscometers, Weighing Balances, Pocket pH Meters, Digital Conductivity Meters, Portable pH/mV/Temperature Meter, Dissolved Oxygen Meter
- Rotameters of all types
- **Whatman** Filter Papers, Membrane Filters, Syringe filters, Nylon Filters, Butter Papers, etc
- **Borosil / Duran / JSil / JSGW** Glasswares
- Test Sieves & Sieve Shaker
- Spares for GC & HPLC Systems
- Ice Flakers, Deep freezers, Refrigerators, Microwave Oven
- Laminar Air Flow, Bio-safety Cabinet, Fume Hoods
- Hydrometers, Thermometers with certificate
- **Tarsons** Make Labware Products
- Oil & Petroleum Products

Major Principal Companies : Mettler Toledo, TCI, Sigma, Thermo, Meck Millipore, Tarsons, Abdos, Athena, NEB, CST, Santacruz, R&D Systems, Eppendorf, Kubota, Avantor, Promega, Bioxcell, Invivogen, Himedia, ElabScience, Epigentek, Veego, Cayman, MPBio, GE (Cytiva), Labman/Wensar, Heidolph, Aczet, Bandelin, Sartorius, Brand, Qiagen, Rocker, Starna, Remi, Miltenyi, Chromotek, Bioassay, Wheaton, Moltox, Medchem Express, TargetMol, Horizon Discovery (Dharmacon), Biologend, Roche, Hanna, TechResource, Waters, Polylab, Lovibond, Sujay, White-Westinghouse, Novita, Ika, Brookfield, Licor, Exciton, Cambridge Isotope, Spectrum (Repligen), Tedpella, Combi-Blocks, Advent, Axygen, Corning, Falcon, Laxbro, Hellma, Shimadzu, PerkinElmer, Bechhmark, Borosil, JSil, Klasspack, JSGW, Ibidi, Matrix, Metalab, Shanti Scientific, PolyScience, TRC, Technics, Trident, Cole-Parmer, Micro Scientific, Oscacr, Eltek, Electrolab, Jayant, Contech, Schott-Duran, Toshniwal, Systronics, Gilson, Kasablanka, Hamilton, BioRad, LabIndia, Leimco, Rescholar, Star, Horiba, Amber, Genaxy, Strem, & many more



ipgi instruments

Technical Support for Electrochemistry, XRD , Polymer & Analytical Instruments.

Electrochemistry:-

Zahner Electrochemical workstation. CIMPS, IMVS, QE

All kinds of cell kits for Electro analytical , corrosion , Battery , high temperature c , Membrane permeation, etc. Custom designed cell kits.

Compact Mini Potentiostat. , MultiChannel Potentiostats

Wireless Potentiostats , redox Flow cell , FCTS , DMFC , PEMFC , SOFC



Simulator:- Sciencetech – Canada`

150W ,300W ,1000W, 1600W Xe light source.

Solar Simulators.

IV testing System. DSSC , PV , Solar cell characterization

IPCE , EQE , IQE efficiency measurements.

Reactors: Customized Reactors , Bio reactors , Fuel cell , Electrolyser etc

High Temperature reference electrode 0°C up to +800°C

Thermo - XRD, XPS,

EQUINOX FAMILY

X Ray Diffractometer

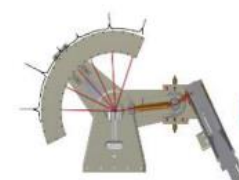
Thermo Inel - France



EQUINOX 100 : Stand Alone Benchtop X-Ray diffractometer

EQUINOX 1000 : Benchtop X-Ray diffractometer

EQUINOX 3000 : Powder X-Ray diffractometer



Electrolyser Fuel cell

Chillers – Cold water circulator:-

Compact chillers, Imported chillers. Labtech -Italy

ipgi chillers from 0.5kw ~ 90kw. Temperature range -20oC ~ RT ~ 95°C.

ipgi instruments , old No.15/1 , New No.46 , Naickamar street , West mambalam, Chennai –

600033 . Ph: 9444345824, 7358082134 , 94444168027, 9094966589. Tel.04443362589.Email:

sales@ipgi.co.in, gbsubramani@ipgi.co.in, aanandharaj@ipgi.co.in **www.ipgi.co.in**

Metrohm solution for electrochemistry in industry, health, and environment

Metrohm India Private Limited is a subsidiary of Metrohm AG, Switzerland, world leader in Ion Analysis. Metrohm is a renowned name in Ion Analysis and is the only company to offer the complete range of Ion Analysis Instrumentation - Titration, Ion Chromatography and Voltammetry. We also have world class pH / Ion/ Conductivity meters/ Electrochemical instruments, Spectroscopy and Stability Measuring Instruments in our comprehensive product portfolio.

Metrohm Autolab sets the standard for electrochemistry instrumentation. Metrohm Autolab creates instruments that are suitable for most application areas including: corrosion, energy, environmental, sensors, and solar. Our customers may not always be electrochemists, but they are engaged in fundamental and applied research harnessing the power of electrochemistry for further understanding. They are driven to understand and improve electrochemical processes with the ambition to deliver new materials with superior properties and future possibilities.

With an Autolab potentiostat/galvanostat and NOVA software there are no limits to where your research can go.



Our electrochemistry portfolio ranges from portable instruments to modular systems for full flexibility and multichannel workstations allowing a number of experiments to be performed simultaneously.

- Compact/Modular Line potentiostat / galvanostat instruments
- Multichannel instruments with up to 12 channels
- Spectroelectrochemical measurements combining electrochemistry and UV-Vis, Vis-NIR or Raman spectroscopy in one measurement
- Screen-printed and interdigitated electrodes



Scan this code for more info.

Metrohm India Private Limited

Metrohm-SIRI Towers, 3&4, Fourrts Avenue, Annai Indira Nagar
Okkiyam, Thoraipakkam, Chennai - 600097, India.
Ph: +91 44 40440440 | Customer support: +91 44 40440444

For details, e-mail us at info@metrohm.in or visit us at www.metrohm.in

 **Metrohm**
India Private Ltd.



LITHIUM BATTERY RESEARCH INSTRUMENTS & RAW MATERIALS

 ALUMINIUM FOIL	 COPPER FOIL	 LITHIUM CHIP	 ELECTROLYTE	 SEPARATOR	 CRIMPING MACHINE	 OXYGEN SENSOR
 ELECTROLYTE FILLING MACHINE	 GLOVE BOX	 BATTERY TESTER	 DESKTOP COATING MACHINE	 LITHIUM TAPE	 CYLINDRICAL CELL CASE	 ULTRASONIC WELDER
 SWAGELOCK CELL	 COIN CELL BATTERY HOLDER	 COIN CELL ASSEMBLY	 DISC CUTTER	 DOCTOR BLADE	 CARBON CLOTH	 HOT ROLL PRESS MACHINE



AEROINCORPRATION

NO. 44/38A, 2ND STREET, SATHIYAVATHI NAGAR, PADI, CHENNAI-600050
E-MAIL ID: sales1@aeroincorp.com, Ph: 9176637255, web: www.aeroincorp.com



PG TECH PVT. LTD.

Manufactures, Exporters & Distributors for Scientific Instruments



Dr. R Chidambaram, DAE-
Homi Bhabha Chair Professor



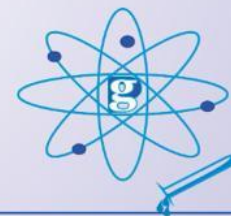
Hon. Dr G Satheesh Red
Chairman DRDO



Prof CNR RAO Bharat
Ratna Awardee



Registered NGO
For Education & Social Cause



PG TECH RESEARCH INSTITUTE

(APPLICATION LAB & TRAINING INSTITUTE)

Training Institute for Pharma
(Wet Lab, HPLC & QC-QA)

38, Electronic Complex, Near Govt. ITI College, Pardeshipura, INDORE (M.P.) – 452010

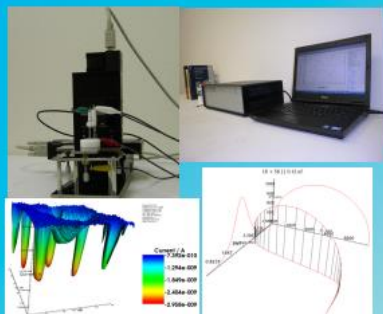
Phone : 0731-4993339, 4996222, Mob.: +91-98269-69100

E-mail : admin@pgtech.in

www.pgtech.in

Sinsil International Pvt Ltd

Your Partner in Scientific Needs



Electrochemical Workstation
CH Instruments
www.chinstruments.com



ZHN Nanoindenter
ZwickRoell
www.zwickroell.com



Confocal Microscope
ISS
www.iss.com



Dielectric Impedance Analyzer
Novocontrol
www.novocontrol.com



Ellipsometer
J.A.Woollam
www.jawoollam.com



3D Profilometer
Filmetrics
www.filmetrics.com



Gravimetric Sorption Analyzer
Rubolab
www.rubolab.de



Solar Simulator
Photo Emission Tech
www.photoemission.com



UV-VIS-Fibre Optics Spectrometer
Ocean Insight
www.oceaninsight.com

SINSIL INTERNATIONAL PVT LTD

NO 31, OPP S J E S College
Old Madras Road,
Medahalli, Virgonagar Post,
Bengaluru-560049.

Email:- bangalore@sinsil.in

WhatsApp : +91-80-50891594

Phone : +91-9341282569

Facebook : Sinsil Intl

Baroda : info@sinsil.in

Delhi : delhi@sinsil.in

Kolkata : kolkata@sinsil.in

Chennai: bangalore@sinsil.in

Mumbai : mumbai@sinsil.in

Hyderabad: bangalore@sinsil.in

+91-9167404043

+91-9312437300

+91-9681442892

+91-9980287123

+91-9833011933

+91-8008999507

www.sinsilinternational.com



Indian Society for ElectroAnalytical Chemistry

www.iseac.org.in